2011

Online Conductivity and Stability in Emulsion Polymerization of n-Butyl Methacrylate

Funian Zhao
Lehigh University

ONLINE CONDUCTIVITY AND STABILITY IN THE EMULSION POLYMERIZATION OF N-BUTYL METHACRYLATE

by

Funian Zhao

A Dissertation

Presented to the Graduate and Research Committee

of Lehigh University

in Candidacy for the Degree of

Doctor of Philosophy

in

Chemical Engineering

Lehigh University

May 2011

Certificate of Approval

Approved and recommended for acceptance as a dissertation in partial fulfillment of the requirements for the degree of Doctor of Philosophy

_____
Date

_____
Dissertation Director
Professor Andrew Klein

_____
Accepted Date

Committee Members:

_____
Professor Andrew Klein
Advisor

_____
Professor Mohamed S. El-Aasser
Co-Advisor

_____
Dr. Eric S. Daniels
Co-Advisor

_____
Dr. E. David Sudol
Co-Advisor

_____
Professor F. Joseph Schork

_____
Dr. (Maria) Rong Hu

Acknowledgements

I wish to express my sincere gratitude and appreciation to:

Professor Andrew Klein for guiding me into the field of emulsion polymers and helping me in my studies and research. His endless support, priceless advice, and invaluable encouragement are my powers to overcome troubles. His personality greatly influences me on my life.

Professor Mohamed S. El-Aasser for his discussion, suggestions, and serving as my co-advisor. His kindness and care made me feel comfortable during the period of these years.

Dr. E. David Sudol for his guidance, extensive discussion, and numerous suggestions. His rigorous and deep approach in research is the great treasures I obtain. Special thanks for editing the draft of my dissertation and papers.

Dr. Eric S. Daniels for his advice, discussion, and support through my research. His dedication to work and research affects my thoughts about the careers. I also appreciate his proofreading for everything I wrote.

Professor F. Joseph Schork and Dr. Rong (Maria) Hu for serving on the Ph.D. committee. Their suggestions and comments are important parts of this research.

All students in the EPI group for sharing ideas and encouragements. The friendship among us is an invaluable gift. The lives we shared are cherished memories and unforgettable experiences.

All my family members of their endless love and support during these years.

Acknowledgements

To my mother, father, and younger brother

and

To my wife and two lovely daughters

Table of Contents

List of Figures

List of Tables

Abstract

A resistance probe and a torroidal probe, which work on different principles, were used to measure conductivity during the course of emulsion polymerizations of *n*-butyl methacrylate (BMA). The purpose of this research was to investigate whether this combination of online conductivity measurements can be used to predict latex stability.

First, online conductivity measurements were used to monitor conductivity in a non-reactive system. In this case, the synthesized latex was charged in a reactor under shear and high temperature to test latex stability. The results showed that some coagulum was formed, but the two conductivity curves obtained from the two conductivity probes were not significantly different. This indicated that this method cannot be used to monitor latex stability in the non-reactive system.

Second, batch emulsion polymerizations of BMA were carried out using sodium lauryl sulfate (SLS) as surfactant at 70 °C. The solids content of the batch polymerizations were 5 % and 20 %, respectively. Semi-batch emulsion polymerizations of BMA (40 % solids content) were also run. In all cases, the profiles of the two conductivity curves changed with the variation of the SLS concentration. Because the deposition on the surfaces of the electrodes of the resistance probe can make the conductivity values obtained from this probe smaller than the true values,

which was measured by the torroidal probe, the final conductivity ratio (R/T) between the two conductivity curves was chosen as a parameter to correlate the conductivity curves to latex stability. Blender tests and turbidity measurements were performed to measure the mechanical stability and the electrolyte stability of the final latexes, respectively. The percent coagulum obtained after the blender test was completed was used to represent the mechanical stability, and the critical coagulation concentration (ccc) calculated through the turbidity measurements was used to indicate the electrolyte stability. R/T was correlated to the percent coagulum and the ccc, respectively. There was a linear relationship between them, which indicated that the online conductivity measurements could be used to predict latex stability.

Third, batch emulsion polymerizations of BMA using mixed anionic-nonionic surfactants were carried out. SLS was used as anionic surfactant and Triton X-100 was chosen as a nonionic surfactant. The total surfactant concentrations were 6, 10, 20 and 30 mM, respectively. The weight ratio between the two surfactants changed for each concentration. For each concentration, the results showed that the reaction rate decreased with the increase in the amount of Triton X-100. Moreover, the R/T values, and the mechanical and electrolyte stability of the final latexes also decreased with a increase in the weight ratio of Triton X-100 to SLS. The correlation between R/T and the percent coagulum, and R/T and the ccc was made. There was a linear relationship between them, which indicated that the online conductivity measurements could be used as online sensors to predict latex stability.

Finally, the DLVO and extended DLVO theories were applied to theoretically calculate the energy barrier between two polymer particles, which is normally used to represent the degree of latex stability. First, the DLVO theory was used to calculate the energy potential, which was caused by the repulsive forces between the particles, for the latexes prepared using SLS as the sole surfactant. Some unreasonable results were obtained. These were caused by an assumption of the DLVO theory (surface potential less than 25 mV), which was not suitable for the experimental results. After changing the electrolyte concentration from the order of 0.001 to 0.1 M, the equations based on the DLVO theory showed much smaller errors and the new results were more reasonable. The extended DLVO theory was used to calculate the energy potential for latexes prepared using mixtures of SLS and Triton X-100 as the surfactants. Both the repulsive and steric forces were included in this system. The theoretically calculated results showed the same trend as those obtained from the blender test and turbidity measurements. Moreover, the results also showed that the contribution of Triton X-100 to latex stability was much smaller compared with SLS, which was caused by the structure of Triton X-100 and its low surface coverage on the latex particle surfaces. This was the reason why the mixed surfactants did not improve latex stability.

Chapter 1
Introduction

1.1 Introduction

Latex stability is the property by which particles remain dispersed as single entities for long periods of time[1]. There is usually a thermodynamic tendency for a hydrophobic colloid to phase separate, because aggregation or coalescence of particles are accompanied by a loss of interface between the two phases, which causes a reduction in the total Gibbs free energy of the system[2]. Brownian motion is a key factor in the aggregation process since the particles dispersed in the medium are continually undergoing Brownian motion[3]. Latex stability depends on the presence of an energy barrier between the particles, which discourages their close approach. These barriers arise from a balance between the various attractive and repulsive forces, such as van der Waals attractive forces and electrostatic repulsive forces. The higher is this barrier, the more stable is the colloid.

Latex stability is one of the most important factors for all commercial emulsion polymers, because it can not only affect the cost and the yield of latexes in large reactors, but also affect the quality of the final products. During emulsion polymerizations, polymer particles must be dispersed in the medium without

significant coagulation. After the reactions, latexes must survive in the following processes, such as pumping under high pressure or shipping, which may expose the latexes to widely varying temperature fluctuations. Moreover, latex stability dictates the shelf-life time for the products. However, so far, there is no effective method or online sensor that can monitor latex stability during polymerizations.

Conductivity probes are inexpensive and easily accessible tools. They can serve as online sensors, which may provide added insight into an emulsion polymerization reaction. Conductivity can be used to monitor the mobility of ion species present in the formulation and responds to changes in the concentrations of ionic species (e.g., surfactant, initiator, etc.), which are related to latex stability. Moreover, if two conductivity probes based on two different measurement principles can be used, some information related to latex stability might be obtained. This is based on the observation that there may be some plating of polymers on the surfaces of the metal electrodes of a conventional resistance probe, which can cause a decrease in the measured conductivity values by this probe. On the other hand, if the plating does not affect the measurements of another conductivity probe, such as torroidal probe, the difference in the values from the two probes may indicate some instability in the latex.

The objective of this project is to determine the feasibility of predicting latex stability through online conductivity measurements. If a relationship between the

conductivity measurements and latex stability can be established, this method may be used as an online sensor to predict latex stability during an emulsion polymerization. This could have significant commercial implications.

1.2 Emulsion Polymerization

Emulsion polymerization is a free-radical-initiated chain polymerization process in which a monomer or a mixture of monomers is polymerized in the presence of an aqueous solution containing surfactant to form a product, known as a latex[4]. Emulsion polymerization has developed into a widely used process for the production of synthetic latexes since its first introduction on an industrial scale in the mid-1930s. Nowadays, many commodity polymers are prepared by the emulsion polymerization process, such as synthetic rubber, latex paints, paper coatings, adhesives and binders for non-woven fabrics.

The emulsion polymerization process has some distinct advantages. This polymerization can proceed at a high rate due to good heat transfer of the aqueous phase. Moreover, high molecular weight can be obtained at a high rate, which is different from bulk polymerization. The viscosity of latex products is low and independent of molecular weight. In some cases, the latexes can be directly employed in final uses such as coatings and paints. On the other hand, there are some disadvantages of this process. For example, the structure of polymer chains is not easy to control compared with bulk and solution polymerizations, and the presence of

surfactants in latexes may affect the quality of the final products.

Since a number of books dealing with emulsion polymerization have been published[4,5,6], the classic theory concerning the kinetics of this process is only briefly introduced here. According to Harkins' mechanism [7], when the surfactant concentration is above its ctitical micelle concentration (CMC), emulsion polymerization is divided into three intervals, which are the particle formation stage (Interval I) and particle growth stages (Intervals II and III). During Interval I, free radicals generated in the aqueous phase by initiator decomposition enter monomer-swollen micelles to initiate polymerization. Monomer-swollen micelles are the main location of particle nucleation in Harkins' theory. The monomer diffuses from the monomer droplets through the aqueous phase and polymerizes in the monomer-swollen nuclei. Free surfactant molecules adsorb onto and stabilize the growing particles. Both the particle number and polymerization rate increase with time. This stage ends when the micelles disappear. During Interval II, the particle number remains constant and the monomer droplets provide the growing polymer particles with the required monomer to maintain saturation swelling and support the propagation reaction. The polymerization rate is classically considered to be constant in this stage. The monomer droplets disappear at the end of Interval II and the reaction continues until the monomer in the monomer-swollen particles is consumed (Interval III). During the final stage, the particle number also remains constant and the polymerization rate decrease due to the decrease in the monomer concentration in the

particles.

A quantitative model to describe this mechanism was developed by Smith and Ewart[8] and further modified by others[9,10]. The expression for the general rate of polymerization is shown in eqn (1.1).

$$R_p = \frac{k_p \bar{n} [M]_p N_p}{N_A} \tag{1.1}$$

where k_p is the propagation rate constant, $\bar{n}$ is the average number of radicals per particle, $[M]_p$ is the monomer concentration in the particles, N_p is the total number of particles and N_A is Avogadro's number. Smith and Ewart described three cases depending on the value of $\bar{n}$ which were determined by the radical desorption rate from the particles, particle size, modes of termination, and the rates of initiation and termination relative to each other[11]. $\bar{n} < 0.5$ is observed when radical desorption from the particles and aqueous phase termination are significant. Monomers with high monomer chain-transfer constants show this behavior. $\bar{n} = 0.5$ is considered to be the predominant behavior in most emulsion polymerizations. In this case, the radical absorption rate is high and the radical desorption rate is either zero or negligible compared with the radical absorption rate. Small particles can contain only one growing radical or no radical: "zero-one" kinetics apply. Thus $\bar{n}$ equals 0.5. Normally, this value is used in eqn (1.1) to calculate k_p. Finally, if the particle size is large or the termination rate constant is low, $\bar{n} > 0.5$ is observed as long as the termination in the aqueous phase and the radical desorption rate constant are

negligible and the initiation rate is not too low.

1.3 Latex Stability

There are three main types of latex stability: mechanical, chemical and thermal (freeze-thaw). Thermal stability is the stability when a latex is exposed to both low and elevated temperatures or repeated freeze-thaw cycles. This stability is was not part of this research. The other kinds of stability will be introduced below.

The term mechanical stability, as applied to a polymer latex, is meant to reflect the ability of a latex to withstand colloidal destabilizative effects of mechanical influences such as shearing and agitation[2]. The mechanical stability of latex is a property of great industrial importance. It has implications for the pumping, transportation, and processing of latexes, where sufficient mechanical stability to withstand the shearing forces is necessary. Although mechanical stability has a very important meaning in a practical sense, it is a difficult property to define quantitatively. In some factories, a trained worker may be able to replicate his results satisfactorily, but agreement between the results obtained from different workers is not always close. Moreover, the results obtained from mechanical stability tests are strongly dependent on the experimental conditions and procedure. There are two distinct principles of mechanical stability tests. One is to determine the time when the first visible coagulum appears, known as the mechanical stability time[12]; the other is to measure the weight of coagulum after a given time of agitation[13]. Because it is hard

to determine the first signs of coagulum during the blender test, which is used in this research to detect the mechanical stability of a latex, the latter principle is being applied.

The term chemical stability means the ability of a latex to withstand destabilizative influences of the further addition of chemical agents[2]. In many cases, but not all, the principal change that facilitates colloidal destabilization is a reduction in the magnitude of the potential energy barrier to the close approach of particles. In this research, the added chemical agent is a water-soluble electrolyte, and the stability to added electrolyte is termed electrolyte stability. The critical coagulation concentration (ccc), which is defined as the critical concentration of added electrolyte which can cause rapid coagulation of latex, is the most important parameter used to estimate electrolyte stability. If the electrolyte concentration is higher than the ccc, the electrostatic repulsive forces between two particles are completely cancelled and rapid coagulation occurs as a result of Brownian motion. On the other hand, if the electrolyte concentration is below this point, coagulation is slow[14]. Turbidity measurements are normally used to determine the ccc of latex samples.

1.4 Surfactant

Surfactants are amphiphilic molecules, which typically comprise a hydrophobic tail and hydrophilic head[15]. There are an enormous variety of commercially available surfactants which are employed in emulsion polymerizations.

Surfactants are generally categorized into four classes[16]: anionic, cationic, nonionic and ampholytic. The anionic and nonionic surfactants are the most widely used because of enhanced compatibility with negatively charged latex particles (usually as a result of persulfate initiator fragments) as compared to the cationic and ampholytic surfactants[17]. The typical anionic surfactants are comprised of sulfate, sulfonate, sulfosuccinate or phosphate groups attached to an extended hydrophobic backbone. Cationic surfactants comprise alkyl quaternary nitrogen bases, amines, nitriles and nonquaternary nitrogen bases. The major examples of nonionic surfactants are alkylaryl poly(ethylene oxide) (EO group) with various chain lengths. Ampholytic surfactants contain both amino and carboxylic acid groups.

When surfactant molecules are dissolved in water, some of them adsorb onto interfaces, such as the air/water and oil/water interfaces while the others exist as single molecules in the aqueous phase. When adding more surfactant molecules into water until a critical point is reached, the surfactant molecules adopt a more energetically favorable conformation by forming aggregates[18], which are called as "micelles". The surfactant concentration at this critical point is called the critical micelle concentration (CMC). The CMC is one of the most important parameters for emulsion polymerizations. In general, emulsion polymerizations carried out below the CMC lead to homogeneous nucleation[19,20], which can lead to a narrow particle size distribution. On the other hand, if emulsion polymerizations are run under conditions above the CMC, micellar nucleation dominates the nucleation process[21,22].

The hydrophile-lypophile balance (HLB) of a surfactant was developed as a systematic method to guide the selection of a surfactant for a specific system in the late 1940s[23]. The HLB range for most anionic and nonionic surfactants is 1 to 20. The smaller the value, the better the solubility in the oil phase. Therefore, surfactants with low HLB (less than 6 or 7) are good water-in-oil surfactants, while those with higher HLB (greater than 8) are good for oil-in-water emulsions. For a nonionic surfactant of alkylaryl poly(ethylene oxide) type, the HLB can be adjusted by varying the length of the EO group. The proper choice of HLB is important to achieve an optimum latex stability.

According to Dunn[24], the roles of surfactants in emulsion polymerization processes can be summarized as follows: (1) stabilization of monomer droplets in the emulsion, (2) solubilization of monomer in micelles, (3) stabilization of polymer latex particles, (4) solubilization of polymer, (5) catalysis of initiation reactions, and (6) action as chain transfer agents or retarders. From these effects, it can be seen that surfactants determine the nucleation mechanisms, the number of particles, and the reaction rate. Moreover, surfactants play a major role in stabilizing polymer particles, which is the main issue of this research.

In industry, mixtures of two or more surfactants are usually used to improve latex stability. The mixed surfactants can provide different surface properties compared with a single surfactant. Specific interactions between two types of

surfactants can lead to beneficial or detrimental effects. In practical applications, the mixtures of anionic and nonionic surfactants are often used to combine their stabilization properties: anionic surfactants provide electrostatic stability, which is caused by the presence of the end group (e.g., sulfate or sulfonate group) of the anionic chain. This repulsion is dependent on parameters such as electrolyte concentration and pH in the aqueous phase. This dependency can adversely affect latex stability under these conditions. On the other hand, nonionic surfactants provide steric stability, which is not related to electrolyte concentration. It is, therefore, practical to use mixtures of these two kinds of surfactants in emulsion polymerizations.

Many studies have been carried out to investigate the effect of mixed surfactants on the kinetics of emulsion polymerizations and latex stability. In the aspect of the kinetics, Colombié[25] investigated the role of mixed surfactants in the emulsion polymerization of styrene and Capek[26] wrote a comprehensive review about the differences between electrostatically and sterically stabilized emulsion polymerizations. Regarding latex stability, which is the focus of this research, few papers have been published. Woods *et al.*[27] varied the ratio of Siponate DS-10 (sodium dodecylbenzene sulfonate) to Triton X-100 (polyethylene oxide isooctylphenyl ether) in the emulsion polymerization of styrene. They found that the latex stability was extremely dependent on the surfactant content and electrolyte content. Chu and Piirma[28] studied the variations in the number of particles during the

emulsion polymerizations of styrene using SLS and Emulphogene BC-840 (tridecyl polyethylene oxide ethanol) as surfactants. The results showed that some surfactant ratios produced macroscopically unstable latexes. Later, Piirma and Sung[29] tried a new type of surfactant [$C_mH_{2m+1}O(CH_2CH_2O)_nSO_3Na$], which combine both anionic and nonionic surfactant characteristics. In their research, different chain lengths were used. A switch in the stabilization mechanism from electrostatic to steric with increasing EO chain lengths was observed.

Overall, the effect of the mixed surfactants on latex stability is extremely complicated. There is no clear understanding of this effect in both industrial and academic fields. Online conductivity measurements may be used as a practical tool to predict this effect during emulsion polymerization processes.

1.5 Electrostatic and Steric Forces

To keep polymer particles dispersed in the continuous aqueous phase as single entities instead of aggregation, repulsive forces between particles are necessary. There are two kinds of repulsive forces that are normally considered in emulsion polymer systems: electrostatic and steric forces.

Electrostatic forces are generated by the charged groups present on the particle surfaces. The charged groups mainly include the end groups of the decomposed initiators and ionic surfactants in the emulsion polymerization system.

Surface charges cause an electric field and this electric field attracts counterions. The layer of surface charges and counterions is called the "electric double layer". As a result of thermal motion of counterions, the surface charge extends over a certain distance from the particle surfaces and dies out gradually with increasing distance (diffuse layer) into the bulk phase. The distribution of cations and anions in the diffuse layer is given by a Bolzmann equation. On the basis of this simple model it can be deduced, as a first approximation for low potentials (less than 25 mV), that at a planar interface the potential (ψ_x) at a distance x from the surface (ψ_0) is given by the following equation:

$$\psi_x = \psi_0 \exp(-\kappa x) \tag{1.2}$$

The Stern layer is a layer of counterions that is directly adsorbed to the surface and that is immobile[30]. The potential at the point where the Stern layer ends is the Stern potential (ψ_s), which controls the colloidal stability of the system. When two charged particles approach each other and the electric double layers overlap, an electrostatic double layer force arises. This force is essential for the stability of the dispersed particles. Because the electrostatic force depends on the surface potential, which is determined by the surface charge density and the electrolyte concentration in the bulk phase, this force is sensitive to the variation of the electrolyte concentration. Obviously, it causes the disadvantage for latexes to resist salts, which is one of the most important considerations in industry. The electrostatic force can be estimated using the DLVO theory. This theory is named after Derjaguin and Landau[31], Verwey and Overbeek[32] who developed it in the 1940s. The details about this theory will be

discussed in Chapter 7.

Steric stabilization is a generic term that encompasses all aspects of the stabilization of colloidal particles by nonionic macromolecules[33]. When two particles covered by nonionic surfactant approach each other, the dangling chains of the nonionic surfactant overlap. This reduces the entropy of the system and results in a repulsive force, which is known as steric force. The applications of steric forces have had an especially long history of technological exploitation. Ancient Egyptian inks were prepared by dispersing carbon black (formed by combustion) in water using natural steric stabilizers, such as gum arabic and egg albumin[34]. Steric stability is very important in many industrial applications because the steric forces generated by the nonionic surfactants are not affected by the presence of electrolyte, which is much different from the electrostatic forces. This means that the addition of the nonionic surfactants can improve latex stability as well as the salt resistance of the latexes. Therefore, different kinds of nonionic surfactants are widely used in industrial products. However, on the other hand, the theories regarding the steric forces are not well-developed due the complication of the interactions. The most successful and widely used model was established by Vincent[35,36]. This model will be discussed later.

1.6 Conductivity and Conductivity Probes

Conductivity is a measure of the ability of a solution to conduct electric current. The conductivity of a solution is affected by charged species present in the

solution (such as electrolyte) and temperature. As temperature increases, the mobility of the charged species will increase, so conductivity will also increase. Since the effect on conductivity from charged molecules and particles in the latex is important in this research, relative conductivity is used to remove the effect of temperature on conductivity. This means that if conductivity is measured at a given temperature, it should be normalized into a value corresponding to its conductivity at 25 °C. This value is relative conductivity. Relative conductivity can be determined from the following temperature compensation equation[37]:

$$k_{25} = \frac{k_T}{[1 + 0.02(T - 25)]} \tag{1.3}$$

where k_{25} (μS/cm) is the relative conductivity at 25 °C, k_T is the measured conductivity at temperature T (°C). The value 0.02 present in Eqn (1.3) is the typical temperature correction factor.

Conductivity can be measured in many different ways. In this research, a conventional resistance electrode probe (manufactured by Control Company) and a novel torroidal probe (manufactured by Invensys Foxboro) were used (Figure 1.1). Both of them have their own advantages and disadvantages due to the way that they measure conductivity, so additional information can be obtained by using both probes together.

The resistance probe works by applying a potential difference between the

electrodes, with alternating current (AC) being used in order to minimize ion migration (Figure 1.2). The resistance probe has a cell constant (K) defined as the ratio of the effective distance (d) between the two electrodes to the effective area (A) (eqn (1.4)). Conductance (k) is the inverse of the resistance of the solution (R) as shown in eqn (1.5) and conductivity (Λ) can be calculated using eqn (1.6). The electrodes are in direct contact with the solution, which allows the probe to obtain very accurate and sensitive measurements. However, if there is some fouling or plating on the surface of the probe because of deposited coagulum, the measurements will not be accurate and the measured value will be smaller than the true conductivity value.

$$K = \frac{d}{A} \tag{1.4}$$

$$k = \frac{1}{R} \tag{1.5}$$

$$\Lambda = k \times K \tag{1.6}$$

The torroidal probe has two coils set up in parallel to each other (Figure 1.2). These coils are insulated and are contained in a donut-shaped polymer, such that they have no direct electrical contact with the solution to be measured. One of the coils creates a magnetic field, which causes a flow of the solution through the opening of the loop. This flow is then detected by the second coil, where the signal created by the induced flow is correlated to the conductivity. Therefore, the torroidal probe measures conductivity through induction. The benefit of measuring conductivity using this approach is that fouling of the surfaces of the torroidal probe does not affect the values it measures. However, this probe needs longer time to obtain a stable value

compared with the resistance probe. Moreover, the head of the torroidal probe is much larger than the resistance probe, so it is not easy to mount this probe into a lab scale reactor.

Figure 1.1: *Resistance conductivity probe (left) and torroidal probe (right).*

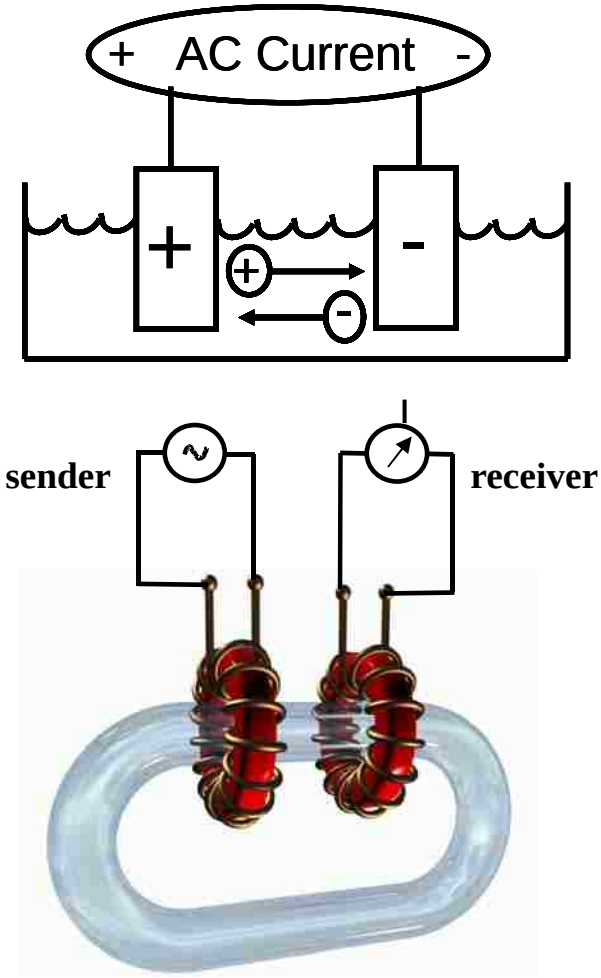

Figure 1.2: *Principle of operation of the resistance (top) and torroidal (bottom) conductivity probes.*

1.7 Online Conductivity Measurements

Studies describing the application of online conductivity measurements have been reported recently. For samples, Santos et al.[38,39] claimed that conductivity measurements corresponded to changes in the concentration of the ionic surfactant in the emulsion polymerization of styrene. In their research, conductivity measurements were used to determine the CMC of Sodium lauryl sulfate (SLS) at different temperatures. Moreover, a conductivity meter was coupled to a calorimetric reactor to provide online conductivity measurements during the emulsion polymerization of styrene (Figure 1.3). They also gave an explanation for the shape of the conductivity profiles. When the emulsion polymerization reaction starts, particles are formed, causing an increase in particle surface area. Surfactant is adsorbed from the aqueous phase onto the newly formed particle surfaces. The mobility of the adsorbed SLS molecules is much smaller compared with free SLS molecules, which results in a decrease in conductivity. Afterwards, the conductivity increases, which probably is due to consumption of monomer, which releases small amounts of the surfactant into the continuous phase. This explanation established a relationship between conductivity and the location of the surfactant. Based on these results, they established a model to predict the number of particles generated during the emulsion polymerizations. However, more work needs to be done to prove this relationship. Moreover, this explanation did not correlate conductivity and surfactant to latex stability during the emulsion polymerization processes.

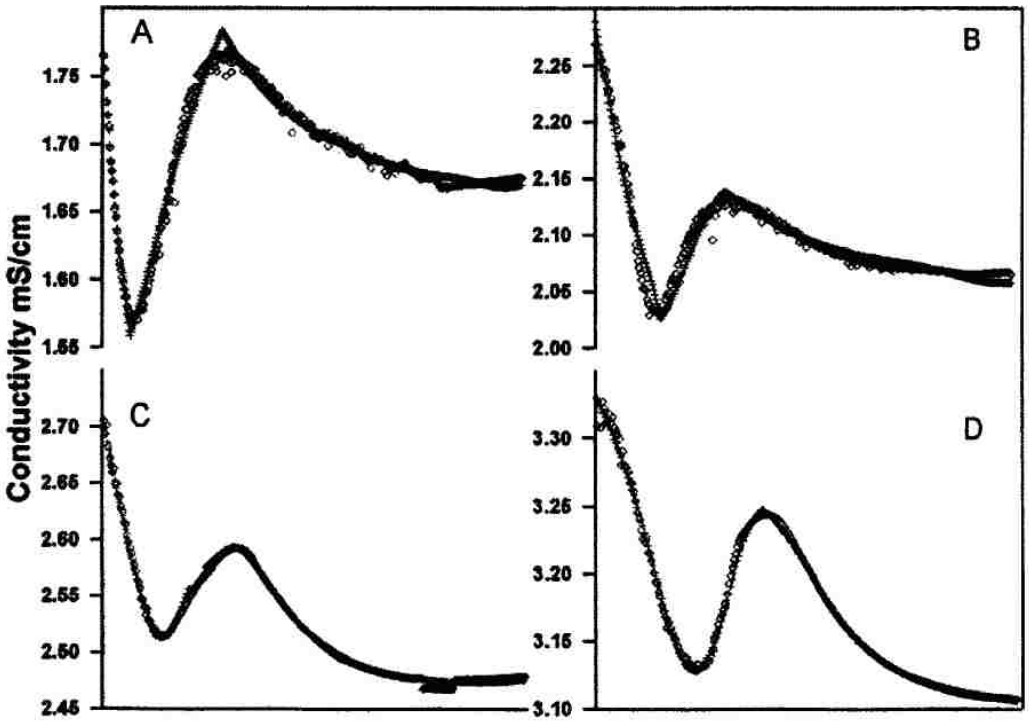

Figure 1.3: *Experimental (o) and predicted (+) conductivity signals for various recipes with different SDS concentrations: (A) 20 mM, (B) 30 mM, (C) 40 mM and (D) 50 mM*[38].

Ortiz Alba[40] reported widely varying conductivity profiles using a resistance probe during emulsion polymerizations of styrene with varying surfactant (Abex EP-110) concentration (Figure 1.4). This figure shows that the conductivity decreases to very low values when the surfactant concentration is 10 mM. He also reported that some coagulum was found on the surfaces of the electrodes of the resistance probe and mentioned that deposited coagulum might influence the conductivity measurements using this probe, which meant that the conductivity values measured by this probe were not correct. Therefore, he suggested that another probe, which works on a different principle, needed to be used to measure conductivity during the reactions to overcome the shortcomings of the resistance probe. A torroidal probe, which measures conductivity through induction, is a good choice.

Engisch [41] used both resistance and torroidal conductivity probes to investigate changes in conductivity during styrene emulsion polymerizations. He found that the values obtained from the two probes were not the same and the differences between them were not constant. The reason for the difference was that there was some plating present on the electrodes of the resistance probe, which decreased the measured conductivity values of the resistance probe. Therefore, there may be a relationship between these conductivity differences and latex stability or the amount of coagulum formed on the surfaces of the probes. Further investigation of this relationship was the focus of this research program.

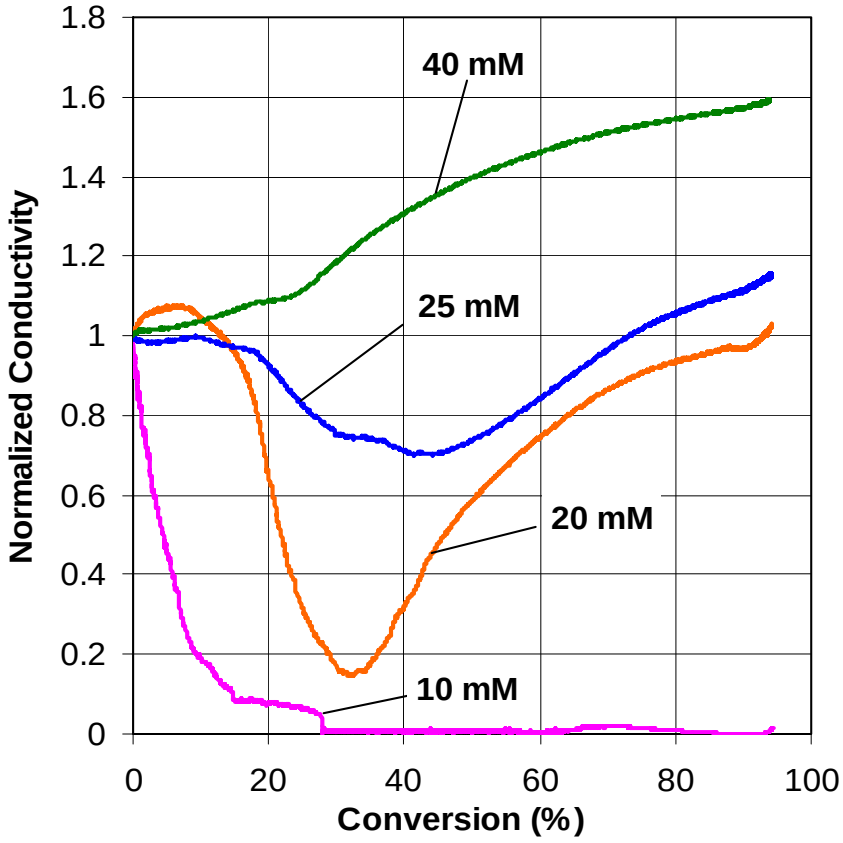

Figure 1.4: *Normalized conductivity-conversion profiles for emulsion polymerizations of styrene at 50 ^{o}C using different concentrations of Abex EP-110 surfactant*[40].

1.8 Objectives of the Research Program

Even though online conductivity measurements have been applied in emulsion polymerization processes previously, the relationship between the conductivity curves and the stability of the final latexes is not clear. The primary objective of this research is to investigate the feasibility of monitoring latex stability during the course of the emulsion polymerizations of *n*-butyl methacrylate (BMA) using online conductivity measurements. The investigations were carried out in non-reactive and reactive systems. In the reactive system, both batch (5 % and 20 % solids content) and semi-batch (40 % solids content) emulsion polymerizations were run. The amount of surfactant, which is directly related to latex stability, was varied in both the cases. In the batch emulsion polymerizations, the effect of the nonionic surfactant (Triton X-100) on latex stability was studied. Moreover, the morphology of coagulum formed in the early stages of BMA emulsion polymerizations was also studied. Blender and turbidity tests were used as means of investigating the mechanical and electrolyte stability of the final latexes. The percent coagulum and the critical coagulation concentration (ccc) were chosen as parameters to represent the mechanical and electrolyte stability of the final latexes. In order to establish the relationship between the conductivity curves and latex stability, the conductivity ratio between the two probes was plotted as a function of the level of latex stability. Finally, the DLVO and extended DLVO theories were studied. The parameters obtained from the experiments were put into the equations to theoretically analyze latex stability.

In Chapter 2, online conductivity measurements, employing a non-reactive system, are described. The non-reactive system means that latex is prepared first, and then changed into a reactor at high temperature and under shear forces to check the stability, so there is no reaction taking place. Latexes at different conversions were used in this system.

For Chapters 3 to 6, investigations using reactive systems are reported. First, a low solids content (5 %) recipe was used in batch BMA emulsion polymerizations. The results, which are presented in Chapter 3, show that the conductivity curves obtained from the resistance and torroidal probes have significant differences. The reason for this is related to the coagulum deposited during the reactions. It is proven that the hypothesis of this research is correct. The solids content was then increased to 20 % (Chapter 4). Some unexpected results were obtained, such as poor repeatability and sensitivity. This was caused by the commercial resistance probe. A homemade probe was built to solve the problems and this probe was used to replace the commercial one. The morphology of coagulum formed in the early stages of the emulsion polymerization is also reported in this chapter. In Chapter 5, seven semi-batch emulsion polymerizations were carried out. All of the reactions had the same seed stage and final solids content (40 %). Different amounts of sodium lauryl sulfate (SLS) were fed in the reactor during the feed stage to provide different latex stabilities. In Chapter 6, mixed surfactants, which are normally used in industries, were employed in batch emulsion polymerizations (20 % solids content). SLS was

used as anionic surfactant and Triton X-100 was chosen as nonionic surfactant. In order to make a comparison with the single surfactant system, the total surfactant concentrations were fixed and the values are the same as the ones used in Chapter 4. The weight ratio between SLS and Triton X-100 was varied for each fixed total surfactant concentration. Reactions using Triton X-100 alone were also run at different concentrations. The surface coverage of each surfactant on the particle surfaces was measured and the contribution of each surfactant to latex stability was estimated. The two conductivity probes were used to measure conductivity during all of the reactions in Chapters 4, 5, and 6. The conductivity curves are similar to the ones shown in Chapter 3. Blender tests and turbidity measurements were used to check the mechanical and electrolyte stability of the latexes prepared by the reactions mentioned in Chapters 3, 4, 5, and 6.

In Chapter 7, the DLVO and extended DLVO theories were studied to obtain a complete view of latex stability. Through the calculations, a limitation of the DLVO theory was found. In order to overcome the limitation, high electrolyte concentrations were used in the equations instead of the original concentrations based on the experimental conditions. The corrected results show good consistency to the experimental results, which proved that the tendency of latex stability obtained from the experiments is correct. Moreover, the theoretical results show the effect of the parameters related to the nonionic surfactants on latex stability. Finally, the conclusions of this research and recommendations are listed in Chapter 8.

1.9 References

[1] R. H. Ottewill, in *Emulsion Polymerization and Emulsion Polymers*, P. A. Lovell and M. S. El-Aasser Ed., John Wiley and Son, Chichester (1997).

[2] D. C. Blackley, in *Polymer Latices*, Chapman and Hall, Volume 1 (1997).

[3] M. J. Perrin, In *Brownian Movement and Molecular Reality*, Taylor and Francis (1910).

[4] M. S. El-Aasser and E. D. Sudol, in *Emulsion Polymerization and Emulsion Polymers*, P. A. Lovell and M. S. El-Aasser Ed., John Wiley and Son, Chichester (1997).

[5] R. G. Gilbert, *Emulsion Polymerization: A Mechanistic Approach*, Academic Press, London (1995).

[6] E. S. Daniels, E. D. Sudol and M. S. El-Aasser, *Polymer Latexes: Preparation, Characterization, and Application*, American Chemical Society Symposium Series, Vol. 492, Washington, DC (1992).

[7] W. D. Harkins, *J. Am. Chem. Soc.*, **69**, 1428 (1947).

[8] W. V. Smith and R. H. Ewart, *J. Chem. Phys.*, **16**, 592 (1948).

[9] W. H. Stockmayer, *J. Polym. Sci.*, **24**, 314 (1957).

[10] B. M. E. Van der Hoff, in *Emulsion Polymerization*, K. Shinoda, Ed., Dekker (1967).

[11] G. Odian, *Principles of Polymerization*, John Wiley and Sons, Inc., New York (1991).

[12] International Organization for Standardization, 35-1989.

[13] International Organization for Standardization, 2006-1985.

[14] M. Fortuny, C. Graillat, and T. F. McKenna, *Ind. Eng. Chem.* Res., **43**, 7210 (2004).

[15] M. S. El-Aasser, in *An Introduction to Polymer Colloids*, F. Candau and R. H. Ottewill Ed., Kluwer, Netherlands (1990).

[16] S. Swarup and C. K. Schoff, *Prog. Org. Coat.*, **23**, 1 (1993).

[17] A. Klein and E. S. Daniels, in *Emulsion Polymerization and Emulsion Polymers*, P. A. Lovell and M. S. El-Aasser Ed., John Wiley and Son, Chichester (1997).

[18] J. Israelachvili, in *Intermolecular and Surface Forces*, Academic Press, London (1992).

[19] F. K. Hansen and J. Ugelstad, in *Emulsion Polymerization*, I. Piirma ed., Academic Press, New York (1982).

[20] F. K. Hansen and J. Ugelstad, *J. Polym. Sci., Polym. Chem. Ed.*, **16**, 1953 (1978).

[21] M. Harada, M. Nomura, H. Kojima, W. Eguchi and S. Nagata, *J. Appl. Polym. Sci.*, **16**, 811 (1972).

[22] J. Ugelstad, P. C. Mork and J. O. Aasen, *J. Polym. Sci., Polym. Chem.*, **5**, 2281 (1967).

[23] W. C. Griffin, *J. Soc. Cosm.Chem.*, **1**, 311 (1949).

[24] A. S. Dunn, in *Emulsion Polymerization*, I. Piirma ed., Academic Press, New York (1982).

[25] D. Colombié, *Ph.D. Dissertation*, Lehigh University (1999).

[26] I. Capek, *Adv. Colloid Interface Sci.*, **99**, 77 (2002).

[27] M. Woods, J. Dodge, I. M. Krieger and R. Pierce, *J. Paint Tech.*, **40 (527)**, 541 (1968).

[28] H. Chu and I. Piirma, *Polym. Bull.*, **24**, 207 (1990).

[29] A. M. Sung and I. Piirma, *Langmuir*, **10**, 1393 (1994).

[30] S. L. Carnie, D. Y. C. Chan, D. J. Mitchell, and B. W. Ninham, *J. Chem. Phys.*, **74**, 1472 (1981).

[31] B. V. Derjaguin and L. Lyklema, *Acta Physicochim,* USSR, **14**, 633 (1941).

[32] E. J. W. Verwey and J. Th. G. Overbeek, *Theory of Stability of Lyophobic Colloids,* Elsevier, Amsterdam (1948).

[33] D. H. Napper, *J. Colloid Interface Sci.*, **58**, 390 (1977).

[34] In *Encyclopaedia Brittanica*, **12**, 257 (1968).

[35] B. Vincent, P. F. Luckham and F. A. Waite, *J. Colloid Interface Sci.*, **73**, 508 (1980).

[36] B. Vincent, J. Edwards, S. Emmett and A. Jones, *Colloid Surf.*, **18**, 261 (1986).

[37] T. S. Light, *Analytical Chemistry*, **56**, 1138 (1984).

[38] A. F. Santos, E. L. Lima, J. C. Pino, C. Graillat and T. Mckenna, *J. Appl. Polym. Sci.*, **90**, 1213 (2003).

[39] A. F. Santos, E. L. Lima, J. C. Pino, C. Graillat and T. Mckenna, *J. Appl. Polym. Sci.*, **91**, 941 (2004).

[40] E. Ortiz Alba, *Ph.D. Dissertation*, Lehigh University (2007).

[41] W. E. Engisch, *M.S. Report*, Lehigh University (2005)**.**

Chapter 2
Online Conductivity Measurements in a Non-Reactive Latex System

2.1 Introduction

In the first part of this research, online conductivity measurements were used to check the conductivity changes in a simple non-reactive system. Non-reactive means that there is no polymerization taking place in a reactor. To achieve this, the latexes were prepared first through bottle polymerizations and then charged into a 2 L reactor at some conditions to check latex stability. Because the only change that can occur in the reactor is coagulation without polymerization, the aim of this series of experiments is to determine the feasibility of predicting coagulum using online conductivity measurements. If the conductivity curves measured by the two conductivity probes show significant differences when coagulum occurs under given experimental conditions, this method can be used to detect latex stability in non-reactive systems, such as in latex storage and shipping.

n-Butyl methacrylate (BMA), a monomer widely used in industry as well as in fundamental studies on film formation[1,2,3], was chosen as the model monomer. This monomer has low water solubility (~ 32mmol/L at 70 °C[4]) and high propagation rate

constant (1243 $dm^3mol^{-1}s^{-1}$ at 70 °C[5]). The recipe used to prepare poly(*n*-butyl methacrylate) (PBMA) latex via bottle emulsion polymerizations was the same recipe used in the seed stage of Hong's research[6]. Because the hardness of PBMA particles, which can be affected by the presence of the BMA monomer, may have an influence on the process of coagulation, latexes having three different conversions (high, intermediate, and low) were used to detect stability and conductivity. The results of these three conversions were used to represent the relationship between the conductivity curves and latex stability in the non-reactive system.

2.2 Experimental

2.2.1 Materials

10 ppm monomethyl ether of hydroquinone (MEHQ) inhibitor was removed from BMA (Sigma-Aldrich) by passing the monomer through an inhibitor-removal column (Sigma-Aldrich). Sodium lauryl sulfate (SLS, Fisher Scientific), sodium bicarbonate ($NaHCO_3$, Sigma-Aldrich), and potassium persulfate ($K_2S_2O_8$, Sigma-Aldrich) were used as surfactant, buffer, and initiator, respectively. Hydroquinone (HQ, Sigma-Aldrich) was used as inhibitor to stop the reactions. All of these chemicals were used as received. Deionized (DI) water was used for all experiments.

2.2.2 Bottle Emulsion Polymerizations of BMA

Bottle polymerizations were run to prepare the PBMA latexes for the tests in

the non-reactive system. Table 2.1 shows the recipe used based on the one developed by Hong[6]. The solids content of this recipe is low (5 %) because this recipe comprised the seed stage in his research. Moreover, the SLS concentration used is 0.6 mM, which is much lower than the CMC of SLS (7.8 mM)[7]. All components were charged into 480 mL bottles and then nitrogen was bubbled into the solution for 15 min in order to remove O_2, which could inhibit the polymerization. The bottle polymerizations were carried out at 70 °C. The reaction was stopped according to the conversion needed by putting the bottles in ice.

Table 2.1: Recipe for the Bottle Polymerization of BMA[6]

Ingredient	Mass
DI water	406 g
BMA	21 g
SLS	0.07 g (0.6 mM)*
KPS	0.21 g (1.9 mM)*
$NaHCO_3$	0.21 g (6.1 mM)*

* Based on the aqueous phase

2.2.3 Characterization

A Nicomp 370 instrument was used to determine the particle size based on dynamic light scattering. The latex was diluted with DI water to obtain the signal corresponding to an average intensity 300 kHz at a sensitivity level of 150. A monochromatic beam of light from a laser is focused onto the dilute suspension of particles and the scattering intensity is measured at some angle θ (90 °) by a detector. The phase and the polarization of the scattered light depend on the position and

orientation of each scatterer. Because particles dispersed in water are in constant Brownian motion, scattered light will result that is spectrally broadened by the Doppler effect[8]. The diffusion coefficient (D) is related to particle diameter (d) through the Stokes-Einstein equation (eq (2.1)).

$$D = \frac{k_B T}{3\pi\eta d} \tag{2.1}$$

where η is the viscosity of the medium, T is the absolute temperature and k_B is the Boltzmann constant.

2.2.4 Latex Stability and Conductivity

Three PBMA latexes with different conversions were used to check stability. First, a latex with high conversion was prepared. The bottle emulsion polymerization of BMA was run for 4 hrs to obtain a fully-converted latex. Ten bottles containing the recipe shown in Table 2.1 were polymerized and the average conversion was 99.4 %, measured by gravimetry. A latex with low conversion was prepared. The bottle polymerization was run for 1 hr. Hydroquinone was added to the latexes to stop the reaction after the bottles were placed in ice. The average conversion of the ten bottles was 8.6 %. Finally, a latex with an intermediate conversion was prepared. Because the reaction rate is relatively fast in the middle of the polymerization, it is hard to control the conversions of the ten bottles over a small range due to the time lag when taking the bottles out of the tumbler and stopping the reaction. Therefore, a latex of 60.0 % conversion was simulated by mixing fully-converted latex with the other components.

864.56 g of the latex (99.4 % conversion) was mixed with 541 g of DI water, 28 g of BMA, 0.093 g of SLS and 0.28 g of $NaHCO_3$.

To carry out latex stability and conductivity tests, the latex was charged into a 2 L reactor without baffles and stirred using a 7 cm diameter Rushton impeller with 6 blades, which can provide high shear. Both the resistance and torroidal probes were used to measure conductivity during the experiments. The reactor was covered using aluminum foil to minimize evaporation as the torroidal probe could not be readily mounted on a conventional reactor kettle lid. The temperature of the water bath was set at 70 °C. The agitation rate was 170 rpm. For the latex with the stimulated 60 % conversion, the agitation rate was also increased to 400 rpm to generate larger shear forces.

2.3 Results and Discussion

2.3.1 Latex with High Conversion

The fully converted latex (99.4 %) was used to check stability at 70 °C and 170 rpm for 200 minutes. The average particle diameter (D_v) was 269 nm. Figure 2.1 shows the results. It can be seen that the conductivity curves obtained from the resistance and torroidal probes overlap, which indicates that the resistance probe shows the correct results as given by the torroidal probe. This demonstrates that there is no plating on the surfaces of the electrodes of the resistance probe during the test. The conductivity curves show a slight increase with time. This is caused by the

evaporation of water during this test because the reactor is not perfectly sealed and only covered using aluminum foil. On the other hand, some coagulum was found on the surfaces of the reactor and the conductivity probes after this test, which indicates that the latex has some degree of instability. Because the conductivity curves do not show any significant changes when coagulum is formed, this shows that the online conductivity measurements cannot be used as sensors to predict latex stability in the non-reactive system. The reason is unknown so far. It may be caused by the system. Because no polymerization reaction is occurring in the reactor, the coagulum formed under the high temperature and shear forces prefers to adsorb onto the other surfaces instead of the electrodes of the resistance probe, which is made of platinum. Moreover, the coagulation rate is slow and the level of coagulum is low. The surface area of the electrodes is small and the electrodes are built inside of the grass holder in the resistance probe. Therefore, the sensitivity of the resistance probe may not be good enough to detect such low level of coagulum. This may be another reason why the online conductivity measurements do not work as expected.

2.3.2 Latex with Low Conversion

The latex with a low conversion (8.6 %) was tested. The average particle diameter (D_v) was 124 nm. The results are shown in Figure 2.2. Similar to the results shown in Figure 2.1, the conductivity curves obtained from the two conductivity probes overlap. Moreover, no visible coagulum was found on the surfaces of the reactor and the conductivity probes, which means that the latex is stable under the

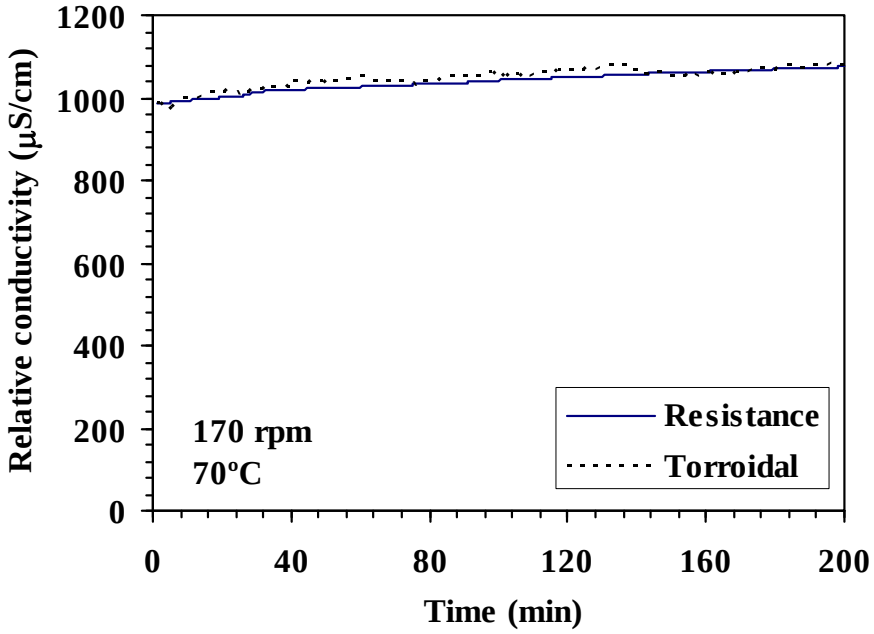

Figure 2.1: *Relative conductivity vs time curves for the PBMA latex with high conversion (99.4 %) (top) and coagulum formed on the surfaces of the reactor and conductivity probes (bottom) in the non-reactive system at 70 °C and 170 rpm.*

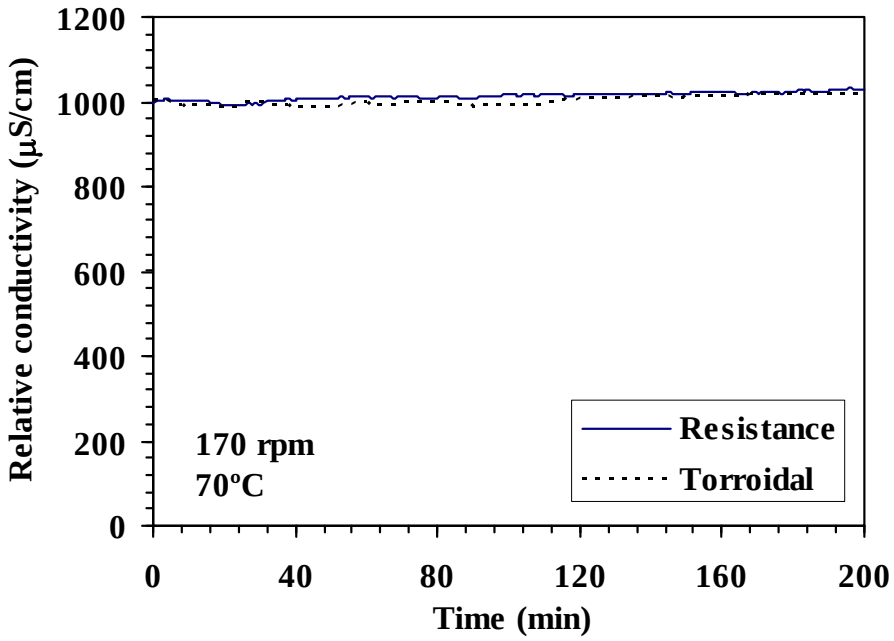

Figure 2.2: *Relative conductivity vs time curves for the PBMA latex with low conversion (8.6 %) in the non-reactive system at 70 °C and 170 rpm.*

experimental conditions. This may be caused by the low conversion and small particle size. Since this latex is stable, no instability can be detected in this case.

2.3.3 Latex with Intermediate Conversion

When the polymer particles are swollen with the monomer, the particles will become soft. Compared with hard particles, the soft particles are sticky and easy to coagulate, which means the latex may be not stable under these conditions. Because the particles are highly swollen by the monomer in the middle of the emulsion polymerization, the stability of the latex of intermediate conversion needs to be checked. The conversion of the simulated latex was 60 %. First, this latex was tested at 70 °C and 170 rpm. The conductivity results are shown in Figure 2.3. No major difference between the two conductivity curves was found. On the other hand, some coagulum was observed as in the pictures shown in Figure 2.1. The agitation rate was increased to 400 rpm to enhance the shear forces. However, the two conductivity curves shown in Figure 2.3 did not have any significant changes compared with the previous results. Therefore, in both of the two cases, the online conductivity measurements cannot be used to predict latex stability.

From the results above, one conclusion can be made: the conductivity curves obtained from the two conductivity probes did not show differences, even though some coagulum was formed in the non-reactive system. This indicated that the online conductivity measurements do not work in this system.

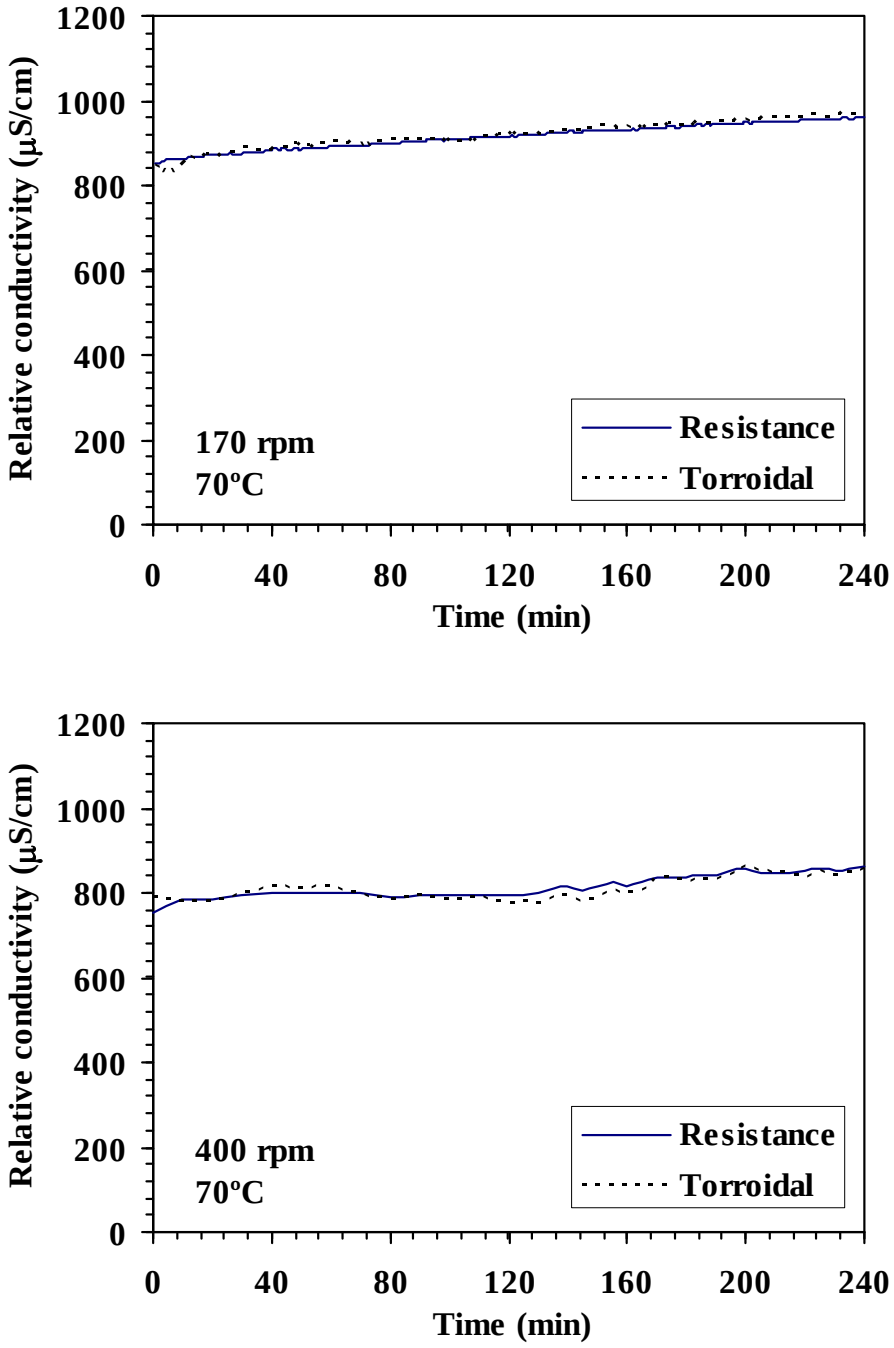

Figure 2.3: *Relative conductivity vs time curves for the PBMA latex with a simulated 60 % conversion in the non-reactive system using the agitation rate of 170 rpm (top) and 400 rpm (bottom) at 70 °C.*

2.4 Conclusions

The investigation of latex stability and conductivity in non-reactive systems was carried out for latexes with three different conversions. When the latexes having high (99.4 %) and intermediate (60.0 %) conversions were used, some coagulum was found on the surfaces of the reactor, the shaft, and the conductivity probes after the experiments, but the conductivity curves obtained from the two conductivity probes did not show any significant differences. When the latex having a low conversion (8.6 %) was used, no coagulum was observed after the test and the conductivity curves did not show any differences. These results indicated that there was no obvious relationship between the conductivity curves and latex stability in the non-reactive system. Therefore, the online conductivity measurements cannot be used as a tool to predict latex stability if there is no polymerization reaction occurring in the system.

2.5 References

[1] Y. Yang, A. Kats, D. Juhue, M. Winnik, R. R. Shivers and C. Dinsdale, *Langmuir*, **8**, 1435 (1992).

[2] J. C. Padget and P. J. Moreland, *J. Coat. Tech.*, **55**, 39 (1983).

[3] B. J. Roulstone, M. C. Wilkinson, J. Hearn and A. J. Wilson, *Polym. Int.*, **24**, 87 (1991).

[4] J. M. Geurts, P. E. Jacobs, J. G. Muijs, S. J. J. G. Van Es and A. L. German, *J. Appl. Polym. Sci.*, **61**, 9 (1996).

[5] S. Beuermann, M. Buback, T. P. Davis, R. G. Gilbert, R. A. Hutchinson, A. Kajiwara and B. Klumperman, *Macromol Chem. Phys.*, **201**, 1355 (2000).

[6] J. Hong, *Ph.D. Dissertation*, Lehigh University (2008).

[7] A. J. Back and F. J. Schork, *J. Appl. Polym. Sci.*, **102**, 5649 (2006).

[8] E. A. Collins, in *Emulsion Polymerization and Emulsion Polymers*, P. A. Lovell and M. S. El-Aasser, Ed., John Wiley and Son, Chichester (1997).

Chapter 3
Online Conductivity Measurements in Batch Emulsion Polymerization of BMA at Low (5 %) Solids Content

3.1 Introduction

As shown in Chapter 2, conductivity probes cannot be used as online sensors to predict latex stability in a non-reactive system. In this chapter, this method was applied in the batch emulsion polymerizations of BMA. The purpose of this research is to investigate the feasibility of monitoring latex stability through online conductivity measurements in a reactive system. In addition, a blender test and turbidity measurements were used as the means to determine the mechanical and electrolyte stability of the final latexes prepared by batch emulsion polymerization of BMA. The percent coagulum obtained after the blender test and the critical coagulation concentration (ccc) calculated based on turbidity measurements were used as the parameters representing the degree of latex stability. Moreover, the degree of latex stability was correlated to the conductivity curves obtained during the batch emulsion polymerization processes to establish the relationship between them.

Because coagulum formed during the seed stage can change the average

particle size, the number of particles, and other properties of the latexes, the latex stability during the seed stage is important and can affect the quality of the final latexes. Therefore, latexes with low solids content were chosen as the first emulsion polymerization system to investigate latex stability. The first recipe used for the batch emulsion polymerization is again based on Hong's research[1]. Hong used this recipe as the seed stage in his semi-batch reactions, so the solids content is low (5 %). However, he reported that the latex was not stable at the end of the seed stage and some coagulum was observed on the surfaces of the reactor and stirrer shaft. Based on his results, it can be seen that the latex can become unstable even at a low solids content. After the first reaction was carried out, some interesting results were obtained, which showed that there may be some relationship between latex stability and the conductivity curves. The SLS concentration in the recipe was then increased to vary the latex stability and investigate the conductivity changes.

3.2 Experimental

3.2.1 Materials

10 ppm monomethyl ether of hydroquinone (MEHQ) inhibitor was removed from BMA (Sigma-Aldrich) by passing the monomer through an inhibitor-removal column (Sigma-Aldrich). Sodium lauryl sulfate (SLS, Fisher Scientific), sodium bicarbonate ($NaHCO_3$, Sigma-Aldrich), and potassium persulfate ($K_2S_2O_8$, Sigma-Aldrich) were used as surfactant, buffer, and initiator, respectively. All of these chemicals were used as received. Deionized (DI) water was used for all experiments.

3.2.2 Batch Emulsion Polymerizations of BMA

Four batch emulsion polymerizations of BMA were run to investigate the changes in conductivity during the polymerization process. Since the surfactant concentration can affect latex stability, the SLS concentration was varied in each reaction (Table 3.1) while the amounts of the other components were the same. In the reaction labeled B-5%-0.6mM (B stands for batch emulsion polymerization, 5% stands for the solids content, and 0.6mM stands for the SLS concentration), the SLS concentration was 0.6 mM, which was much lower than the CMC of SLS. The SLS concentration was increased in the following reactions. In the reaction B-5%-7.8mM, the SLS concentration was 7.8 mM, which is around the CMC of SLS. Moreover, this concentration was relatively high for a recipe of low solids content. All reactions were run in a 1 L reactor without baffles at 70 ^{o}C and stirred at 250 rpm using a 7 cm diameter Rushton impeller with 6 blades. Both the commercial resistance and torroidal probes were used to measure conductivity during the polymerizations. The setup of the reactor lid is shown in Figure 3.1. The resistance probe was inserted into the reactor through a long glass tube because the commercial probe is not long enough. The torroidal probe was mounted in one of the necks on the lid and fixed there due to the size of the head of this probe. The reactor was flushed with nitrogen through a needle during the polymerizations to prevent O_2 inhibition. $K_2S_2O_8$ was used as initiator and an aqueous solution was added to the reactor to begin the polymerization. The reactions were run for 90 min. The conductivity values measured by the two probes were recorded every minute for the first 10 minutes of each reaction, and then

were recorded every 5 minutes. Samples were taken at periodic intervals through a plastic tubing to measure the conversion by gravimetry. The particle size was measured using Nicomp 370 instrument based on dynamic light scattering.

Table 3.1: Recipes Used for the Batch Emulsion Polymerizations of BMA

Ingredient	**B-5%-0.6mM***	**B-5%-1.2mM**	**B-5%-2.4mM**	**B-5%-7.8mM**
DI water	725 g			
BMA	37.5 g			
SLS	0.125 g (0.6 mM)**	0.250 g (1.2 mM)	0.500 g (2.4 mM)	1.625 g (7.8 mM)
$K_2S_2O_8$	0.375 g (1.9 mM)			
$NaHCO_3$	0.375 g (6.1 mM)			

***** In the notation "B-5%-0.6mM", B stands for batch emulsion polymerization, 5% stands for the solids content, and 0.6mM stands for the SLS concentration.

** Concentration based on water phase

3.2.3 Blender Tests

A standard test used to determine the mechanical stability of a latex is given in American Standard Test Methods (ASTM)[2] (D1417-03D): "A sample of latex is subjected to mechanical shear by the use of a high-speed stirrer. The amount of coagulum formed after a given time of agitation is considered a measure of latex stability". Based on this principle, a blender test was used to analyze the mechanical stability of various latex samples. A Hamilton Beach Blender was used to run this test. The rotational speed was around 8000 rpm at the highest setting. 200 g of the latex

sample was directly used for this test without any dilution. At the beginning of the blender test, the temperature of the latex was 25 ^{o}C. After 20 minutes of the blender test, the temperature rose to 60 ^{o}C. According to the ASTM (D1417-03D)[2], the temperature should not exceed 60 ^{o}C, so it was reasonable to run the blender test for 20 minutes. During this process, a great deal of foam was formed, so the blender was stopped every 5 min in order to take a sample from the liquid phase present at the bottom of the blender. After the experiment was stopped, a 100 μm mesh was used to filter the coagulum out of the latex. DI water was used to wash the foam and the blender during the filtration. The mesh holding the coagulum was placed in an oven (90 ^{o}C) for 24 h to dry and remove entrapped water, and the weight of the coagulum was measured. Moreover, the solids content of each sample obtained during the test was measured. The percent coagulum of these samples was calculated based on the solids content of the sample before and after the blender test.

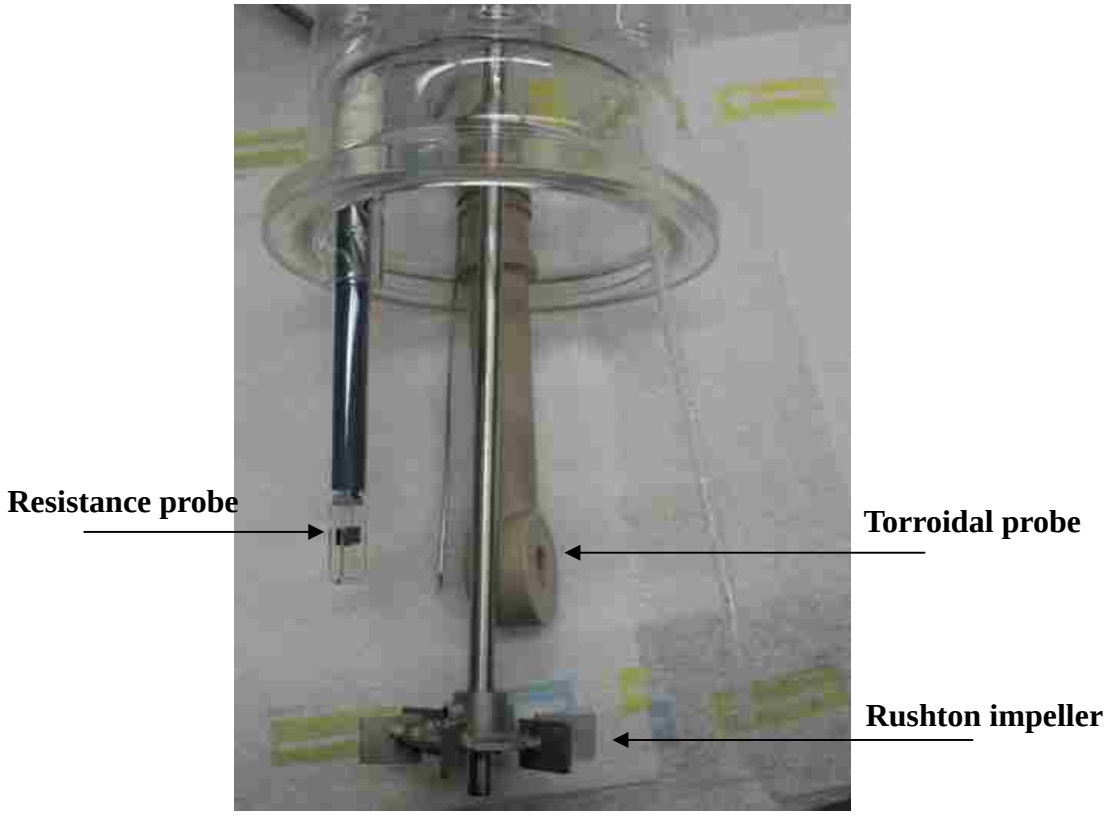

Figure 3.1: *The setup of the 1 L reactor lid.*

3.2.4 Turbidity Measurements

The electrolyte stability of latex was evaluated using turbidity measurements, where the kinetics of coagulation was followed by the measurement of the slope of the optical density (OD) vs. time curve. All measurements were performed at a constant temperature, which was around 25 °C. The OD was measured using a Shimadzu UV-2101PC Spectrophotometer set at a wavelength of 600 nm. All latex samples were diluted to 0.13 wt % before the measurement. 1 mL of the diluted sample was charged into both the reference and sample cells. Different volumes of 4 M KCl solution were added to the sample cell and the OD was recorded automatically after quick shaking. The stability ratio (W) is defined as the ratio of the rate of rapid to slow coagulation processes and is calculated using eqn (3.1).

$$W = \frac{(d\tau / dt)_{0,C_E > ccc}}{(d\tau / dt)_{0,C_E}} \tag{3.1}$$

where τ is the optical density and C_E is the electrolyte concentration. If the electrolyte concentration is higher than the ccc, the electrostatic repulsive forces between two particles are completely canceled and rapid coagulation occurs as a result of Brownian motion. In this case, W = 1 and log(W) = 0. On the other hand, if the electrolyte concentration is below this point, coagulation is slow. In this case, W > 1 and log(W) > 0. Therefore, the ccc can be estimated from the log(W) vs. log(C_E) curve.

3.2.5 Surface Coverage

Fractional surface coverage (θ), which represents the degree of surface

saturation of surfactant on a polymer particle, is an important factor which affects latex stability. The surface coverage of the PBMA particles with the adsorption of SLS molecules was calculated as followings. First, the serum of a latex sample was obtained using a serum replacement cell and the surface tension of the serum was measured with a Du Nouy ring. The free SLS concentration ($[SLS]_{free}$) in the aqueous phase could be calculated using a calibration curve (surface tension vs. SLS concentration). Then, the amount of SLS adsorbed on the surfaces of the latex particles ($[SLS]_p$) could be calculated based on a mass balance using eqn (3.2).

$$[SLS]_p = [SLS]_{total} - [SLS]_{free} \tag{3.2}$$

where $[SLS]_{total}$ is the total SLS concentration which was calculated from the recipe. Second, the particle number, N_p (no. per dm^3 water), and the total surface area of the particles, A_p ($Å^2$), were calculated using eqns (3.3) and (3.4).

$$N_p = \left(\frac{mx}{w}\right)\left(\frac{\rho_w}{\rho_P}\right)\left(\frac{N}{\pi D_V{}^3}\right) \tag{3.3}$$

$$A_p = N_p \pi D_S{}^2 \tag{3.4}$$

where m (g) is the mass of monomer in the recipe, x is the gravimetric conversion, w (g) is the mass of water in the recipe, ρ_w (g/cm^3) is the density of water, ρ_p (g/cm^3) is the density of polymer, and N is Avogadro's number (6.023×10^{23}). D_V and D_S are the volume-average and surface-average particle diameters, respectively. Third, the packing area (the area occupied by one surfactant molecule at a saturated monolayer on particle surface), a ($Å^2$/molecule) was calculated by eqn (3.5).

$$a = \frac{N_p A_p}{[SLS]_p N} \tag{3.5}$$

Finally, the area covered per surfactant molecule at surface saturation, a_s (Å^2/molecule) which was around 54 Å^2/molecule in the PBMA-SLS system[3,4], was used to calculate the fractional surface coverage through eqn (3.6).

$$\theta = \frac{a_s}{a} \tag{3.6}$$

3.3 Results and Discussion

3.3.1 Batch Emulsion Polymerizations of BMA

Four batch emulsion polymerizations were carried out using the recipes shown in Table 3.1. The particle sizes of these four latexes are shown in Table 3.2. As expected, the particle size becomes smaller as the surfactant concentration increases. The particle size of latex B-5%-7.8mM is much smaller than the others. This is caused by the relatively high SLS concentration used in this recipe compared with the other recipes. Moreover, the particle size distribution (PDI) is narrow, because the SLS concentrations are lower than the CMC of SLS in the first three recipes, which enable homogeneous nucleation to take place, which often leads to narrow PDI. In the last recipe, the SLS concentration is around the CMC. The number of the micelles is low and homogeneous nucleation may still dominate the nucleation phase compared with micellar nucleation, so the particle size distribution is narrow.

The fractional conversion vs. time curves for the four reactions are compared in Figure 3.2. It can be seen that the higher was the SLS concentration, the faster was the

reaction rate. Especially for reaction B-5%-7.8mM, the reaction rate was very fast and the reaction was finished in 10 minutes because of the high SLS concentration. The first three reactions were completed at 45, 40, and 30 minutes, respectively.

No coagulum was found in any of the latexes. The weight of coagulum adsorbed on the surfaces of the impeller and reactor was measured after each reaction. The coagulum weights were 0.79, 0.49, 0.34, and 0.01 g, respectively. The highest level of coagulum was 2 %, which meant that the coagulum could be considered negligible. These results show that the degree of coagulum was low and all of the four batch emulsion polymerizations could be considered as successful reactions.

Table 3.2: Particle Size* Obtained from the Batch Emulsion Polymerizations (5 % Solids Content) of BMA

	D_n (nm)	D_V (nm)	D_I (nm)	PDI
B-5%-0.6mM	205	214	218	1.06
B-5%-1.2mM	184	186	187	1.02
B-5%-2.4mM	159	160	161	1.01
B-5%-7.8mM	73	75	77	1.05

* DLS, Nicomp 370

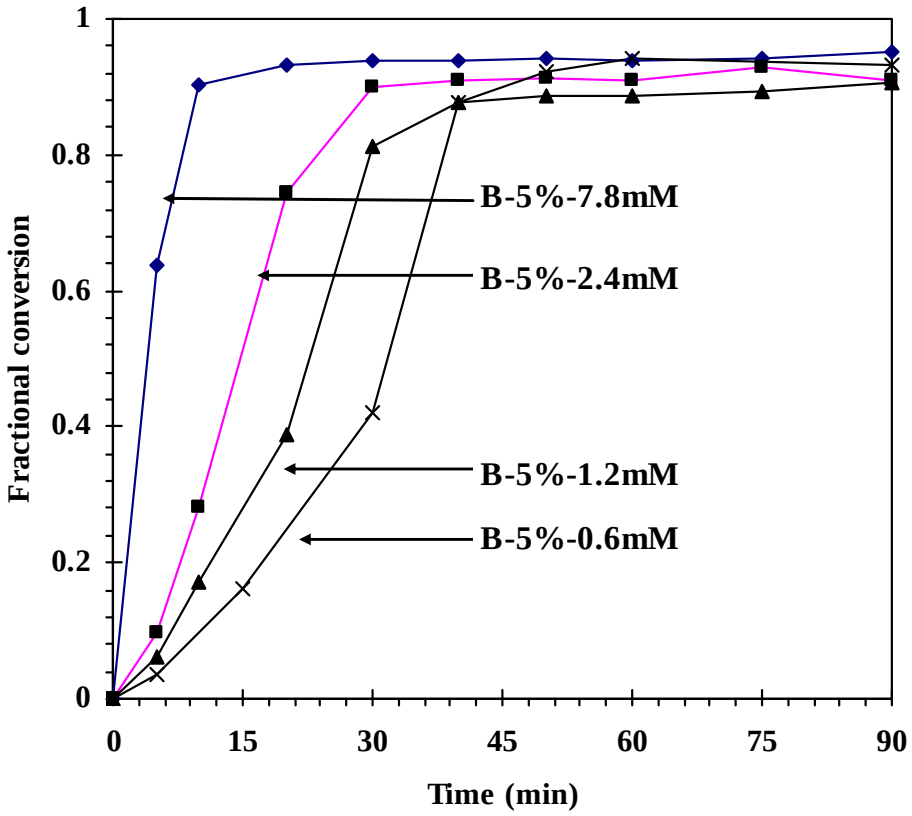

Figure 3.2: *Fractional conversion vs. time curves for the batch emulsion polymerizations of BMA shown in Table 3.1 at 70* °C *and 250 rpm.*

3.3.2 Online Conductivity Measurements

Figure 3.3 shows the fractional conversion and relative conductivity curves for reaction B-5%-0.6mM. At the very beginning of the reaction, the conductivity values measured by the resistance and torroidal probes rose after the addition of initiator (KPS), an electrolyte. However, the values obtained from the two probes showed significant divergence after this initial rise in conductivity. The conductivity values obtained from the torroidal probe appeared almost constant after 5 minutes. On the other hand, the conductivity values measured by the resistance probe decreased dramatically after 3 minutes. This phenomenon did not occur previously when the conductivity was measured using the two probes in the non-reactive system (Chapter 2), so it should be related to the emulsion polymerization processes. Between 10 and 45 minutes, the values of the resistance probe became almost constant. After 45 minutes, the values slightly increased and then became constant. From the relative conductivity curves, it can be seen that the conductivity values obtained from the two probes are not the same during the reaction. This is caused by some plating (adsorbed coagulum) on the surfaces of the electrodes of the resistance probe (Figure 3.3). Thus, the actual conductivity values measured by the resistance probe were smaller than the true values during this time period. This indicates that the difference in conductivity values obtained from the two probes might be used to predict latex stability in the reactive emulsion polymerization system.

The resistance probe was rinsed and dried in air after the reaction. The

conductivity of a standard sodium chloride solution was measured using this resistance probe. The measured value was 132 μS/cm, while the standard value was 987 μS/cm. The resistance probe was then cleaned using toluene, acetone, and DI water. After cleaning, the resistance probe was again used to measure the standard solution and the measured value became normal. These results prove that the plating on the surfaces of the resistance probe decreased the measured conductivity values during the reaction.

The relative conductivity profiles of reactions B-5%-1.2mM, B-5%-2.4mM, and B-5%-7.8mM are shown in Figures 3.4, 3.5, and 3.6, respectively. Divergence between the two conductivity curves occurred in reactions B-5%-1.2mM and B-5%-2.4mM. On the other hand, the two conductivity curves did not diverge and almost overlapped for reaction B-5%-7.8mM. This may be caused by the relatively high SLS concentration, which is much higher than in the other reactions. It is well known that latex stability can be improved by the increase in the surfactant concentration. During this reaction, the polymer particles may be stabilized well enough that no plating occurred, so the resistance probe correctly measured conductivity and the two conductivity curves were similar during the period of this reaction. Therefore, these results prove that the SLS concentration can affect latex stability as well as the shapes of the conductivity curves, which indicates that there may be some relationship between latex stability and the conductivity curves.

The shapes of the relative conductivity curves obtained by the torroidal probe in these three reactions were very similar to the one in reaction B-5%-0.6mM (Figure 3.3). However, the shapes of the relative conductivity curves obtained by the resistance probe are significantly different for each reaction and the four curves are plotted together for a comparison (Figure 3.7). The curves of the first three reactions exhibited sharps decrease at 3, 5, and 10 minutes, and the conversions at these times were 2, 6, and 28 %, respectively. This indicates that the time to reach the sharp decrease is delayed and the conversion becomes higher because of the increase in the SLS concentration. It can also be seen that as the SLS concentration increases, the final conductivity value measured by the resistance probe increases. As shown in eqns (1.4), (1.5), and (1.6), if the conductance of the solution and the distance between the two electrodes do not change, the measurement of the resistance probe is proportional to the surface area of the electrodes. The ratio of the measured conductivity value to the true value can be used to represent the degree of the coverage by plating on the surfaces of the electrodes. Because plating does not affect the measurements of the torroidal probe, the measured conductivity value by the torroidal probe can be seen to give true conductivity values. Therefore, the final conductivity ratio (R/T) can be defined as the ratio between the final conductivity values obtained by the two probes (the values circled in Figure 3.3) as shown in eqn (3.7).

$$\frac{R}{T} = \frac{\text{Final conductivity value measured by the resistance probe}}{\text{Final conductivity value measured by the torroidal probe}} \tag{3.7}$$

If there is no plating on the surfaces of the electrodes, the measured conductivity

values obtained by the two probes should theoretically be the same and R/T would have a maximum value, which would equal 1; if the surfaces of the electrodes are fully covered by adsorbed coagulum, the R/T would have a minimum value, which is equal to 0. Because the degree of plating formed during the reactions may be related to latex stability, R/T can be used as a parameter to correlate the conductivity curves to latex stability in the following discussion.

From Figure 3.7, one phenomenon can also be seen. There is a slight increase in the conductivity curves obtained by the resistance probe in the middle of the reactions, which is named as the second increase. The exact reason for this phenomenon is not clearly known. Some details and discussion about the second increase will be presented in the next chapter.

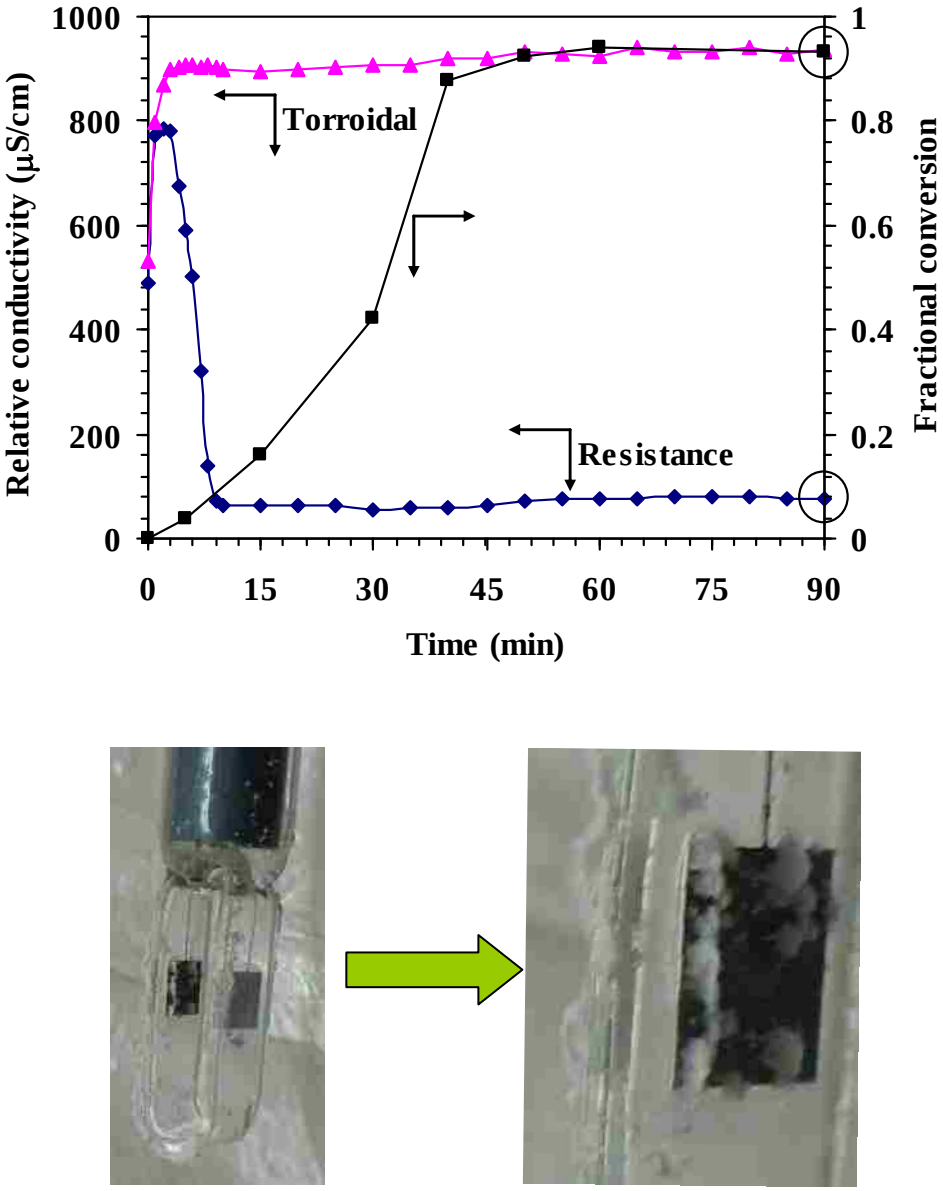

Figure 3.3: *Relative conductivity and fractional conversion vs. time curves for reaction B-5%-0.6mM (Table 3.1) at 70 °C and 250 rpm (top); photograph of the resistance probe with plating on the surface of the electrodes (bottom).*

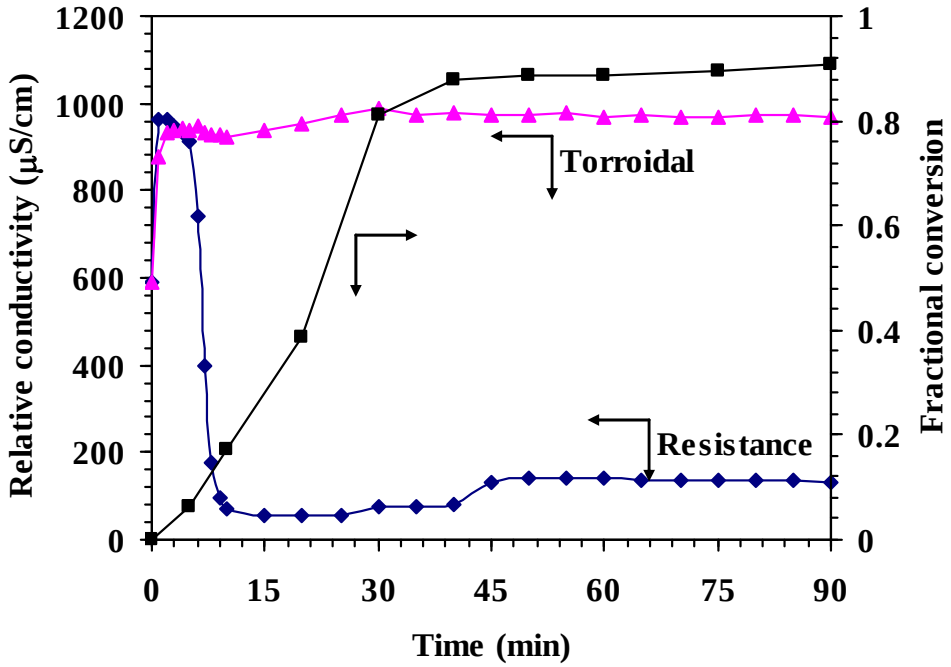

Figure 3.4: *Relative conductivity and fractional conversion vs. time curves for reaction B-5%-1.2mM (Table 3.1) at 70 °C and 250 rpm.*

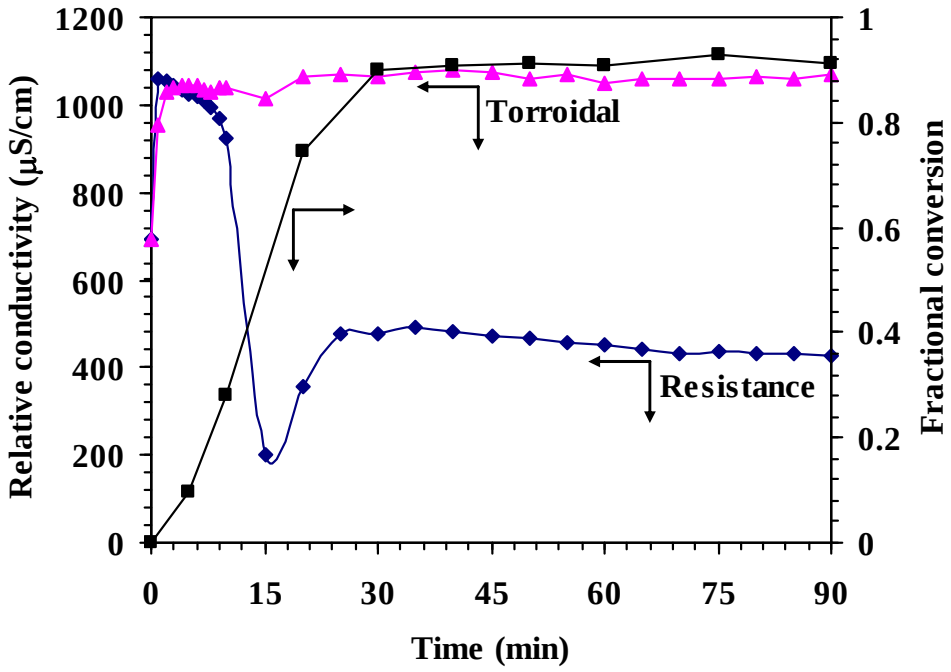

Figure 3.5: *Relative conductivity and fractional conversion vs. time curves for reaction B-5%-2.4mM (Table 3.1) at 70 °C and 250 rpm.*

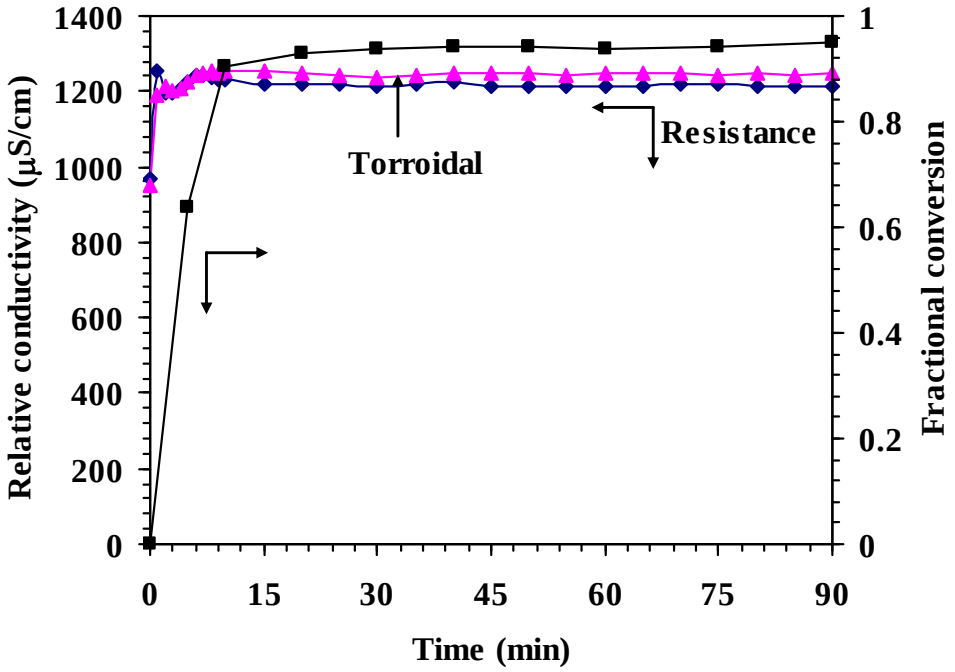

Figure 3.6: *Relative conductivity and fractional conversion vs. time curves for reaction B-5%-7.8mM (Table 3.1) at 70 °C and 250 rpm.*

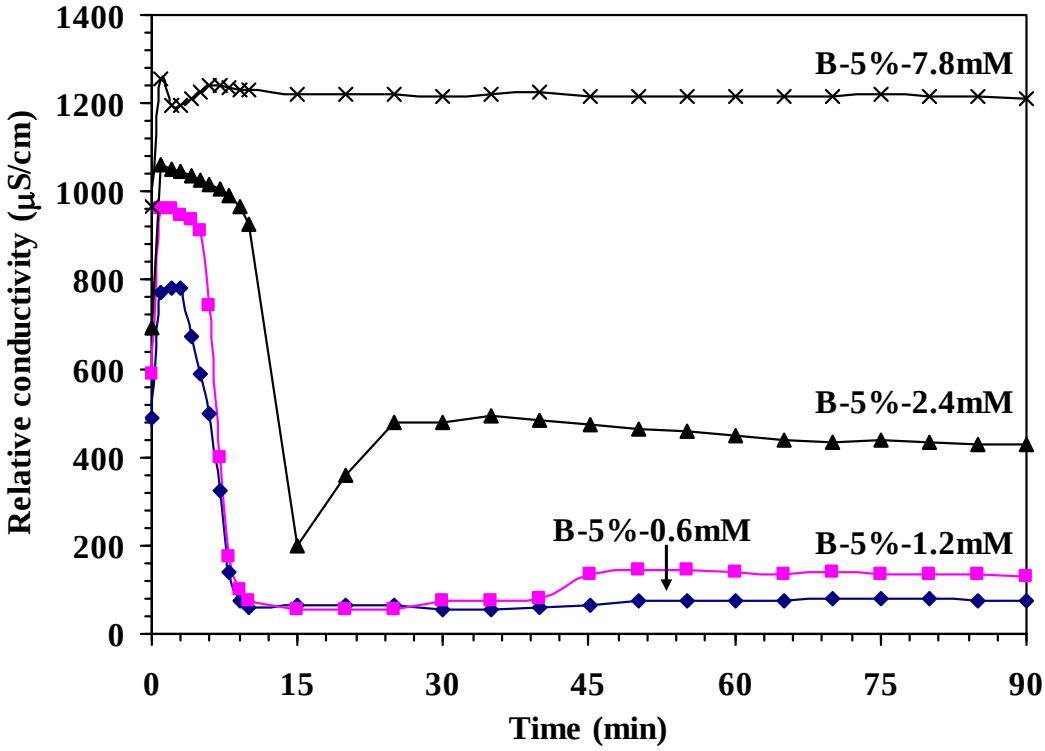

Figure 3.7: *Comparison of relative conductivity obtained by the resistance probe vs. time curves for the four reactions (Table 3.1).*

3.3.3 Blender Tests

Figure 3.8 shows a photograph of the latex samples removed from the bottom of the blender container during the blender test of latex B-5%-0.6mM. Because polymer particles were dispersed in the water phase, the original latex was white. However, in this picture, it can be seen that the samples become clearer as time passes. Especially in samples 3 and 4 (taken at 15 and 20 min), the samples contain almost no polymer particles, so they are transparent. This picture illustrates that the latex becomes unstable and that coagulum is formed during this test. Obviously, the latexes with greater stability should have higher solids content in the samples and less coagulum after this test.

The solids contents of these samples taken during the blender test were measured and the percent coagulum was calculated based on a mass balance. The results are shown in Figure 3.8. From this figure, it can be seen that the percent coagulum of each latex increased with time. Moreover, by comparing the curves of the four latexes, the degree of their stability can be compared. Latex B-5%-0.6mM had poor stability and lost almost all solids during the blender test. Latexes B-5%-1.2mM and B-5%-2.4mM had better stability compared with the first one, but they were still unstable. Latex B-5%-7.8mM was stable and only lost a slight amount of solids content during the 20 minutes. These results show that the four latexes have different degrees of stability, even though they were prepared by successful batch emulsion polymerizations.

5 min 10 min 15 min 20 min

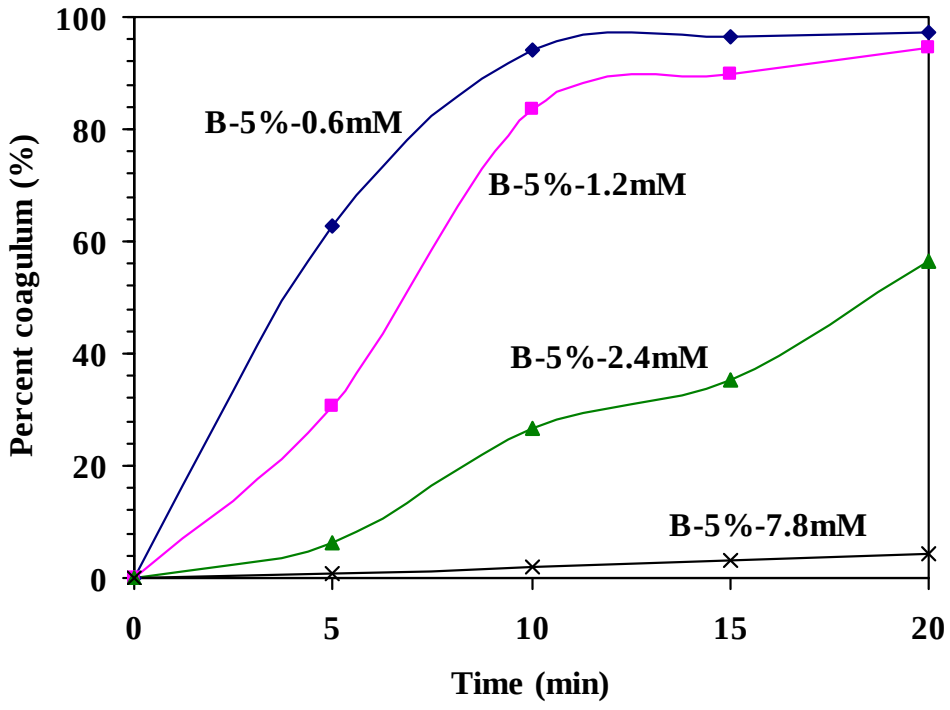

Figure 3.8: *Photograph of the latex samples (B-5%-0.6mM) after shearing in the blender for varying amounts of time (top) and percent coagulum vs. time curves for the four latex samples (bottom).*

To calculate the surface coverage, the SLS concentration in the serum needs to be measured. A calibration curve was generated (Figure 3.9) to achieve this. From this curve, it can be seen that there is a parabolic relationship between the surface tension and SLS concentration before reaching the CMC point (as the arrow indicator), where the curve shows a plateau. The surface coverage of these latexes was calculated following the procedure discussed previously. The surface coverages of these four latexes were 0.8, 1.1, 6.7, and 41.9 %, respectively. The adsorbed SLS molecules generate the electrostatic forces to stabilize the polymer particles, so the particles with higher surface coverage exhibit better stability. The results of the surface coverage explain why these latexes exhibit different stabilities during the blender test.

The final conductivity ratio between the two probes (R/T) is correlated to latex stability. Percent coagulum and surface coverage vs. R/T curves are plotted in Figure 3.10. The results show that there is a linear relationship between them, which means that the percent coagulum can be determined using the R/T value at the end of the emulsion polymerization without running the blender test. The results also indicate that the online conductivity measurements can be used to predict the mechanical stability of the latexes in this system, which is obviously different from the non-reactive system.

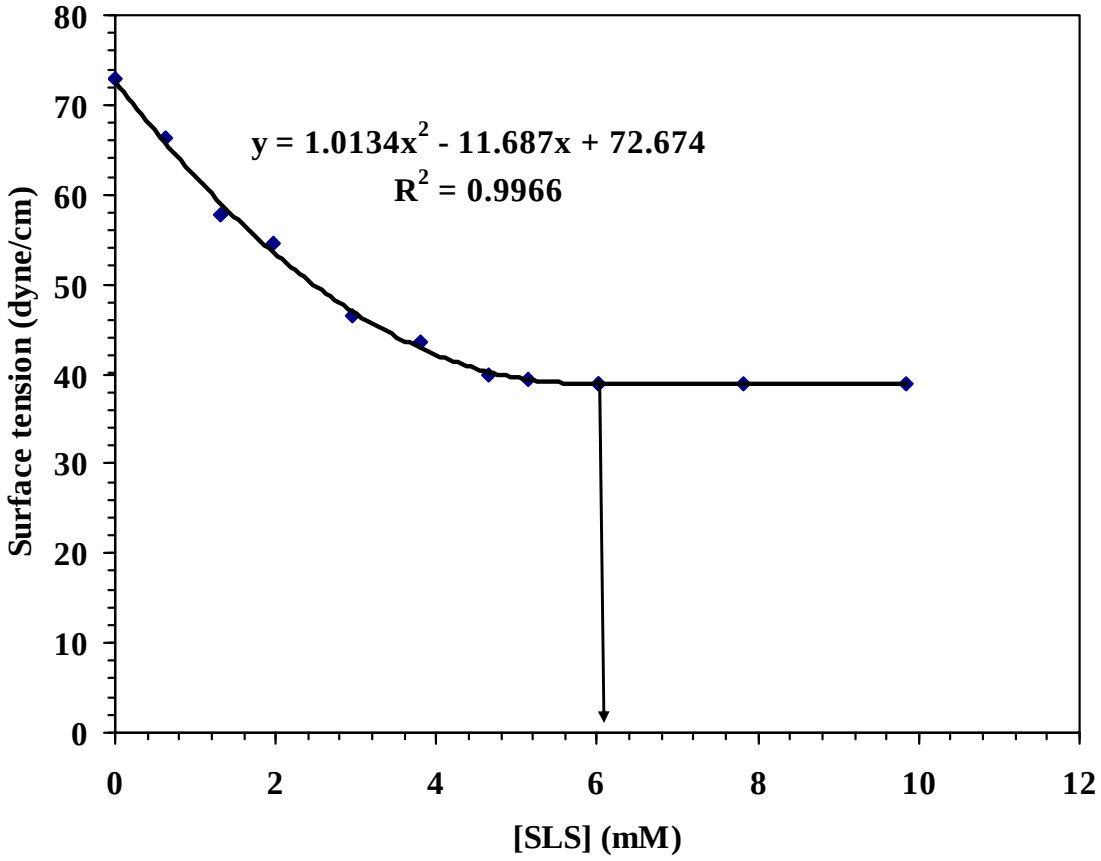

Figure 3.9: *Surface tension profile as a function of the SLS concentration.*

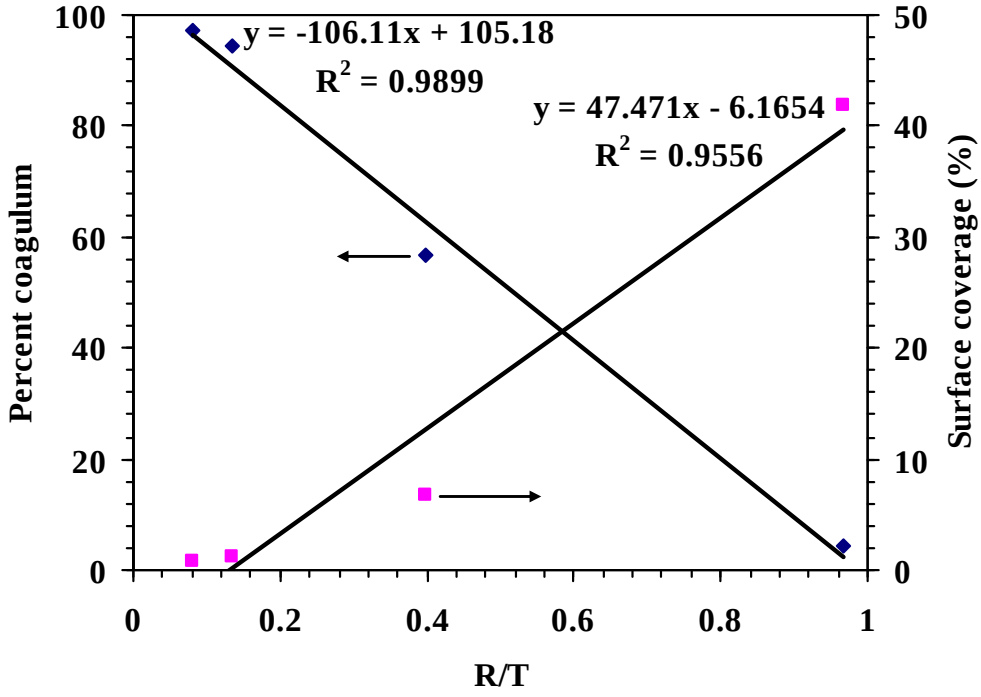

Figure 3.10: *Correlation between the percent coagulum obtained after the blender test and the final conductivity ratio (R/T), and the surface coverage and R/T.*

3.3.4 Turbidity Measurements

The critical coagulation concentration (ccc) of these four latexes was estimated using the turbidity measurements. This calculation is illustrated taking latex B-5%-0.6mM as an example. The results are shown in Figure 3.11. The top figure shows the changes of the optical density (OD) with time. The first recorded data point was taken at four seconds, since it took approximately three seconds to add the electrolyte to the latex and mix it before an OD measurement could be recorded. In some cases, the coagulation rate was too fast to monitor due to the high electrolyte concentration, so the curves were not straight lines. Under these conditions, the first point was used to estimate the initial slope of this line. Among these curves, the first five electrolyte concentrations exhibited slow coagulation and the last two points caused fast coagulation, which can be judged from the slopes. The stability ratio, W, was then calculated using eqn (3.1) and plotted against the added electrolyte concentration (C_E) in Figure 3.11 (bottom). The ccc value can be obtained at the intersection point.

The ccc of these latexes is 0.445, 0.531, 0.581, and 0.682 M, respectively. The correlation between the ccc and R/T is shown in Figure 3.12. The results show that there is a linear relationship, which means that the online conductivity measurements can be used as a tool to predict the electrolyte stability of the latexes in this system.

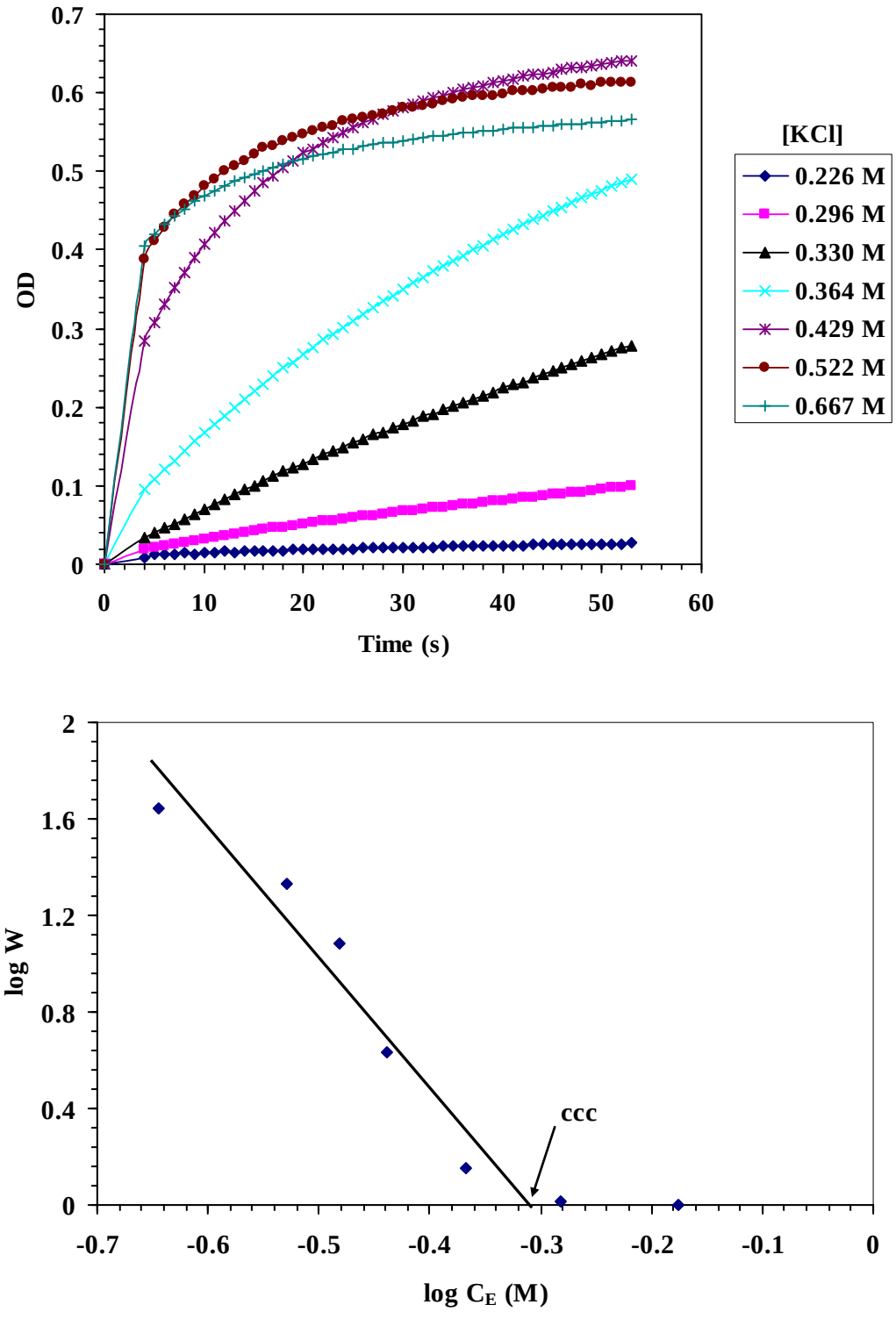

Figure 3.11: *Optical density (OD) vs. time curves in the turbidity measurements (top) and log W vs. log C_E curve to estimate the ccc (bottom).*

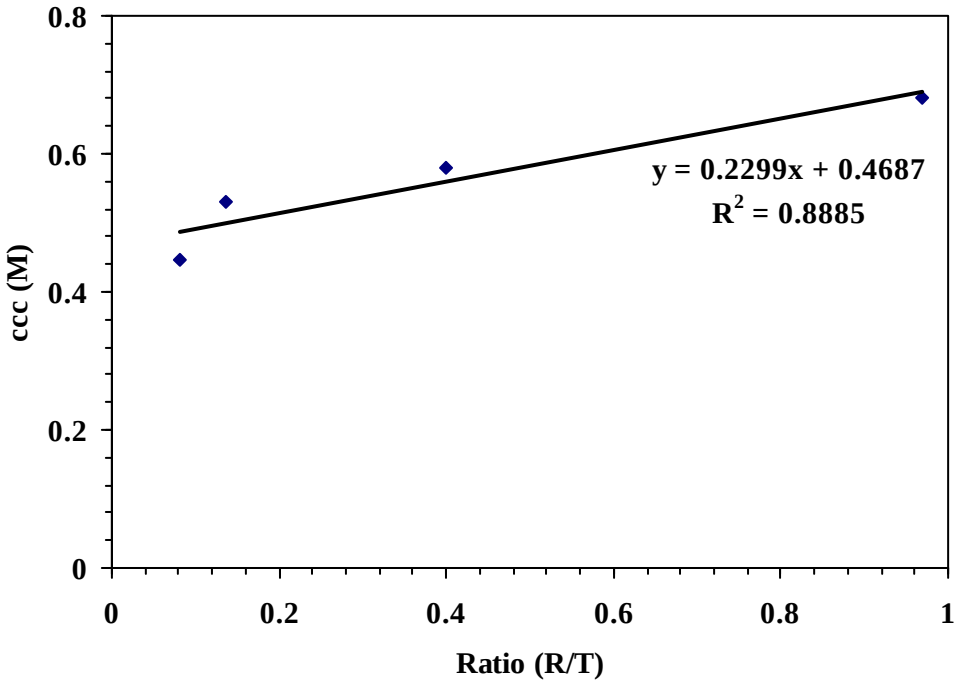

Figure 3.12: *Correlation between the critical coagulum concentration (ccc) estimated by the turbidity measurements and the final conductivity ratio (R/T).*

3.4 Conclusions

Conductivity was monitored using a resistance and torroidal probes during the batch emulsion polymerizations (5 % solids content) of BMA. Four reactions were carried out using different SLS concentrations. The relative conductivity curves obtained from the torroidal probe showed similar shapes. On the other hand, the conductivity curves obtained from the resistance probe showed significant differences. Moreover, the relative conductivity values between the two probes diverged early in some reactions, which is different from the profiles obtained in the non-reactive system. This was caused by some coagulum plated on the surfaces of the electrodes of the resistance probe. A blender test and turbidity measurements were carried out to check the mechanical and electrolyte stability of the prepared latexes. The percent coagulum and the ccc are used to represent latex stability. The final conductivity ratio (R/T) between the two probes is used as a parameter to correlate the conductivity curves to latex stability. The results indicate that there exists a linear relationship between them, which means that the online conductivity measurements can be used to predict the mechanical and electrolyte stability of the final latexes in this system.

3.5 References

[1] J. Hong, *Ph.D. Dissertation*, Lehigh University (2008).

[2] *American Standard Test Method* D1417-03D.

[3] N. Sutterlin, in *Polymer Colloids II*, R. M. Fitch, Eds., Plenum, New York (1980).

[4] S. Krishnan, *Ph.D. Dissertation*, Lehigh University (2002).

Chapter 4
Online Conductivity Measurements in Batch Emulsion Polymerizations of BMA at 20 % Solids Content

4.1 Introduction

In the previous chapter, the relative conductivity curves obtained using the resistance and torroidal probes showed divergence during the batch emulsion polymerizations of BMA (5 % solids content), which differed from the curves obtained for the non-reactive system. These results indicate that it is possible to use online conductivity measurements to predict latex stability in this emulsion polymerization system. Further investigations at a higher solids content were carried out in this chapter.

The solids content of the batch emulsion polymerizations of BMA carried out in this chapter was increased to 20 %. The SLS concentrations were chosen as 5, 6, 8, 10, 20, and 30 mM. Among these, the first two concentrations are below the CMC of SLS (around 7.8 mM), the third one is around the CMC, and the last three are above the CMC. Two goals can be achieved through this series of reactions: one is to investigate the effect of the SLS concentration on latex stability; the other is to check

whether the divergence between the two conductivity curves still occurs when the SLS concentration is above the CMC.

Repeatability was checked for these reactions. The conductivity curves measured using the torroidal probe were repeatable. However, for some of the reactions, the conductivity curves obtained using the commercial resistance probe showed poor repeatability. Moreover, the results of the latex stability tests could not be correlated to the conductivity curves in some cases, which meant that the sensitivity of this resistance probe was not good. Under these conditions, it was not reliable to use the commercial resistance probe. Therefore, a homemade probe was built to overcome the shortcomings of the commercial one. Using the homemade resistance probe with the torroidal probe, the batch emulsion polymerizations of BMA (20 % solids content) were run again.

Blender tests and turbidity measurements were used to check latex stability as before. The results showed that latex stability was improved by the increase in the SLS concentration. Moreover, the final conductivity ratio (R/T) was correlated to latex stability.

Besides the studies relating the online conductivity measurements and latex stability, the effect of the reaction kinetics on the changes in conductivity was investigated. The second increase in the conductivity curves also occurred during this

series of reactions. The reason for this increase was analyzed. Moreover, the formation of coagulum in the early stages of the emulsion polymerization was studied using a designed reactor and some images of coagulum were obtained.

4.2 Experimental

4.2.1 Materials

10 ppm monomethyl ether of hydroquinone (MEHQ) inhibitor was removed from *n*-butyl methacrylate (BMA, Sigma-Aldrich) by passing the monomer through an inhibitor-removal column (Sigma-Aldrich). Sodium lauryl sulfate (SLS, Fisher Scientific) and sodium bicarbonate ($NaHCO_3$, Sigma-Aldrich) were used as surfactant and buffer, respectively. Potassium persulfate ($K_2S_2O_8$, Sigma-Aldrich) and 2,2'-azobis(isobutyronitrile) (AIBN; Aldrich) were used as initiators. All chemicals were used as received. Deionized (DI) water was used for all experiments.

4.2.2 Batch Emulsion Polymerizations of BMA

Compared with the batch emulsion polymerizations described in Chapter 3, the latex solids content was increased from 5 % to 20 % in this chapter. Moreover, the concentration of $NaHCO_3$ was decreased from 6.1 to 1.7 mM, which is the same molar concentration as $K_2S_2O_8$. The SLS concentration was varied from 5 mM to 6, 8, 10, 20, and 30 mM in this series of reactions (Table 4.1), which meant that the SLS concentration increased from below the CMC to around and over the CMC. All reactions were run in a 1 L reactor without baffles at 70 ^oC and stirred at 250 rpm

using a 7 cm diameter Rushton impeller with 6 blades. Both the resistance and torroidal probes were used to measure conductivity during the polymerizations. The reactor was blanketed with nitrogen during the polymerizations to prevent O_2 inhibition. $K_2S_2O_8$ initiator was added as an aqueous initiator solution (1.7 mM) to the reactor to start the reaction. The reactions were run for 60 minutes. The conductivity values from the two probes and the temperature in the reactor obtained from a sensor in the torroidal probe were recorded every minute until the temperature decreased during the reaction, and then were recorded every 5 minutes. Samples were taken at periodic intervals to measure the conversion by gravimetry. The particle size of the latexes obtained from the reactions was measured by dynamic light scattering (Nicomp 370).

Table 4.1: Recipes Used for the Emulsion Polymerizations of BMA

Ingredient	DI Water	BMA	SLS**	$K_2S_2O_8$	$NaHCO_3$
B-20%-5mM*	600 g	150 g	0.865 g (5 mM)	0.280 g (1.7 mM)	0.084 g (1.7 mM)
B-20%-6mM			1.038 g (6 mM)		
B-20%-8mM			1.385 g (8 mM)		
B-20%-10mM			1.731 g (10 mM)		
B-20%-20mM			3.461 g (20 mM)		
B-20%-30mM			5.191 g (30 mM)		

* In the notation "B-20%-5mM", B stands for batch emulsion polymerization, 20% stands for the solids content, and 5mM stands for the SLS concentration.

****** Concentration based on the aqueous phase

One batch emulsion polymerization was carried out using AIBN as initiator to investigate the second increase in the conductivity curves during the reactions. The recipe is shown in Table 4.2. The reaction was carried out under the same conditions as discussed previously and the conductivity was recorded during the reaction. Different from KPS, AIBN initiates the reaction from the oil phase instead of the aqueous phase. Moreover, the decomposition of AIBN does not change the pH value in the system, so no buffer was used in this recipe. The SLS concentration used was 6 mM to compare with reaction B-20%-6mM shown in Table 4.1.

Table 4.2: Recipe Used for the Emulsion Polymerization of BMA Using AIBN as Initiator (B-20%-AIBN)

Ingredient	Amount
DI water	600 g
BMA	150 g
SLS	1.038 g (6.0 mM)*
AIBN	0.043 g (1.8 mM)**

* Concentration based on water phase

** Concentration based on oil phase

4.2.3 Latex Stability Tests

The blender test and turbidity measurements were carried out to check the mechanical and electrolyte stability of the latexes prepared by the batch emulsion polymerizations (Table 4.1). The procedure was the same as used previously and the details were presented in Chapter 3 (Section 3.2.3 and 3.2.4).

4.2.4 Homemade Resistance Probe

The principle of the commercial resistance probe was shown in Chapter 1 (Figure 1.2). Alternating voltage is applied to two electrodes, which are comprised of two pieces of platinum, so there is an alternating current passing through the solution in which the electrode is immersed, which is caused by the motion of ionic species. Even though the electrodes have a face-to-face structure in the commercial resistance probe used previously, some resistance probes apply other structures. As shown in Figure 4.1, the current line follows a curve if the two electrodes are not placed face-to-face and then the current signal is correlated to conductivity. Based on this principle, a homemade resistance probe was built using two pieces of platinum (10×10×0.1 mm) connected with platinum wires (Figure 4.1). The platinum pieces were fixed on a Teflon jacket, which was fixed to the head of the torroidal probe. In this manner, the two conductivity probes were combined into one probe. Moreover, the electrodes of the new resistance probe are totally exposed to the solution in which the probe is immersed. This is different from the commercial resistance probe used previously which encapsulates the electrodes inside glass. The benefit of this design is that much more surface areas of the electrodes can contact the solution, which provides more sensitivity. On the other hand, the position of the two electrodes is back-to-back instead of face-to-face. In this case, the current lines in the aqueous phase are in an arc and are longer compared with the face-to-face electrodes. The back-to-back configuration caused a disadvantage that the measurements can be affected by the presence of monomer droplets dispersed in the aqueous phase. This

will be discussed later. The homemade probe was connected to the original conductivity meter and the signals obtained from this probe were correlated to the standard conductivity values using NaCl solutions. The results (Figure 4.2) showed that there was a linear relationship between the signal and conductivity values, which indicated that this homemade probe could be used to measure conductivity.

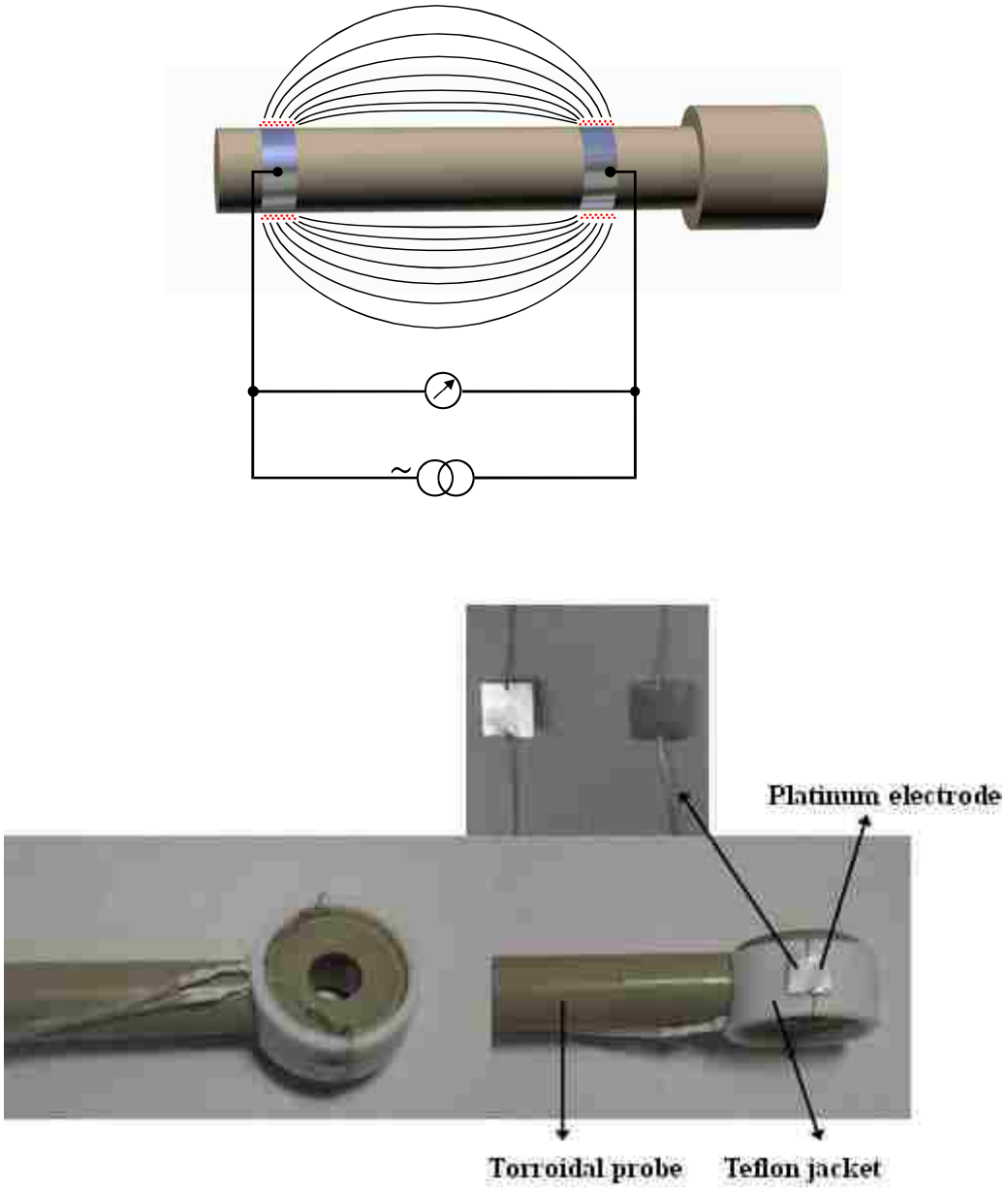

Figure 4.1: *Principle of the resistance probe in a back-to-back configuration (top) and a homemade resistance probe built on the torroidal probe (bottom).*

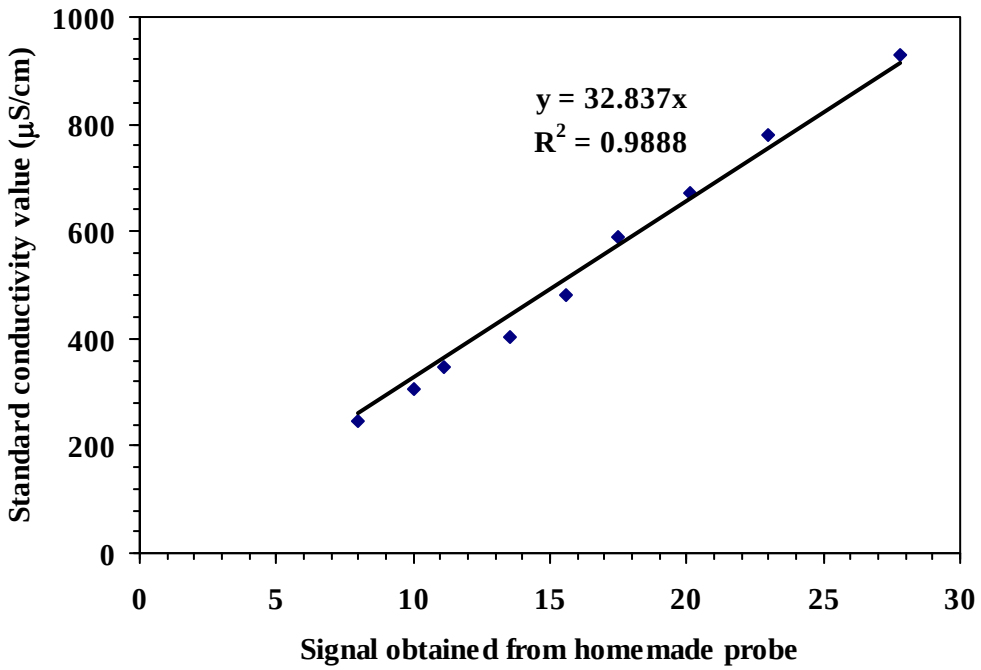

Figure 4.2: *Calibration curve for the homemade resistance probe.*

4.2.5 Investigation of the Morphology of Coagulum

To investigate the morphology of coagulum formed in the early stages of the emulsion polymerizations, a batch polymerization of BMA was carried out in a 500 mL reactor with six baffles at 70 °C and stirred at 300 rpm using a magnetic stirred bar. As Figure 4.3 shows, the baffles were covered by gold films, which are normally used as a material for electrodes. The gold film was fixed by Teflon tape, which is safe under the conditions of the emulsion polymerization of BMA. The baffles were inserted into the reactor through holes on a homemade Teflon lid, so the baffle could be taken out of the reactor at any time. The reactor was blanketed with nitrogen during the polymerization to prevent O_2 inhibition. $K_2S_2O_8$ initiator was added as an aqueous initiator solution (1.7 mM) to the reactor to start the reaction. Samples were taken at periodic intervals to measure the conversion by gravimetry. A baffle was also taken out and placed into ice right after a sample was taken. All baffles were rinsed with DI water and dried in air after the reaction. The particle size was measured by DLS (Nicomp 370).

The recipe for this reaction was the same as reaction B-20%-5mM. The weights of all components were half of the original recipe shown in Table 4.1 due to the smaller reactor. The SLS concentration was chosen as 5 mM because the reaction rate at the beginning of the polymerization was relatively slow compared with the other reactions. It provided enough operation time, such as taking samples, taking out baffles and sealing holes with Teflon film, during the reaction, especially at the very

beginning.

The morphology of coagulum formed in the early stage of the BMA emulsion polymerization on a gold film was examined by field-emission scanning electron microscopy (FESEM, Hitachi, 4300 LV) at an accelerating voltage between 1 and 10 kV. All of the scanning electron microscopy (SEM) samples were air-dried on a stub and sputter-coated with a thin layer (5 sounds) of iridium (Electron Microscopy Science, EMS 575X Turbo Sputter Coater) to obtain a conductive surface and prevent charging during SEM imaging.

The morphology of coagulum was also investigated using a standard tapping mode MFP-3D atomic force microscope (AFM) (Asylum Research, CA). A dried gold film was directly used as the sample. After a sample was loaded on the x-y stage of the AFM, the isolation table was turned on to avoid scan errors introduced by vibration. By looking at through a microscope integrated on the scan head of the AFM, the area covered with coagulum could be observed. The scan speed varied between 0.5 μm/s and 1 μm/s with varied scan size.

Figure 4.3: *A baffle covered by a gold film (left) and the setup of a 500 mL reactor with six baffles (right).*

4.3 Results and Discussion

4.3.1 Batch Emulsion Polymerizations of BMA

The batch emulsion polymerizations shown in Table 4.1 were carried out. The particle size of the obtained latexes is shown in Table 4.3 and the kinetic curves are summarized in Figure 4.4. The particle size decreased as the SLS concentration increased, which is expected. The particle size distribution (PDI) was narrow for all of the latexes no matter if the SLS concentration was below, around or above the CMC. The reaction rate increased with an increase in the SLS concentration. The reaction rates of reactions B-20%-30mM and B-20%-20mM were fast and finishing within 10 minutes. On the other hand, reaction B-20%-5mM was slow, especially in the early stages of this reaction. This is good for the investigation of plating formed during the reaction and will be discussed later. For all reactions, no coagulum was found in the latexes and coagulum adsorbed on the surfaces of the reactor, probes, and impeller was negligible, so these reactions can be considered as successful stable reactions.

Table 4.3: Particle Size Obtained from the Batch Emulsion Polymerizations (20 % Solids Content) of BMA

	D_n (nm)	D_V (nm)	D_I (nm)	PDI
B-20%-5mM	212	212	212	1.00
B-20%-6mM	162	169	174	1.07
B-20%-8mM	138	147	153	1.11
B-20%-10mM	120	122	124	1.03
B-20%-20mM	92	98	103	1.12
B-20%-30mM	85	89	93	1.09

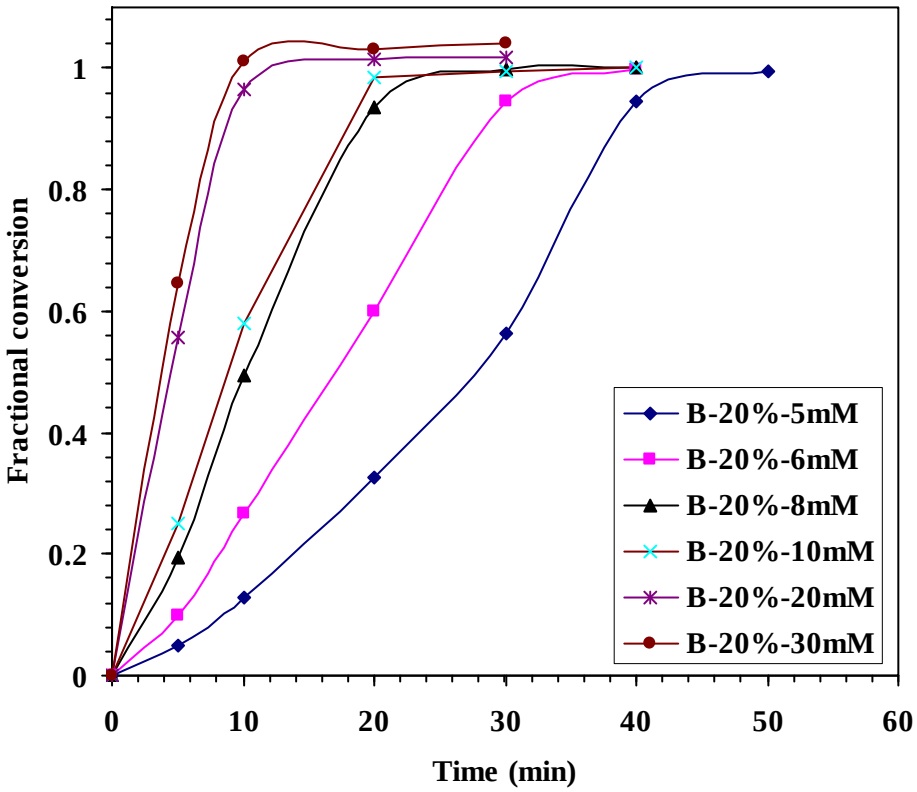

Figure 4.4: *Fractional conversion vs. time curves for the batch emulsion polymerizations of BMA shown in Table 4.1 at 70* °C *and 250 rpm.*

4.3.2 Online Conductivity Measurements Using Commercial Resistance Probe

4.3.2.1 Batch Emulsion Polymerizations of BMA

The relative conductivity curves of the batch emulsion polymerizations (Table 4.1) are shown in Figure 4.5. The results can be divided into two cases. The first represents the first three reactions (Figure 4.5 (a), (b), and (c)), in which the SLS concentrations were 5, 6, and 8 mM, respectively. Divergence between the two conductivity curves is observed during these reactions. For the reactions B-20%-5mM and B-20%-6mM, the sharp decrease occurred early during the reactions and the conversion at that time was less than 20 %. The conductivity curves obtained from the resistance probe decreased to very low values, which meant that the electrodes of this probe were almost fully covered by deposited coagulum formed during the reactions. Therefore, the final conductivity ratio (R/T) is small and close to zero. For reaction B-20%-8mM, the decrease occurred relatively later and the conversion at that time was more than 35 %. Moreover, different from the first two reactions, the conductivity values obtained from the resistance probe just decreased to intermediate values, which meant that the electrodes were partly covered by polymer.

The other case represents the last three reactions (Figure 4.5 (d), (e), and (f)), in which the SLS concentrations were 10, 20, and 30 mM, respectively. There was no obvious divergence between the two conductivity curves for these three reactions, which meant that no plating of the electrodes of the resistance probe occurred during these reactions. Therefore, the R/T values are large and close to 1.

Two questions arise based on the discussion above. One concerns the relationship between the CMC of SLS and the divergence. The main hypothesis of this research project is that the divergence between the two conductivity curves is caused by plating on the surfaces of the electrodes, which may be related to latex stability. However, the results show another view of this phenomenon. The SLS concentrations in the first three reactions, in which divergence occurred, are below and around the CMC. On the other hand, the last three reactions, in which the SLS concentrations are above the CMC, did not show any divergence. Especially, for the reaction B-20%-10mM, the SLS concentration is just above the CMC and not very high based on the weight of the monomer, but the conductivity curve obtained from the resistance probe is significantly different from that of reaction B-20%-8mM. Therefore, the question is whether the divergence is related to the CMC instead of latex stabilities. The other question is that whether the latexes prepared in the last three reactions have similar stability. Because no divergence occurred in these three reactions, the prepared latexes should be stable based on the previous results. Whether these latexes are stable or the sensitivity of the online conductivity measurements has some limitation needed to be tested. Both questions will be discussed and answered later.

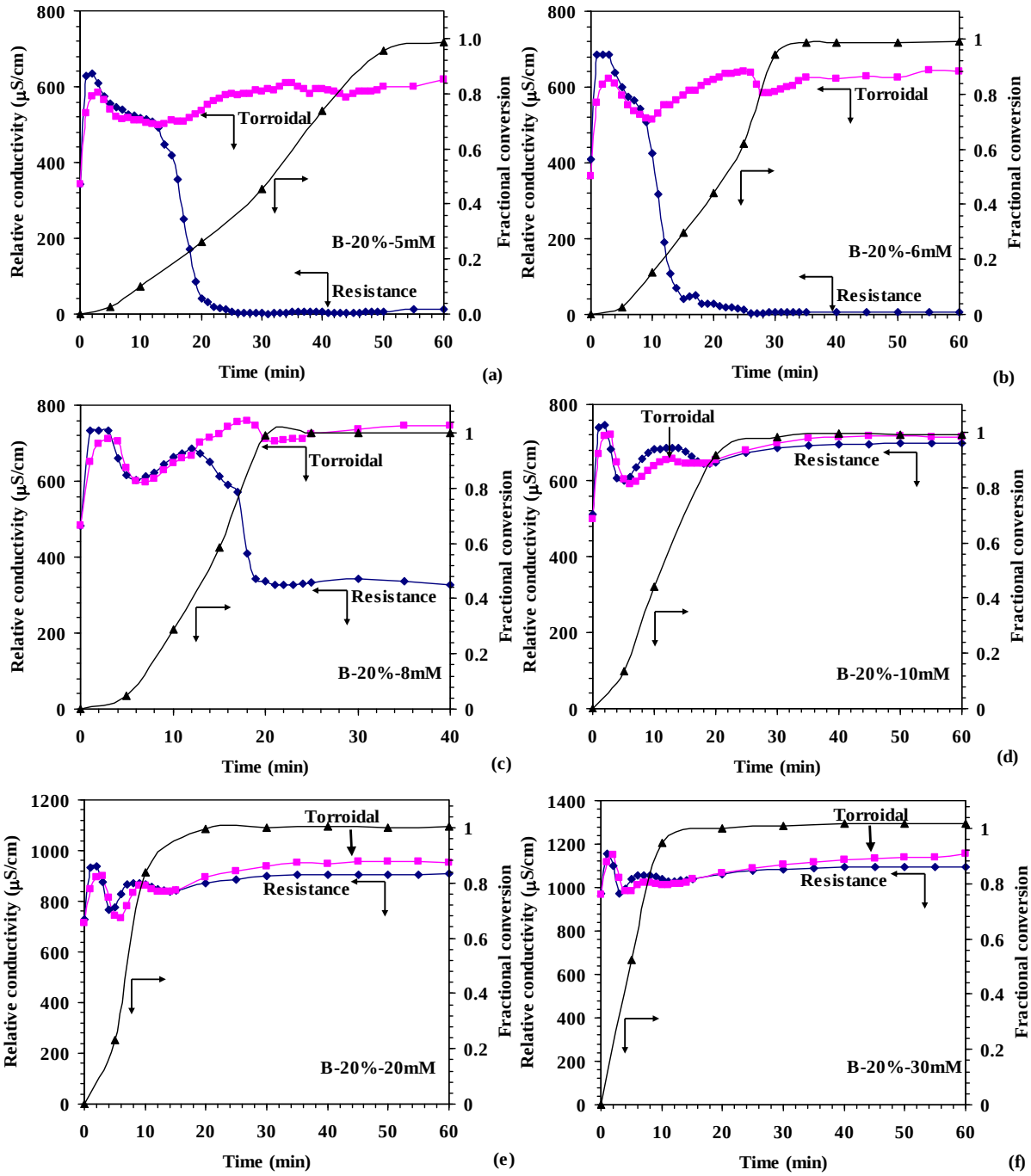

Figure 4.5: *Relative conductivity and fractional conversion vs. time curves for the reactions shown in Table 4.1 at 70 °C and 250 rpm: (a) B-20%-5mM; (b) B-20%-6mM; (c) B-20%-8mM; (d) B-20%-10mM; (e) B-20%-20mM; and (f) B-20%-30mM.*

4.3.2.2 Non-Reactive System

Reaction B-20%-6mM (Table 4.1) was carried out in order to investigate the effect of plating on the surfaces of the electrodes of the resistance probe on the conductivity measurements of this probe during the course of the polymerization and post-polymerization. During this reaction, the resistance probe was taken out of the reactor at 35 min and cleaned with acetone and DI water as fast as possible. The probe was then put back into the reactor. The reaction was run for an additional one hour. The results are shown in Figure 4.6. There was a significant divergence between the two conductivity curves after 8 minutes of the reaction and the resistance probe did not exhibit true conductivity values (as indicated by the torroidal probe) after the divergence. From the fractional conversion curve, it can be seen that the conversion was 96 % at 35 min, when the resistance probe was taken out of the reactor to clean. After cleaning, the measurements of the resistance probe returned to the correct values. The change in the measurements of this probe proves that the decrease in the conductivity curves obtained from the resistance probe is caused by the presence of plating on the surfaces of the electrodes, which is the foundation of this research. In the following hour, there was no decrease in the conductivity values obtained with this probe. After this experiment, the resistance probe was taken out, rinsed with DI water and dried in air. Figure 4.6 shows a picture of this probe. It can be seen that some coagulum was formed on the surfaces of the glass tubing after cleaning at 35 minutes, but no decrease appeared in the conductivity curve. This phenomenon was the same as the previous results shown in the non-reactive system (Chapter 2), which

indicated that the online conductivity measurements did not work in the non-reactive system. Moreover, this system exhibited two different kinds of adsorption mechanisms. First, during the reaction, because there was not enough SLS to stabilize all particles, some latex adsorbed on or flocculated onto the surfaces of the electrodes of the resistance probe. This plating on the surfaces affected the measurements of this probe. Second, after the reaction, some coagulum formed under agitation and high temperature. However, the formed coagulum did not adsorb readily on the electrodes. That is why this method did not work in the non-reactive system. The exact reason for this phenomenon is not yet known. It may be caused by the shape of this probe. Figure 1.1 shows that the electrodes are in the inside of the probe. So coagulum may not attach readily. On the other hand, it may be related to materials. The tubing is made of glass and the electrode is made of Pt metal. Different materials have different surface characteristics, which can directly affect the adsorption.

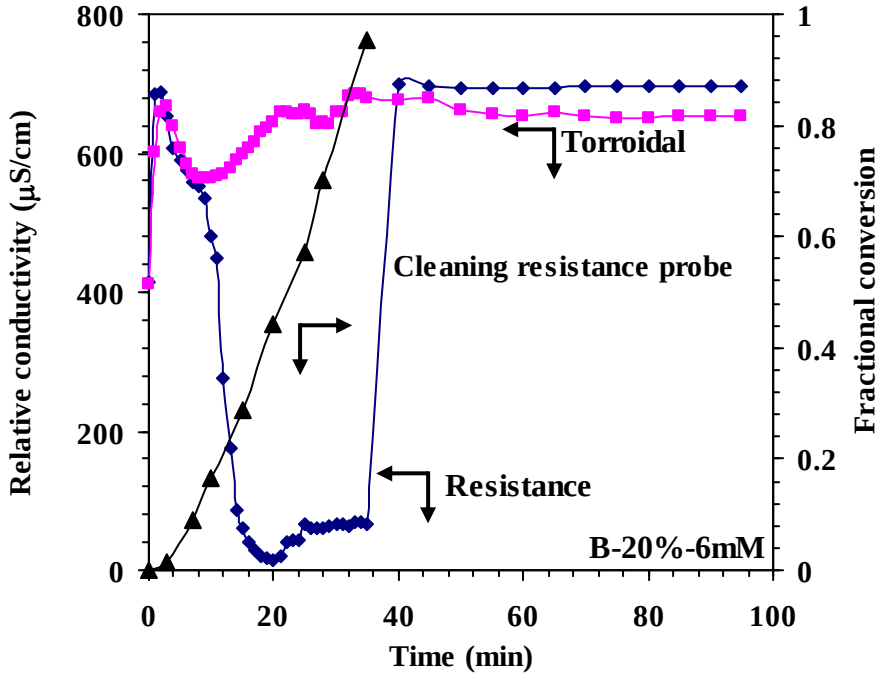

Figure 4.6: *Relative conductivity and fractional conversion vs. time curves for reaction B-20%-6mM (Table 4.1) at 70 °C and 250 rpm (top) and photograph of the resistance probe after the reaction (bottom).*

4.3.2.3 Repeatability Problem

The repeatability of the conductivity curves obtained from these reactions (Table 4.1) was checked. Among these reactions, some problems were found for reaction B-20%-8mM. This reaction was run three times. From the kinetic curves (Figure 4.7) and the particle size (Table 4.4), it can be seen that the repeatability of this reaction was good. Moreover, the relative conductivity curves obtained from the torroidal probe were also reproducible as shown in Figure 4.8. However, the curves obtained from the commercial resistance probe showed obvious differences (Figure 4.8). All of the three curves showed a decrease in the middle of the reactions, but the decrease occurred at different times and the final conductivity values were not the same. Under this condition, the R/T values calculated from these three curves are significantly different, which means that the R/T value cannot be used as a parameter to predict latex stability due to poor repeatability. This is caused by the structure of the commercial resistance probe. As shown in Figure 1.1, the electrodes are built in the glass and the liquid flow needs to pass through a slot between the two electrodes to have contact with them, so the orientation of this probe and the position of the slot relative to the flow direction strongly affect the interaction between the liquid and electrodes, which may affect the formation of any plating. Lots of efforts were carried out to solve this problem, but the poor repeatability could not be overcome. Moreover, other resistance probes were tried, but different shapes of the conductivity curves were obtained even though all these probes are from the same company. Therefore, the better way to solve this problem is to make a better resistance probe.

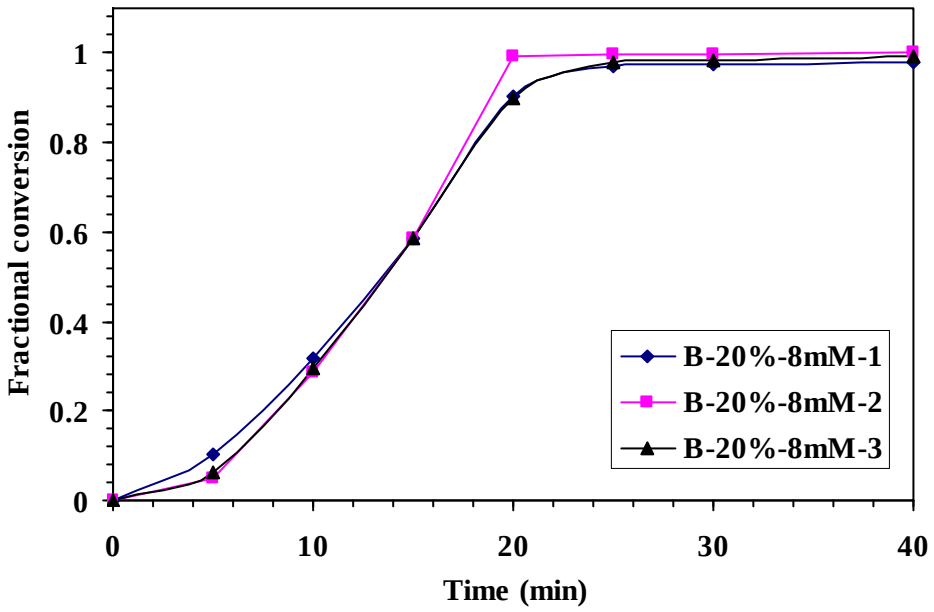

Figure 4.7: *Repeatability of fractional conversion vs. time curves for Reaction B-20%-8mM (Table 4.1).*

Table 4.4: Repeatability of Particle Size of the Latexes Prepared in Reaction B-20%-8mM

Sample	B-20%-8mM-1	B-20%-8mM-2	B-20%-8mM-3
D_n (nm)	138 ± 12	136 ± 13	140 ± 7
D_I (nm)	153 ± 1	152 ± 1	149 ± 1
D_V (nm)	147 ± 5	145 ± 6	145 ± 3

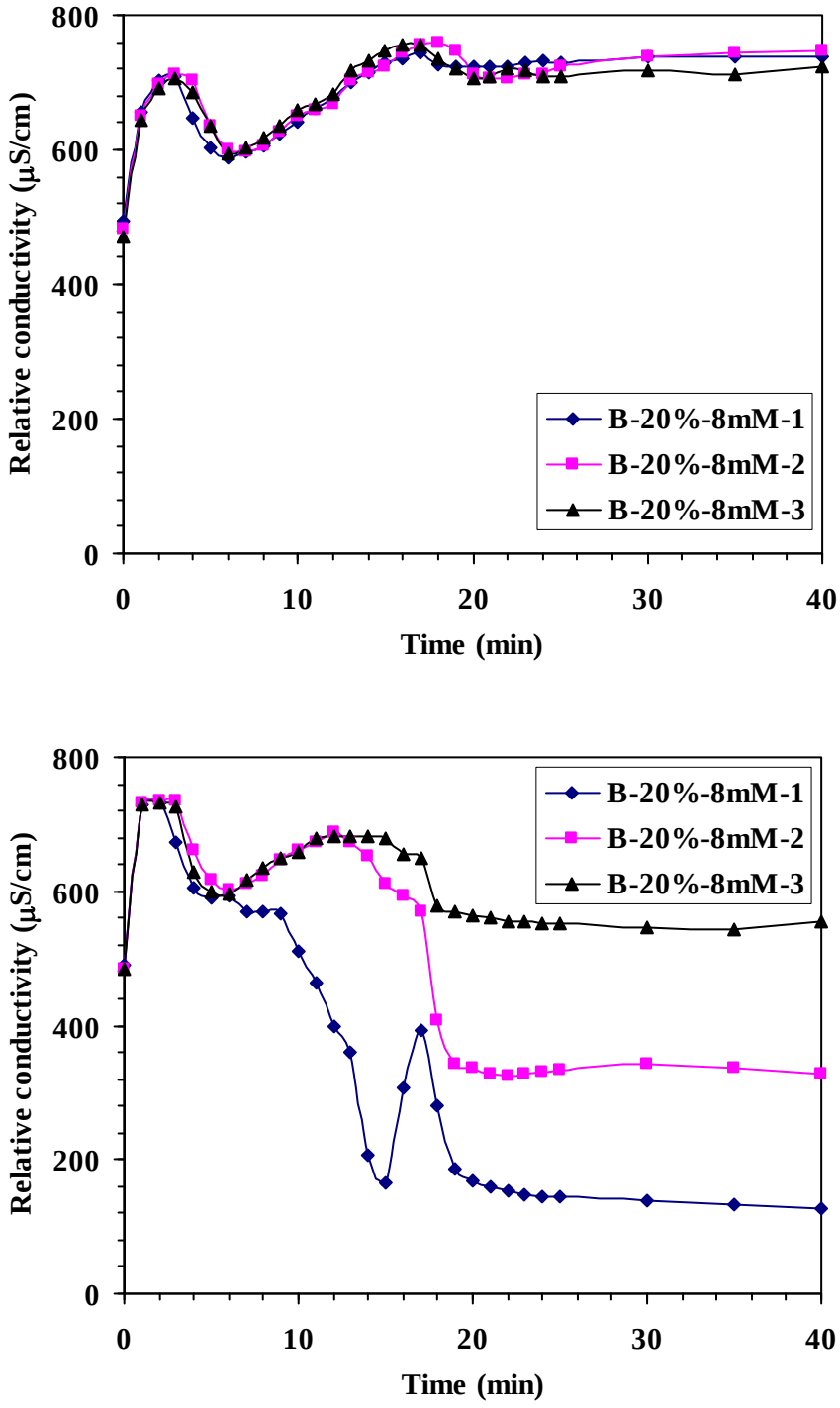

Figure 4.8: *Repeatability of relative conductivity vs. time curves for Reaction B-20%-8mM (Table 4.1) obtained from the torroidal probe (top) and commercial resistance probe (bottom).*

4.3.3 Latex Stability

4.3.3.1 Blender Tests

The blender test was carried out to test the mechanical stability of the latexes prepared previously. The procedure is the same as described in Chapter 3 (3.2.3) and the results are shown in Figure 4.9. Latex B-20%-30mM had the best stability. This latex did not lose solids during the blender test, which meant that no coagulation occurred under the applied shear forces. Latex B-20%-20mM was stable within the first 5 minutes and then lost solids at a slow rate. Because a 5 minute test is normally long enough for a latex under such tough conditions in industry, this latex can be considered as stable even though it is not as good as latex B-20%-30mM. The positions of latexes B-20%-10mM and B-20%-8mM were switched and the results for latexes B-20%-6mM and B-20%-5mM were close. All of these four latexes lost more than 40 % solids during the test and thus, were not stable. Among these, the results of latex B-20%-10mM need to be pointed out. The relative conductivity curves (Figure 4.5 (d)) obtained during this reaction do not show any divergence, which indicates that this latex should be stable based on the assumption of this research. However, the blender test indicates that this latex is not stable. These contradictory results show that the sensitivity of the commercial resistance probe is really limited. This probe shows poor repeatability for reaction B-20%-8mM and does not predict any instability for latex B-20%-10mM. Therefore, 8 mM SLS seems to be a transition point for this probe. If the SLS concentration is above 8 mM, the commercial resistance probe does not work to correctly predict latex stability.

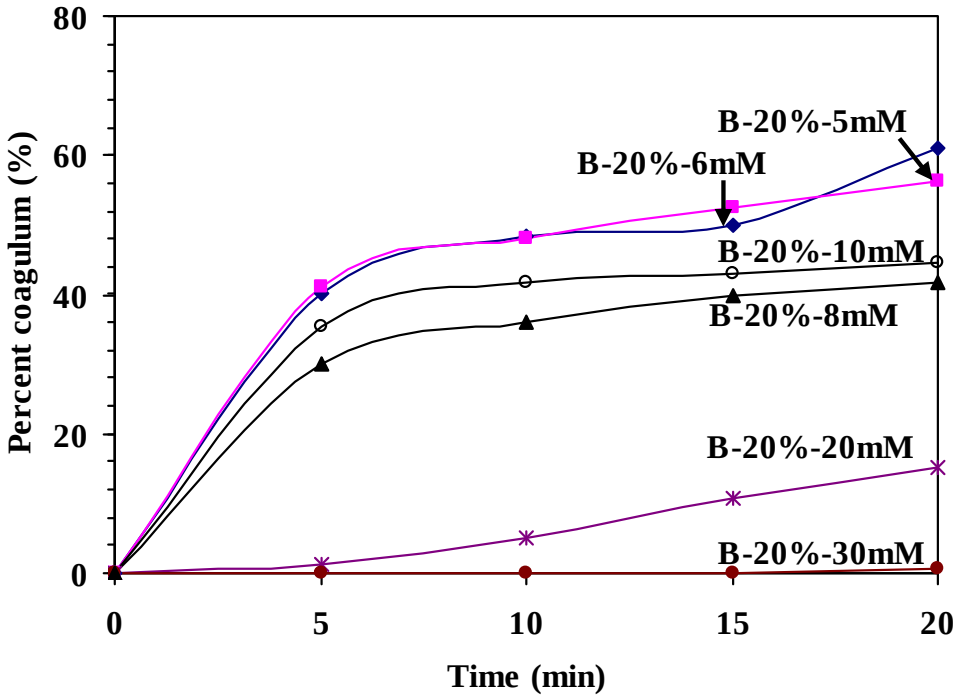

Figure 4.9: *Percent coagulum vs. time curves for the latexes prepared in the reactions shown in Table 4.1.*

4.3.3.2 Turbidity Measurements

The critical coagulation concentration (ccc) of the latexes prepared in the previous reactions (Table 4.1) was estimated through turbidity measurements. The results are shown in Table 4.5. The ccc of latexes B-20%-5mM and B-20%-6mM is close. The ccc increased with the increase in the SLS concentration in the recipe. But the differences among these latexes are not as significant as those obtained from the blender tests. This is most likely caused by the dilution of the latexes before the turbidity measurements. Some SLS molecules are released to the aqueous phase from the particle surfaces during the dilution, which reduces the differences in stability among these latexes. However, the ccc values change with the variation in the SLS concentration, so the latexes still have different degrees of stability after dilution and the ccc values can be used to represent the degree of the electrolyte stability of these latexes even though the stability of the diluted and original latexes is not exactly the same.

Table 4.5: Critical Coagulum Concentration (ccc) of the Latexes Obtained from the Reactions in Table 4.1

Latex	ccc (M)
B-20%-5mM	0.527
B-20%-6mM	0.522
B-20%-8mM	0.550
B-20%-10mM	0.560
B-20%-20mM	0.616
B-20%-30mM	0.699

4.3.4 Online Conductivity Measurements Using Homemade Resistance Probe

4.3.4.1 Batch Emulsion Polymerizations of BMA

As discussed previously, the commercial resistance probe showed poor repeatability and limited sensitivity. Even though the exact reason is unknown, obviously, it is not reliable to use this kind of probe in further experiments. Therefore, a homemade probe was made and the details about this probe were shown in the experimental section (4.2.4). Using this homemade resistance probe, all the reactions shown in Table 4.1 were run again and the new results are shown in Figure 4.10. To distinguish the conductivity curves obtained from the commercial resistance probe, the new results obtained from the homemade resistance probe were labeled as "new resistance" in the figures.

Comparing the new results with the previous results (Figure 4.10 vs. Figure 4.5), two major differences are observed. First, before the addition of the initiator (time = 0 min in the figures), the conductivity values obtained from the two probes were similar to the previous results (Figure 4.5). On the other hand, the conductivity values obtained from the new combined (resistance and torroidal) probes were different and the values obtained from the homemade resistance probe were smaller than those obtained from the torroidal probe (Figure 4.10). This was caused not by plating because the reaction was not even started, but by the presence of the monomer droplets. Monomer droplets dispersed in the continuous aqueous phase acted as insulators and interrupted the movement of the ionic species present in the emulsion

which could affect the current lines passing between the two electrodes. Because the homemade resistance probe has a back-to-back configuration and works on long current lines, which is different from the commercial resistance probe with the face-to-face configuration and short distance pathway between the two electrodes, the effect of the monomer droplets on the conductivity measurements obtained from the homemade probe are much more significant compared with the commercial probe. To illustrate this phenomenon, an experiment is presented in Figure 4.11. In this experiment, the torroidal, the commercial (labeled as original resistance in the figure) and homemade (labeled as new resistance) resistance probes were used to measure conductivity at the same time. 500 g of DI water, 20.28 g of 0.24 M NaCl solution, 81.73 g of 0.07 M SLS solution, and 150 g BMA monomer were added into the reactor at 70 °C stirred at 250 rpm in sequence. Before adding monomer, the homemade resistance probe showed the same conductivity values as the other two probes. However, after the addition of the monomer, the values obtained from the homemade resistance probe became smaller than the other two probes. This was resulted from the influence of the monomer droplets.

Second, in the new results, there were obvious divergences between the two conductivity curves for reactions B-20%-5mM, B-20%-6mM, B-20%-8mM, and B-20%-10mM. On the other hand, in the old results, no divergence could be detected in reaction B-20%-10mM using the commercial resistance probe, but the subsequent blender test showed that this latex was not stable. The difference between the old and

new results is very important and can be used to answer the questions presented before, which concern the relationship between the divergence and the CMC of SLS and the limitation of the online conductivity measurements. Based on the new results, both questions can be answered clearly. First, the divergence still occurred when the SLS concentration (10 mM) was higher than the CMC. Therefore, this proves that the divergence between the two conductivity curves is not related to the CMC but caused by latex stability. Second, using the homemade probe, the instability of the latex B-20%-10mM can be detected through the divergence, which cannot be achieved by the commercial probe. This demonstrates that the online conductivity measurements have limitations depending on the resistance probe used to make the measurements.

As the conclusion about the homemade resistance probe, both the advantage and disadvantages need to be mentioned. The measurements of the homemade probe are more easily to be affected by the monomer droplets dispersed in the aqueous phase compared with the commercial probe. This causes the differences in the conductivity values measured by the two probes from the beginning of each reaction. The disadvantage of this is that it is hard to judge the exact time when the divergence occurred during the reactions. On the other hand, the homemade probe can detect the instability of latex B-20%-10mM. Moreover, after the disappearance of the monomer droplets, the two conductivity curves can be overlapped for the stable latexes, such as B-20%-20mM (Figure 4.10 (e)). These results indicate that the homemade probe has better sensitivity and can be used to detect latex stability.

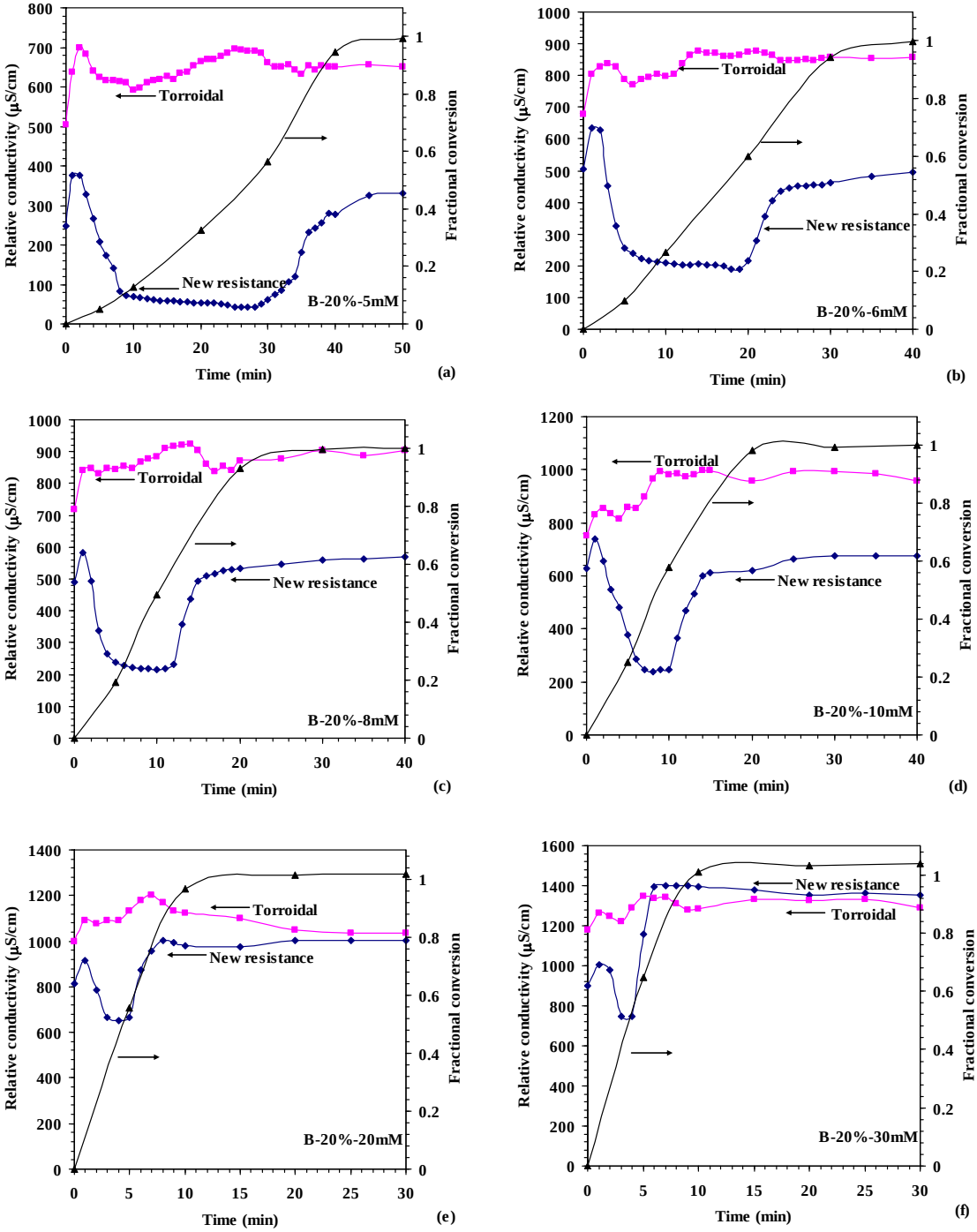

Figure 4.10: *Relative conductivity and fractional conversion vs. time curves for the reactions shown in Table 4.1 using the homemade resistance probe at 70 °C and 250 rpm: (a) B-20%-5mM; (b) B-20%-6mM; (c) B-20%-8mM; (d) B-20%-10mM; (e) B-20%-20mM; and (f) B-20%-30mM.*

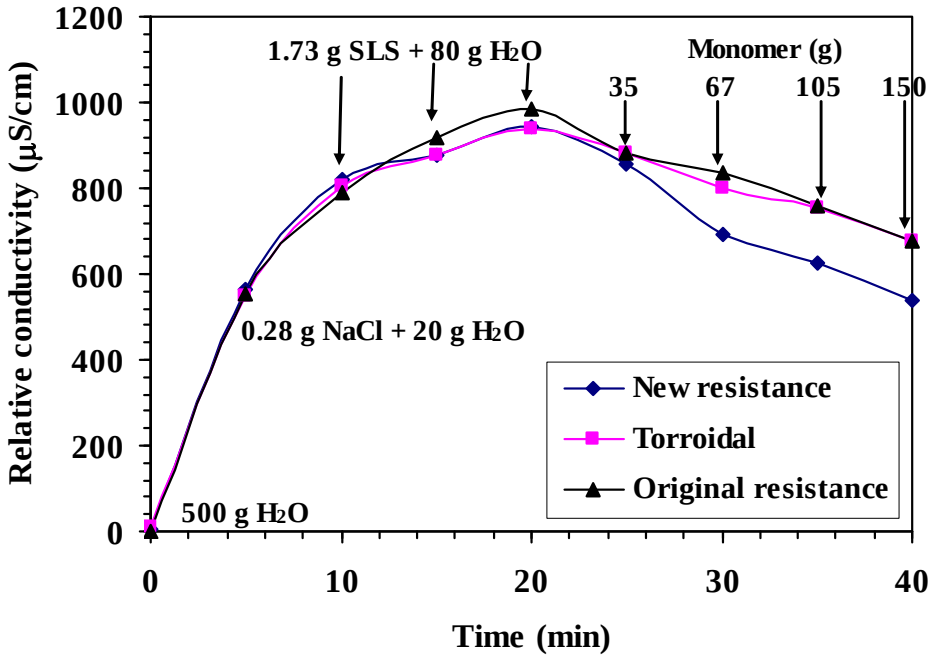

Figure 4.11: *Effect of the monomer droplets on the conductivity measurements using the new homemade resistance probe.*

4.3.4.2 Correlation

Because the homemade resistance probe has better sensitivity to detect latex stability due to the large surface area of the electrodes, the final conductivity ratio (R/T) between the two conductivity curves shown in Figure 4.10 is calculated and correlated to latex stability. Moreover, the surfactant surface coverage of each latex, which can determine the degree of latex stability, was also measured. The surface coverages of these latexes from B-20%-5mM to B-20%-30mM were 21.3, 19.1, 23.8, 24.1, 36.5, and 48.6 %, respectively.

First, R/T is correlated to the percent coagulum obtained after the blender test and the surface coverage. Figure 4.12 shows the results. Because both latexes B-20%-20mM and B-20%-30mM are stable, the R/T values are close to 1. Latex B-20%-20mM was used to represent the results of the stable latexes. The percent coagulum after 5 minutes of the blender test (Figure 4.9) was used in the correlation. The results show that there is a linear relationship between the percent coagulum and R/T, and the surface coverage and R/T. This indicates that the online conductivity measurements can be used to predict the mechanical stability of the final latexes. Second, R/T is correlated to the critical coagulum concentration (ccc) estimated based on the turbidity measurements (Table 4.5) and the results are shown in Figure 4.13. A linear relationship between them is also obtained, which means that this method can predict the electrolyte stability of the final latexes. Therefore, using the homemade probe, the online conductivity measurements work in this system.

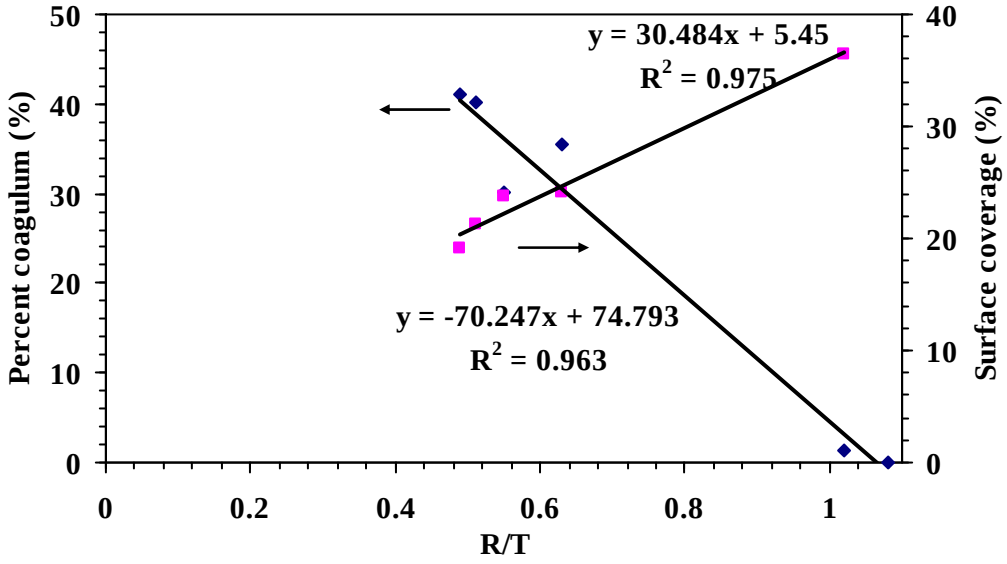

Figure 4.12: *Correlation between the percent coagulum obtained after the blender test and the final conductivity ratio (R/T), and the surface coverage and R/T.*

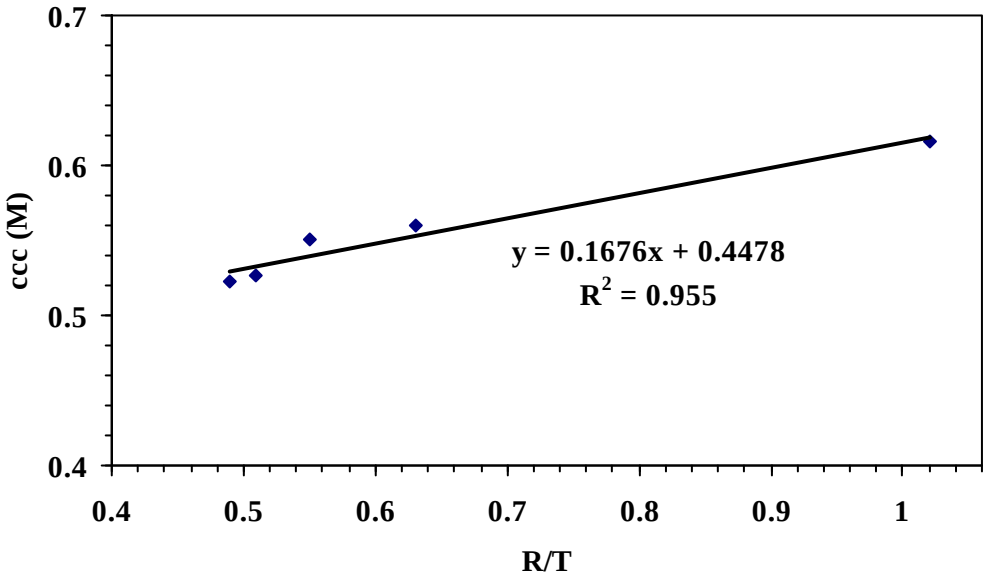

Figure 4.13: *Correlation between the critical coagulation concentration (ccc) estimated by the turbidity measurements and the final conductivity ratio (R/T).*

4.3.5 Investigation of the Second Increase

From the previous results (Figure 3.7 and Figure 4.10), it can be seen that there is an increase in the conductivity curves obtained from the resistance probe in the middle of the batch emulsion polymerizations of BMA, which is referred to as the second increase. The exact reason for this phenomenon is not clearly known so far. Some explanations were given in prior research. For example, Santos et al.[1] mentioned that this increase was probably caused by the monomer consumption in the medium, which could release small amounts of the surfactant into the continuous phase. Schork et al.[2] also gave an explanation based on the comparison of the emulsion and miniemulsion polymerizations of MMA using SLS as the surfactant under the same conditions. In the emulsion polymerization, the conductivity curve showed a significant increase. On the other hand, no increase was observed in the miniemulsion polymerization. They claimed that the increase corresponded to the disappearance of excess monomer and a desaturation of the aqueous phase in the emulsion polymerization. In the miniemulsion polymerization, there is little change in surface characteristics of the monomer droplets. The explanations from these two research groups are not the same, but both of them mentioned that this increase was related to the consumption of the monomer droplets during the reactions. In this research, an investigation was carried out and the results will be discussed below.

4.3.5.1 Kinetics Analysis

All of the conductivity curves obtained from the homemade resistance probe

and the fractional conversion curves were combined in Figure 4.14. It can be seen that all of the second increases in conductivity occurred in the same range of the fractional conversion, which was between 50 and 60 %, no matter what the SLS concentration was in the recipe. Based on the classical theory of emulsion polymerization, the second interval ends around 40 % conversion, which corresponds to the disappearance of monomer droplets. The experimental results of the conversion when the second increase occurred were higher than 40 %. However, if the fast reaction rate in this range and the time lag of sampling and stopping the reaction are taken into account, the real conversion at the beginning of the second increase should be very close to the conversion at the end of second interval. Therefore, the disappearance of the monomer droplets in the aqueous phase is the most likely reason to cause the second increase in conductivity. This explanation is reasonable. Because the disappearance of the monomer droplets implies that "insulated material" is removed from the continuous aqueous phase, so the interruption to the movement of the charged species disappears, which causes the increase in conductivity. As shown in Figure 4.10, the conductivity curves obtained from the homemade resistance probe are lower than the one obtained from the torroidal probe before the second increase, which is caused by the presence of the monomer as discussed previously. However, the two conductivity curves become close after this increase if the SLS concentration is high enough to stabilize the particles. This proves that the disappearance of the monomer droplets is the reason of the second increase.

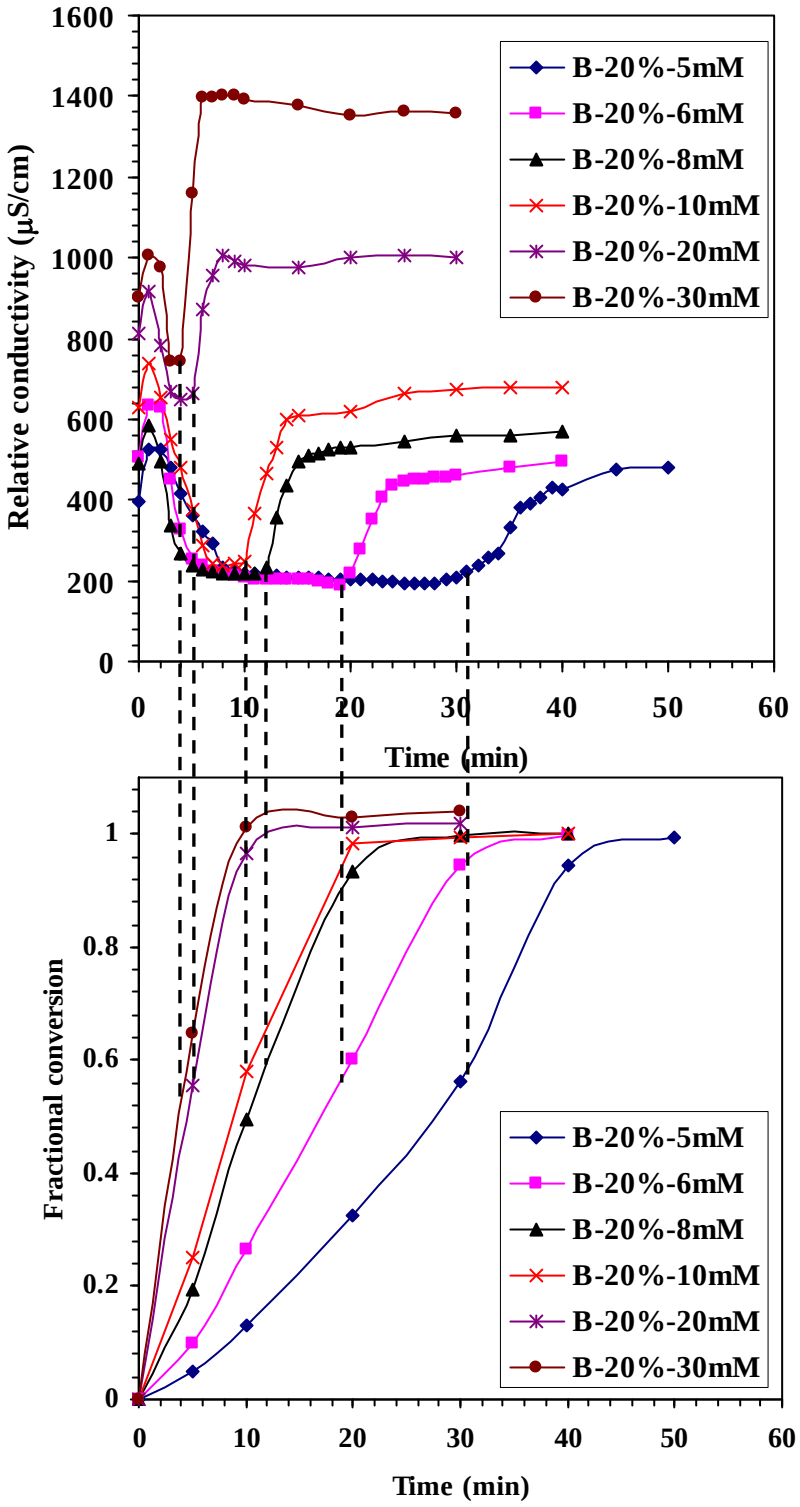

Figure 4.14: *Summary of all conductivity curves obtained from the homemade resistance probe (top) and the fractional conversion curves of the batch emulsion polymerizations (bottom) shown in Table 4.1.*

4.3.5.2 Batch Emulsion Polymerization Using AIBN as Initiator

A batch emulsion polymerization of BMA using AIBN as initiator (Table 4.2) was run to investigate the second increase. Because a low SLS concentration was used, this reaction was not successful. Lots of viscous coagulum was formed and absorbed on the torroidal probe and impeller during the reaction (Figure 4.15). However, from the conductivity curves shown in Figure 4.15, some useful information can be obtained. There was no increase in the conductivity curve obtained from the resistance probe. Because the polymerization occurred in the monomer oil phase, there were little change in surface characteristics of the monomer droplets and no obvious transition point of the disappearance of the monomer droplets compared with using KPS as initiator. This may be the reason why there was no increase in conductivity during this reaction.

Even though the two evidences discussed above are indirect, they still show some means to determine the reason for the second increase. If this increase is really caused by the disappearance of the monomer droplets, the online conductivity measurements can provide more information during emulsion polymerizations and the moment when the second interval ends can be clearly seen. Therefore, this method will become a very useful and accurate tool in studies related to emulsion polymerizations for both academia and industry.

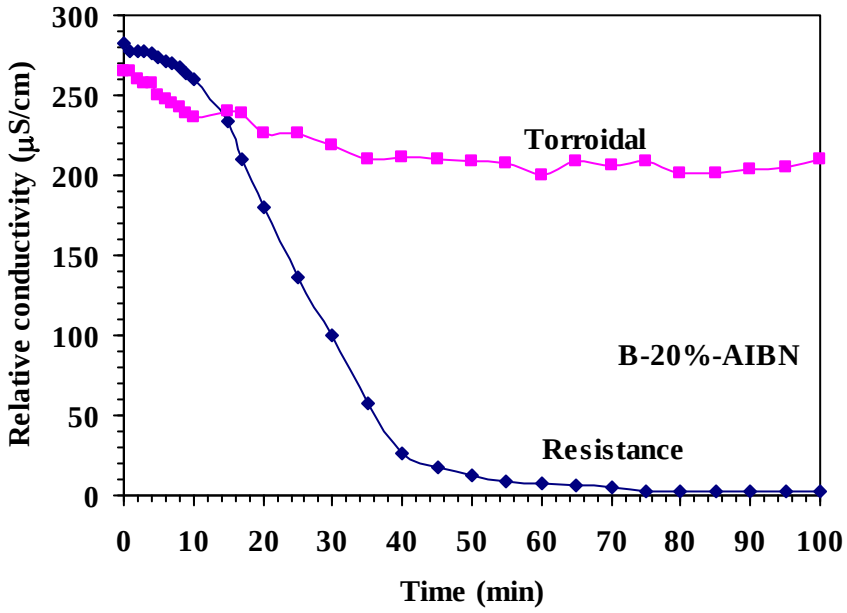

Figure 4.15: *Photograph of the viscous coagulum (top) and relative conductivity vs. time curves (bottom) obtained during the batch polymerization of BMA using AIBN as initiator (Table 4.2) at 70 °C and 250 rpm.*

4.3.6 Coagulum Morphology

To obtain evidence that can prove that coagulum is adsorbed on the surfaces of the electrodes of the resistance probe in the early stages of the reactions, an emulsion polymerization was carried out using a special reactor (Figure 4.3). Recipe B-20%-5mM (Table 4.1) was chosen due to its slow reaction rate at the beginning of this reaction. The kinetic results for this reaction showed good repeatability compared with the previous results (Figure 4.4), in which the conductivity probes were used. This means that the previous conductivity curves can be fitted to the new reaction.

During this reaction, the first baffle was taken out of the reactor at 5 min. The conversion was 2.3 % and particle size was 78 nm at this time. The gold film looked clean and there was no visible coagulum present (Figure 4.16 (a)). Under SEM examination, some small white dots were found at the 500 μm scale. After changing the scale to 20 μm, coagulum was found. However, the coagulum level was very low at this point, so the effect of coagulum on the measurements of the resistance probe should be small and conductivity value obtained by the resistance probe was even a little higher than the value obtained by the torroidal probe (Figure 4.5 (a)). The second baffle was taken out of the reactor at 10 min with 8.7 % conversion and 112 nm particles. Some visible white dots were found on the film (Figure 4.16 (b)). From the SEM images, obvious plating was found. It can be seen that some individual particles were accumulated onto the previous areas of the electrodes where plating occurred. However, in Figure 4.5 (a), it is hard to observe any major difference between the two

conductivity curves at 10 min. Since the resistance curve shown in Figure 4.5 (a) was measured using the commercial resistance probe, the results indicate that the sensitivity of the commercial resistance probe is not sufficient. The third baffle was taken out at 16 min when the conversion was 20.0 % and particle diameter was 155 nm. White plating on the film can be seen clearly (Figure 4.16 (c)). The SEM images show that the amount of coagulum grew. At this time, the conductivity curve obtained using the resistance probe sharply decreased, and an obvious divergence between the two conductivity curves can be seen easily.

AFM imaging was also carried out to visualize the coagulum morphology. Because the coagulum level was very low for the first sample and the scanning area of AFM was small, it is hard to find coagulum in this case. On the other hand, because coagulum increased significantly for the third sample and the plating layer was thick, a good image cannot be obtained under AFM due to the small distance of the movement for the AFM tip. The second sample was found to be suitable to obtain good images and the results are shown in Figure 4.17. From the height image (Figure 4.17 (a)) and phase image (Figure 4.17 (b)), it can be seen that the surface of this area was covered by coagulum. The height image also shows that the plated surface is not smooth and the 3D image (Figure 4.17 (c)) shows that the highest level of plating is over 400 nm.

Differing from the picture of plating shown previously (Figure 3.3), which

was taken at the end of the reaction, the samples for the SEM and AFM images were obtained at early stages of the reaction. The results clearly show that coagulum can be formed in these early stages. This provides direct evidence that the divergence between the two conductivity curves is caused by coagulum, which proves that the hypothesis of this research is correct.

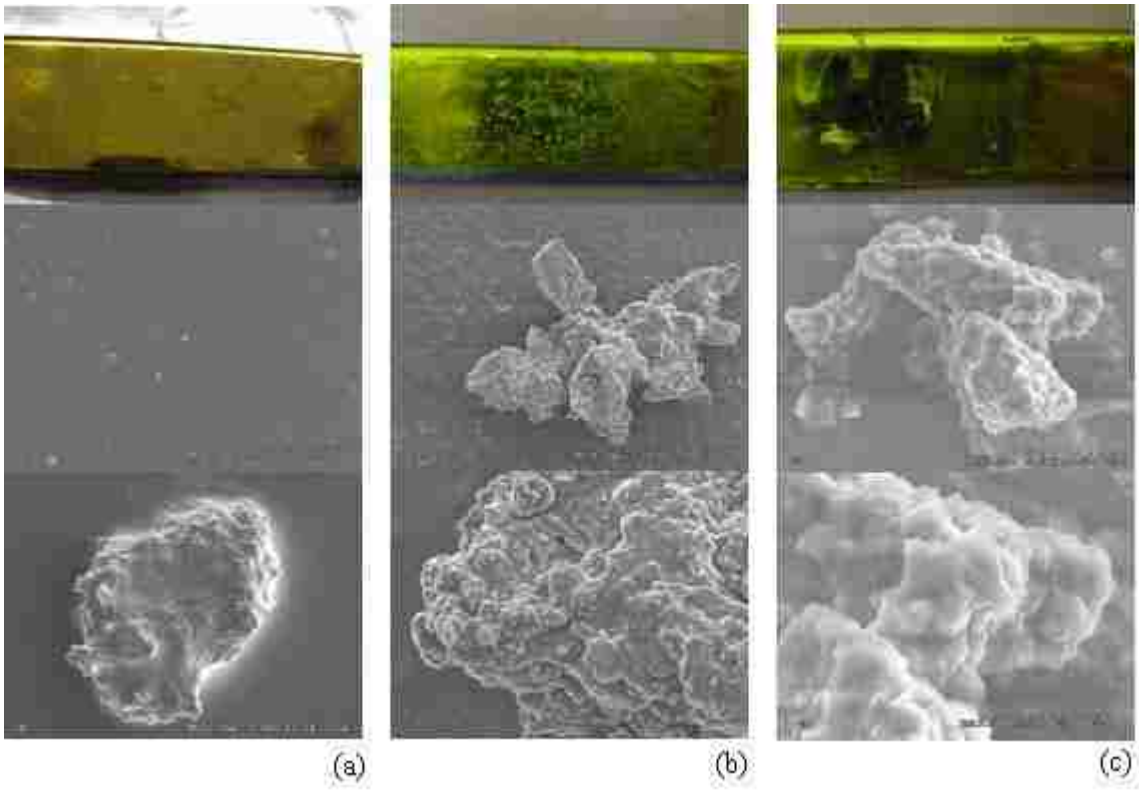

Figure 4.16: *Pictures and SEM images of the gold films taken out of the reactor at early stages of the BMA emulsion polymerization reaction: (a) 5 min with 2.3 % conversion, (b) 10 min with 8.7 % conversion, and (c) 16 min with 20.0 % conversion.*

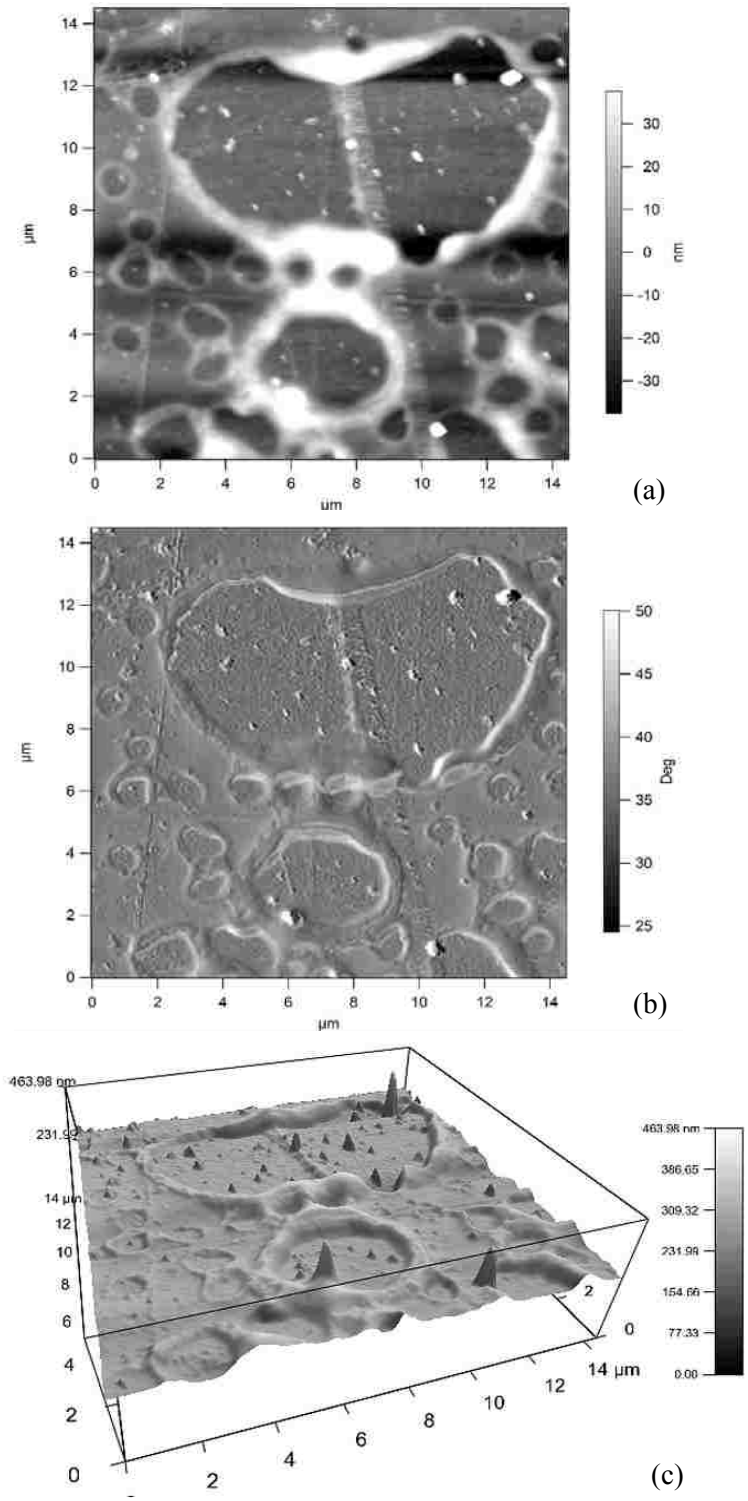

Figure 4.17: *AFM images of the gold film taken out of the reactor at 10 min: (a) height image, (b) phase image, (c) 3D image.*

4.4 Conclusions

Online conductivity measurements were carried out during the batch emulsion polymerizations (20 % solids content) of BMA. Six recipes were used with the various SLS concentrations. The commercial resistance probe showed poor repeatability and limited sensitivity in some cases. Therefore, a homemade resistance probe was built and used to measure conductivity during the reactions. The new results were much more reliable than the old results. The blender test and turbidity measurements were also carried out to check latex stability. The final conductivity ratio (R/T) between the two probes was correlated to latex stability. The results indicate that there exists a linear relationship between them, which is similar to the results shown previously in Chapter 3. Therefore, online conductivity measurements can be used to predict latex stability in this system. The reason for the second increase was also investigated and the results show that this increase is related to the disappearance of the monomer droplets. SEM and AFM were used to investigate the morphology of coagulum formed in the early stages of an emulsion polymerization reaction. The results show that coagulum may be formed at a very low conversion on the gold film surfaces. This provides a direct and strong evidence to prove that the divergence between the two conductivity curves is caused by coagulum.

4.5 References

[1] A. F. Santos, E. L. Lima, J. C. Pino, C. Graillat and T. Mckenna, *J. Appl. Polym. Sci.*, **90**, 1213 (2003).

[2] K. Fontenot and F. J. Schork, *J. Appl. Polym. Sci.*, **49**, 633 (1993).

Chapter 5
Online Conductivity Measurements in Semi-Batch Emulsion Polymerizations of BMA

5.1 Introduction

Semi-batch (also referred to as semi-continuous) emulsion polymerization is the most important process used to produce emulsion polymers in industry. Differing from batch processes, in which all the reactants are completely added to the reaction vessel at the start of the polymerization, only part of the total reaction formulation is introduced at the beginning of the reaction in semi-batch processes and the remainder is added during the course of the polymerization[1]. Because any proportion of any reaction component can be added at any time, the semi-batch emulsion polymerization is very versatile and widely used to control latex and polymer properties, such as particle size, reaction rate and copolymer composition.

There are normally two stages in a semi-batch emulsion polymerization: seed stage and feed stage. It is typical to add 5-10 % of the total monomer and to allow complete conversion of this monomer in the seed stage. The remaining monomer is added to provide the growth of the formed particles in the feed stage. Other components may also be added during the feed stage, such as initiator and surfactant.

The seed stage can be run *in situ* or as a separate batch. The advantage of this process is to separate particle nucleation from particle growth, which is beneficial to control the particle size and particle size distribution. Moreover, the surfactant concentration is also a key factor to control particle size and particle size distribution. If the surfactant concentration is too high, new particles can be formed during the addition of monomer resulting in a broad particle size distribution. This is known as secondary nucleation and is usually undesirable. On the other hand, if the surfactant concentration is too low, coagulation of polymer particles will occur, which should also be avoided. Therefore, the surfactant concentration is a critical parameter that affects the particle size distribution as well as latex stability in semi-batch processes.

The monomer feed rate is another important aspect, which may affect the semi-batch emulsion polymerization process. When the monomer concentration is saturated in the polymer particles, the polymerization will reach the maximum rate R_{max}. If the monomer feed rate is faster than R_{max}, the excess monomer will accumulate in the reactor and monomer droplets will be present. Under these monomer-flooded conditions, the reaction rate equals R_{max} and the semi-batch polymerization has no major differences from the equivalent batch polymerization. On the other hand, if the monomer feed rate is slower than R_{max}, the concentration of monomer in the particles will fall below the saturation value and no monomer droplets will exist in the reactor. This situation is known as monomer-starved conditions. In order to take full advantage of semi-batch emulsion polymerizations, it

is necessary to use monomer-starved conditions. The instantaneous conversion is measured in order to judge whether the monomer-starved conditions are achieved. Normally, if the instantaneous conversion is above 80 %[1], the semi-batch reaction can be considered to be under monomer-starved conditions.

To obtain a better understanding of the influence of the key parameters on the particle growth and latex properties during the feed stage of emulsion polymerization, many studies have been carried out. Chern and Hsu[2] investigated the effect of different types of surfactant on the particle nucleation and growth in semi-batch emulsion copolymerizations of methyl methacrylate (MMA) and butyl acrylate (BA). The relationship between the number of particles and surfactant concentration was established. Castelvetro et al.[3] studied the evolution of the main colloidal parameters in the seeded, starved-feed, semi-batch emulsion polymerizations of BMA. The surfactant/monomer feed ratio was optimized to achieve a target particle size. Moreover, the surface tension and the particle surface coverage were correlated with secondary nucleation or particle aggregation. Sajjadi[4] investigated the influence of the rate of the feed addition on the particle formation and coagulation in the seeded semi-batch emulsion polymerizations of BA. A quantitative correlation was found between the surface tension and particle surface coverage (θ). If θ was less than 0.25, coagulum would be formed. On the other hand, if θ was more than 0.55, secondary nucleation would occur. If θ was between these two values, the number of particles remained constant and stable latexes were obtained.

In the previous chapters, the results showed that online conductivity measurements can be used to predict latex stability during the batch emulsion polymerizations. Since the semi-batch emulsion polymerizations are important and widely used in industry, this method was used in a semi-batch system in this chapter. The purpose is to investigate whether this method can be used to predict latex stability in the semi-batch system. If this method works, it will provide more practical meanings for this research.

5.2 Experimental

5.2.1 Materials

10 ppm monomethyl ether of hydroquinone (MEHQ) inhibitor was removed from BMA (Sigma-Aldrich) by passing the monomer through an inhibitor-removal column (Sigma-Aldrich). Sodium lauryl sulfate (SLS, Fisher Scientific), sodium bicarbonate ($NaHCO_3$, Sigma-Aldrich), and potassium persulfate ($K_2S_2O_8$, Sigma-Aldrich) were used as surfactant, buffer, and initiator, respectively. All of these chemicals were used as received. Deionized (DI) water was used for all experiments.

5.2.2 Semi-Batch Emulsion Polymerizations of BMA

Semi-batch emulsion polymerizations of BMA were carried out in a 1 L reactor without baffles at 70 °C with stirring at 250 rpm using a 7 cm diameter Rushton impeller with 6 blades. Both the homemade resistance and torroidal probes were used to measure conductivity during the polymerizations. The reactor

wasblanketed with nitrogen during the polymerizations to prevent O_2 inhibition. $K_2S_2O_8$ initiator was added as an aqueous initiator solution (1.7 mM) into the reactor to start the reaction. During the reactions, the conductivity values from the two probes and the temperature in the reactor obtained from a sensor in the torroidal probe were recorded manually. Samples were taken at periodic intervals to measure the instantaneous and overall conversions by gravimetry.

The recipes for all the reactions are shown in Table 5.1. The seed stages of each reaction were the same; these were run for 30 minutes to achieve more than 98 % conversion and were formulated for latexes with 20 % solids content. The SLS concentration of the seed stage was 20 mM. The use of this recipe as the seed stage is based on the consideration of the online conductivity measurements and latex stability. First, the latex prepared during the seed stage should have good stability. If an unstable latex is applied as the seed, it would be hard to judge the reason for instability of the final latex prepared by the semi-batch process. Moreover, if the latex is not stable at the end of the seed stage, which may cause a divergence between the two conductivity curves, it would be difficult to analyze the information of the changes in the conductivity curves during the feed stage. Second, if the SLS concentration is too high in the seed stage, the final latex may have good stability even though no SLS solution is added during the feed stage. Therefore, it would be impossible to distinguish the differences in the stability of the final latexes prepared using the different recipes. Based on these considerations, recipe B-20%-20mM used

in Chapter 4 (Table 4.1) was chosen as the recipe for the seed stage and the amount each component was scaled down. The latex prepared using this recipe has good stability. Moreover, the two conductivity curves are close at the end of this reaction, which means that any further differences between the two conductivity curves are caused by changes in the properties of the latexes during the feed stage.

The feed stage was run for 137 minutes, where the solids content was increased from 20 to 40 %. The only difference in the seven reactions was the amount of SLS added during the feed stage. In the first reaction (Semi-0.7%), no SLS was added. In the other six reactions, the amount of added SLS was increased from 0.807 to 8.750 g. So the total weight ratios (including the seed stage and the feed stage) between SLS and the monomer of the seven reactions were varied: 0.7, 1.0, 1.4, 1.7, 2.0, 2.5, and 3.6 %, respectively. The monomer and SLS solution were fed in two different streams using two syringes pumps during the feed stage. The monomer feed rate was 1.5 g/min (1.678 mL/min), which was designed based on Krishnan's research[5]. In his research, monomer-starved conditions were achieved using this monomer feed rate. The SLS solution feed rate was 0.511 mL/min.

Table 5.1: Recipes Used for the Semi-Batch Polymerizations of BMA at 70 °C

	Ingredient	Semi-0.7%**	Semi-1.0%	Semi-1.4%	Semi-1.7%	Semi-2.0%	Semi-2.5%	Semi-3.6%
Seed Stage	DI water	380 g						
	BMA	95 g						
	SLS*	2.193 g (20.0 mM)						
	$K_2S_2O_8$*	0.178 g (1.7 mM)						
	$NaHCO_3$*	0.178 g (5.5 mM)						
	Time	30 min						
Feed Stage	DI water	70 g						
	BMA	205 g						
	SLS	--	0.807 g	1.882 g	2.907 g	3.807 g	5.307 g	8.750 g
	Time	137 min						

* Concentration based on water phase

** In the notation “Semi-0.7%”, Semi stands for semi-batch emulsion polymerization, 0.7% stands for the total weight ratio of BMA to SLS.

5.2.3 Characterization

The particle diameter of the latexes obtained from the reactions was measured by capillary hydrodynamic fractionation (CHDF-2000, Matec Applied Sciences). The principle measurement of CHDF is based on particle separation by size due to the radial velocity profile occurring in flow through a capillary. Because larger particles are not able to approach the capillary walls and smaller particles approach closer to the capillary walls, the larger particles will elute first, followed by the smaller particles[6]. The employed 20 μm diameter capillary can be used to measure particle sizes between 15 and 600 nm. The 1X-GR-500 solution was diluted to 10 wt% with DI water and used as eluant. The latex samples were diluted to a solids content between 0.5 and 3 wt% prior to analysis in order to prevent blockage of the capillary. Approximately 45 μL of the diluted latex samples were injected into the 25 μL sample loop.

5.2.4 Latex Stability Tests

The blender test was used to analyze the mechanical stability of the final latexes prepared by the semi-batch emulsion polymerizations (Table 5.1). Due to the high solids content (40 %) of these latexes, the test procedure for these samples was different from the one used in Chapters 3 and 4, which was used for the latexes of 5 % and 20 % solids content. In the case of 40 % solids content, the blender test was run only 5 minutes instead of 20 minutes. 200 g of the latex sample was directly used for this test without any dilution. Because water was trapped in the coagulum, it was hard

to isolate the water phase from the samples after this test was complete. Under this condition, the sample obtained after the blender test was washed using DI water under agitation with a stirring bar in order to remove the entrapped and uncoagulatedparticles, which were adsorbed on the surfaces or inside of the coagulum. Then, a 100 μm mesh was used to filter out the coagulum. The mesh holding the coagulum was placed in an oven (90 ºC) for 24 h to dry, removing any entrapped water. The percent coagulum was calculated based on the dried coagulum weight and was used to represent the mechanical stability of the latexes.

Turbidity measurements were also carried out to estimate the electrolyte stability of the final latexes prepared by the semi-batch emulsion polymerizations. The procedure was the same as used previously. The details were described in Chapter 3 (3.2.4).

5.3 Results and Discussion

5.3.1 Semi-Batch Emulsion Polymerization of BMA

Seven semi-batch emulsion polymerizations of BMA were run, where only the amount of SLS was varied during the feed stage (Table 5.1). The results of the fractional instantaneous and overall conversions for reaction Semi-0.7% are shown in Figure 5.1. From this figure, it can be seen that the fractional instantaneous conversions were more than 0.95, which indicated that this semi-batch reaction was run under monomer-starved conditions. Moreover, high overall conversions were

achieved, which meant that the reaction was run as designed. The particle size and particle size distribution are shown in Table 5.2. Because the only difference among these reactions is the variation of the added SLS amount during the feed stage, the particle size of these latexes should theoretically be the same. The results show that the particle size of these latexes varies over a small range (80 ± 3 nm). Furthermore, the particle size distribution (PDI) is narrow. These results demonstrate that there is no secondary nucleation during the feed stage, which means that the added SLS amount is not too high. After these reactions were complete, no coagulum was found in the latexes. The coagulum adsorbed on the surfaces of the probes, impeller, and reactor was negligible, so these semi-batch reactions were run successfully. Moreover, the similar particle sizes and narrow size distributions of these latexes are beneficial for the theoretical calculation of latex stability based on the DLVO theory because the effect of particle size on the potential energy is removed when the stability of these latexes is compared. This will be shown and discussed later (Chapter 7).

Table 5.2: Particle Size Obtained from the Latexes Produced in Semi-Batch Emulsion Polymerizations of BMA (Table 5.1)

	D_n (nm)	D_V (nm)	PDI
Semi-0.7%	95	107	1.13
Semi-1.0%	110	117	1.06
Semi-1.4%	95	107	1.12
Semi-1.7%	111	118	1.06
Semi-2.0%	102	111	1.09
Semi-2.5%	97	109	1.12
Semi-3.6%	96	108	1.12

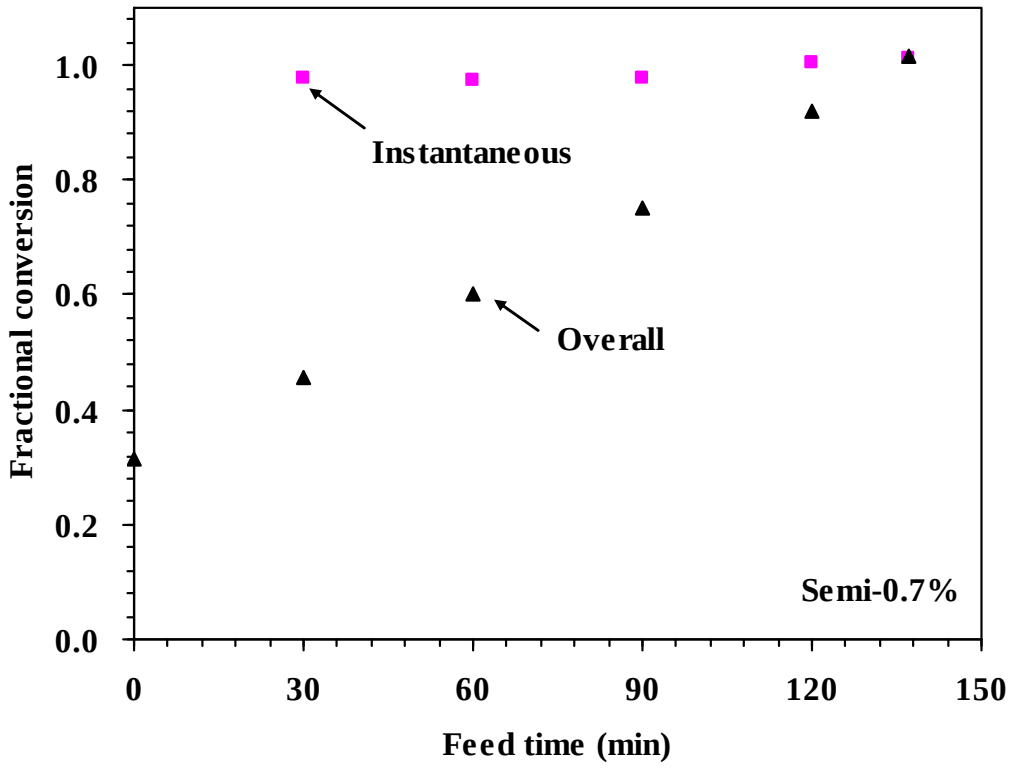

Figure 5.1: *Fractional instantaneous and overall conversions vs. feed time for reaction Semi-0.7% (Table 5.1).*

5.3.2 Online Conductivity Measurements

Figure 5.2 shows the conductivity changes during the reaction Semi-0.7%. It can be seen that the two conductivity curves are almost overlapped at the end of the seed stage. At the very beginning of the feed stage, the conductivity curve obtained using the homemade resistance probe exhibited an obvious decrease in conductivity and the curve obtained from the torroidal probe showed a small increase. These phenomena resulted from two different reasons. The former should be related to the processes of diffusion and swelling of monomer in the polymer particles. At the end of the seed stage, there was no monomer remaining; at the beginning of the feed stage, the monomer was introduced in the system and the presence of the monomer droplets influenced the measurements of the homemade resistance probe as discussed in Chapter 4 (4.3.4.1) since the monomer droplets act as insulators. As the monomer diffused through the aqueous phase, swelling the latex particles, and being consumed in the polymerization reactions, the effect on the measurements of the homemade resistance probe was eased because the monomer feed rate was slower than the monomer reaction rate. So the conductivity curve obtained from the homemade resistance probe exhibited an increase in conductivity following the first decrease. Another experiment was carried out to illustrate these processes (Figure 5.3). At room temperature, 10 g of BMA monomer was added to 500 g of the latex B-20%-30mM under agitation. Before this addition of monomer, the conductivity values obtained from the two probes were similar. Both curves showed a decrease after the addition. However, the curve obtained from the torroidal probe only decreased slightly while a

sharp decrease occurred for the one obtained from the homemade resistance probe. Because the torroidal probe works on induction, the monomer droplets do not affect the measurements of this probe, which means that the slight decrease in conductivity obtained from this probe showed the true decrease in conductivity by the addition of monomer. However, the conductivity curve obtained from the homemade probe decreased to a very low value and then increased gradually as time passed. This showed the effect of the transfer of monomer from the droplets to the polymer particles. During this process, the number of monomer droplets decreased as the monomer swelled the particles, so the effect on the measurements of the homemade resistance probe decreased and the measured values increased. When the added monomer was totally dissolved in the particles, the monomer droplets disappeared from the aqueous phase, which caused the two conductivity curves to overlap. The process took 40 minutes. When 10 g more monomer was added, a similar process occurred. Because the monomer concentration reached saturation in the particles, some monomer droplets remained after 100 min and the conductivity values obtained from the homemade resistance probe were lower than the true values.

On the other hand, the increase in the conductivity curve obtained from the torroidal probe at the very beginning of the feed stage was caused by a change in the liquid volume. Because the liquid level in the seed stage just covered the head of the torroidal probe, which is required to obtain correct measurements of this probe, at the beginning of the feed stage, a small change in the liquid volume would affect the

magnetic field, which would result in a change in the conductivity measurements of the torroidal probe. Therefore, the divergence, which occurred at the very beginning of the feed stage, was caused by the effect of the changes in the reactive system on the measurements of the probes and was not related to plating or latex stability.

The results of the other six reactions are shown in Figure 5.4. From these figures, it can be seen that the changes in the amount of SLS used in these reactions affected the shapes of the conductivity curves. For reactions Semi-0.7% and Semi-1.0%, the divergence between the two conductivity curves occurred early. However, during these two reactions it was hard to judge when the divergence occurred due to the interruptions on the measurements at the beginning of the feed stage, which was discussed before. For reactions Semi-1.4%, Semi-1.7%, and Semi-2.0%, this divergence occurred later in the polymerization and the degree of the divergence became smaller. For reactions Semi-2.5% and Semi-3.6%, there was no major difference between the two conductivity curves obtained at the end of the reactions. These results are similar to the ones obtained in the batch emulsion polymerization systems as shown in Chapters 3 and 4.

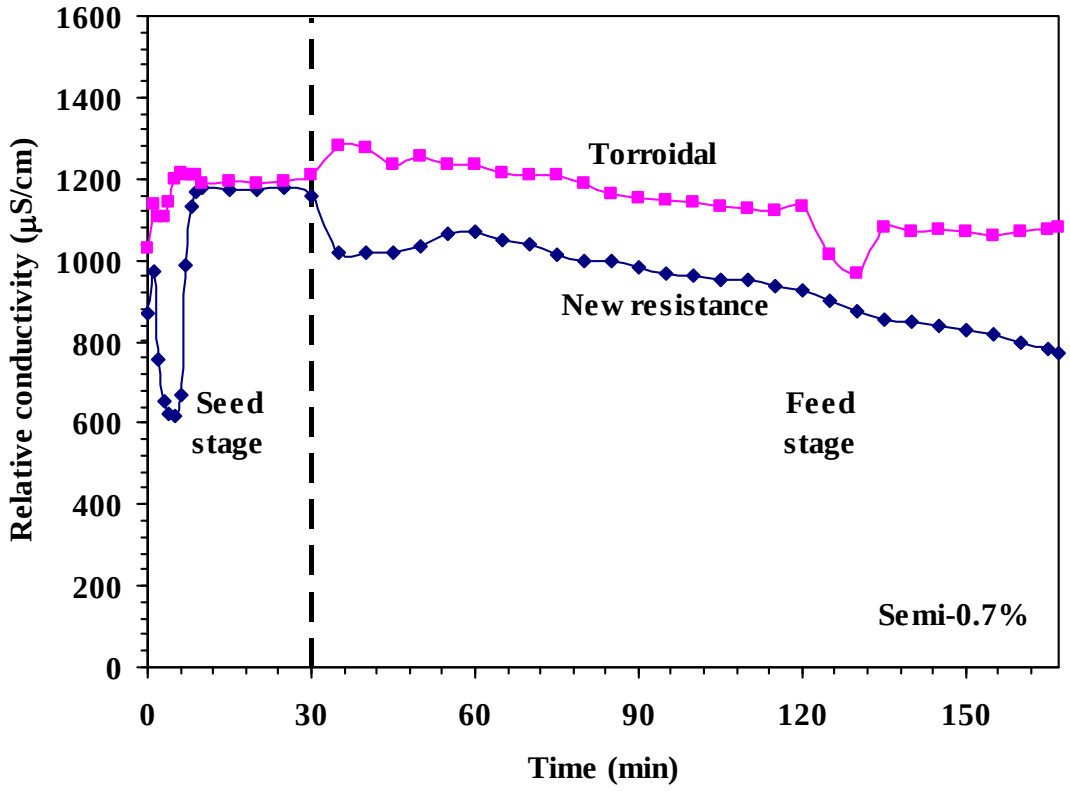

Figure 5.2: *Relative conductivity vs. time curves for reaction Semi-0.7%.*

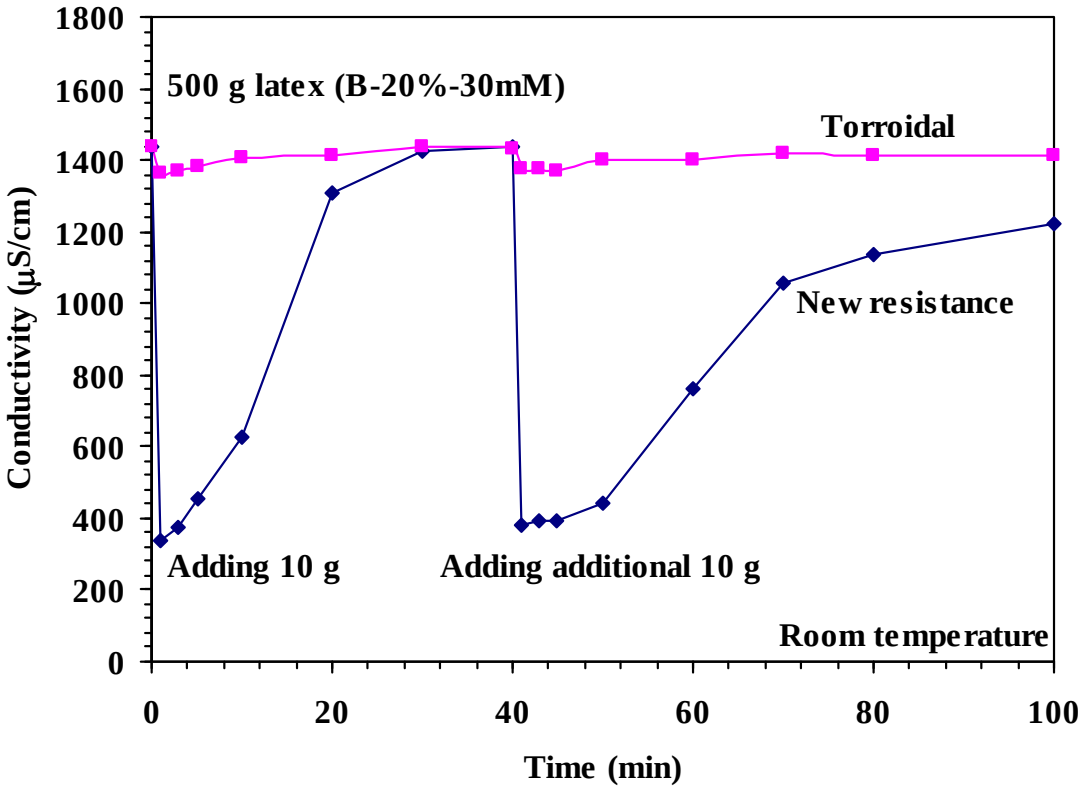

Figure 5.3: *Effect of monomer droplets on the conductivity measurements.*

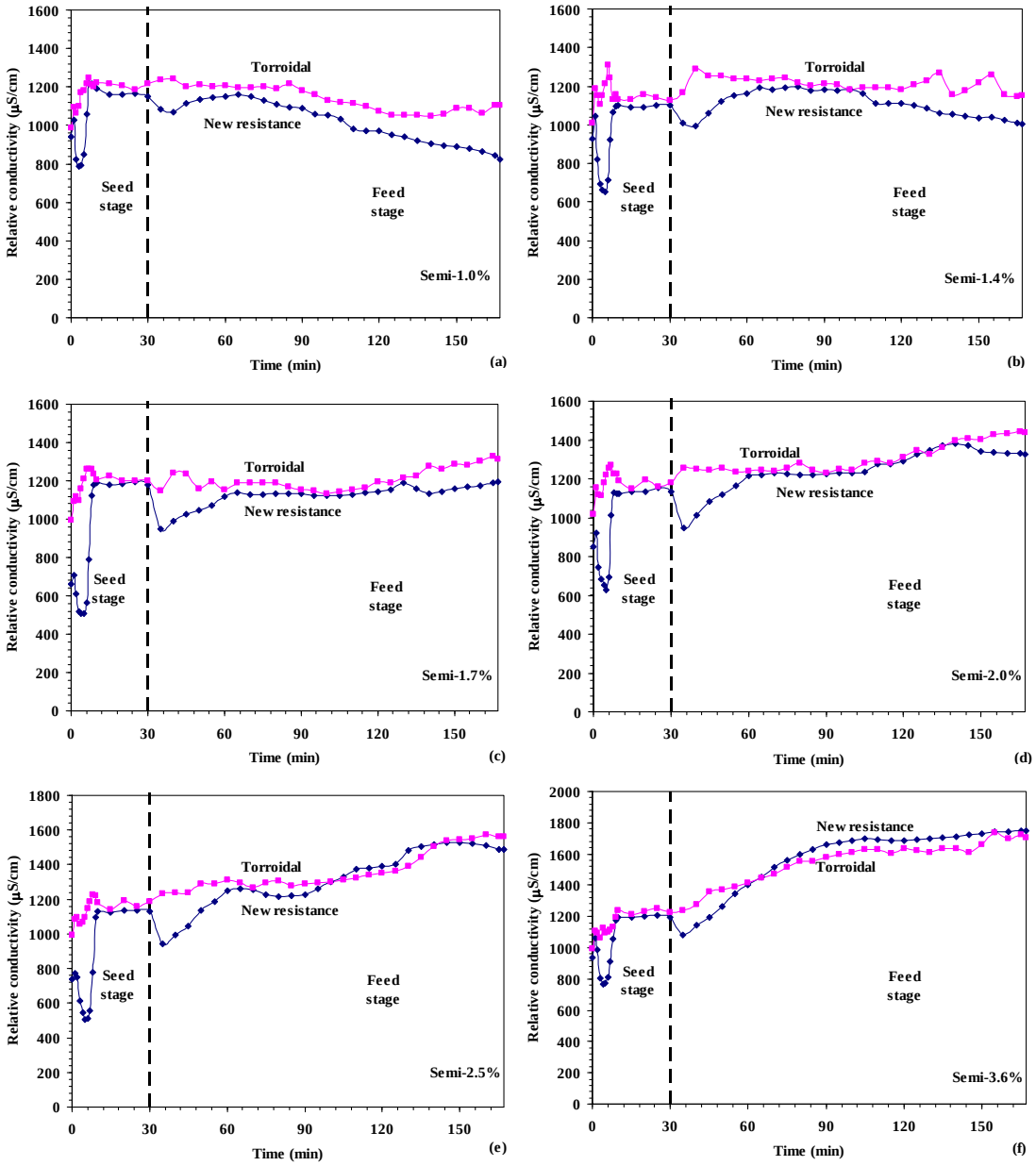

Figure 5.4: *Relative conductivity vs. time curves for the other six reactions listed in Table 2: (a) Semi-1.0%, (b) Semi-1.4%, (c) Semi-1.7%, (d) Semi-2.0%, (e) Semi-2.5%, and (f) Semi-3.6%.*

To correlate the conductivity curves to latex stability, the final conductivity ratio (R/T) between the two curves was calculated. However, the degree of divergence shown in Figure 5.4 was not as significant as those found in the batch emulsion polymerization systems (Chapters 3 and 4), and the R/T values were more than 0.9 in some cases, which meant that only a small part of the electrodes was covered by coagulum. This was caused by the high viscosity of the latexes due to the high solids content (40 %). As shown in Figure 5.5 (top), viscous latexes was found on the surfaces of the combined conductivity probes at the end of the semi-batch reactions. However, most of the attachment is not plating or coagulated particles. It can be removed easily by rinsing and the degree of the actual plating is not high (Figure 5.5 (bottom)). Because the adsorbed viscous latexes may work as a membrane and prevent the further deposition on the surfaces of the electrodes, the differences in divergence among these reactions were not as significant as shown previously in Chapters 3 and 4.

Since the R/T values are relatively high as discussed above, it is possible that the divergence is caused by the experimental errors instead of plating. To test this, another ratio was also calculated. After each semi-batch reaction, the electrodes were rinsed with DI water and put into a standard NaCl solution. The conductivity was then recorded using the homemade resistance probe. After soaking in toluene and cleaning using acetone and DI water, this probe was again used to measure conductivity in the same electrolyte solution. The ratio between the measured conductivity values before

and after cleaning was calculated. To distinguish between the two types of conductivity ratios, the one between the final values of the two probes at the end of the semi-batch reactions was termed the dynamic ratio; the other between the conductivity values of the same solution measured for the “dirty” and “clean” homemade resistance probe is called the static ratio. All of the results are listed in Table 5.3. It can be seen that the values are close. Because it is clear that the static ratio is caused by plating on the surfaces of the electrodes, which causes the measured conductivity values to be smaller than the true conductivity values, it proves that the divergence during the semi-batch reactions is caused by plating instead of experimental error.

Table 5.3: Dynamic Ratio and Static Ratio of the Conductivity Values

Reaction	Dynamic ratio	Static ratio
Semi-0.7%	0.715	0.689
Semi-1.0%	0.742	0.711
Semi-1.4%	0.871	0.857
Semi-1.7%	0.912	0.914
Semi-2.0%	0.924	0.916
Semi-2.5%	0.954	0.952
Semi-3.6%	1.026	0.964

Figure 5.5: *Pictures of the combined conductivity probe taken right after the reaction Semi-0.7% (top) and after rinsing and drying (bottom).*

5.3.3 Latex Stability Tests

The 5-minute blender test was applied to all the final latexes with 40 % solids content obtained from the semi-batch reactions (Table 5.1). The percent coagulum of each sample after this test is shown in Table 5.4. For the samples having the low amount of fed SLS (Semi-0.7% and Semi-1.0%), the results were 32.7 % and 29.5 % coagulum, which indicated that the latexes were not stable. These were not as high as imagined, since the latexes were severely coagulated on the bottom of the blender after several seconds of agitation during the test and looked fully coagulated. For the samples having the high amount of fed SLS (Semi-2.5% and Semi-3.6%), lots of foam was formed during the test and the liquid could be mixed throughout the entire testing time. Little coagulum was found attached to the surfaces of the blade and no coagulum was evident in the latex. These two samples could survive under the high shear force applied in the blender test. Figure 5.6 shows the comparison of the blender blade before and after the blender test using samples Semi-1.0% and Semi-2.5%. The obvious difference in the amount of coagulum stuck on the surface of the blade can be seen, which illustrates the difference in the stability between the two samples. The other three samples (Semi-1.4%, Semi-1.7%, and Semi-2.0%) exhibited intermediate results for the percent coagulum.

Turbidity measurements were used to estimate the electrolyte stability of these latexes and the surface coverage of these latexes was also measured. All of these results are summarized in Table 5.4.

Table 5.4: Percent Coagulum, Critical Coagulum Concentration (ccc) and Surface Coverage of the Latexes Prepared by the Semi-Batch Emulsion Polymerizations (Table 5.1)

Latex	Percent coagulum (%)	ccc (M)	Surface coverage (%)
Semi-0.7%	32.7	0.471	14.0
Semi-1.0%	29.5	0.566	20.5
Semi-1.4%	12.7	0.590	27.3
Semi-1.7%	11.2	0.675	36.6
Semi-2.0%	4.9	0.741	40.9
Semi-2.5%	0.5	0.777	50.9
Semi-3.6%	0.2	0.787	73.3

(a) (b)

Figure 5.6: *Comparison of the blender blade after the blender test (left) and before the test (right)***:** *(a) latex Semi-1.0% and (b) latex Semi-2.5%.*

The correlation between the conductivity curves and latex stability was determined as previously described. Because the conductivity ratio (R/T) measured in the static way (static ratio in Table 5.3) is more reliable, this data was used to represent the degree of plating on the surfaces of the electrodes of the homemade resistance probe. The results are shown in Figures 5.7 and 5.8. Similar to the previous results, there is a linear relationship between the mechanical stability and static R/T, and the electrolyte stability and static R/T. These results indicate that the online conductivity measurements can be used to predict latex stability during the course of the semi-batch emulsion polymerizations. Since the semi-batch emulsion polymerizations are widely used in industry, the results show that it is possible for this method to be applied in industrial processes.

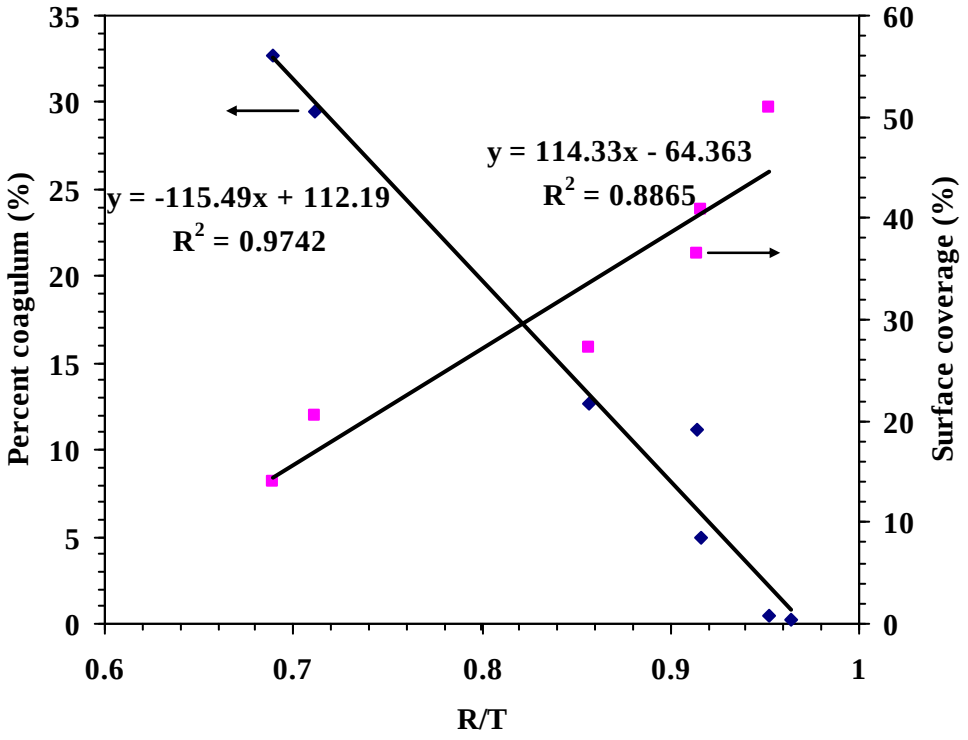

Figure 5.7: *Correlation between the percent coagulum obtained after the blender test and the final conductivity ratio (R/T), and the surface coverage and R/T.*

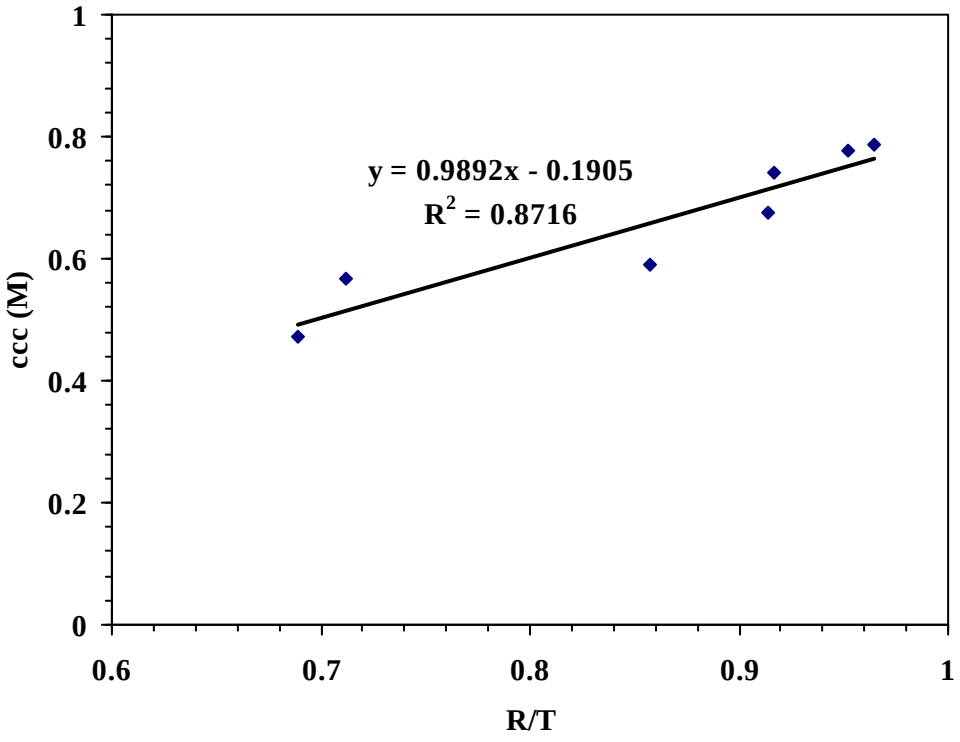

Figure 5.8: *Correlation between the critical coagulum concentration (ccc) estimated by the turbidity measurements and the final conductivity ratio (R/T).*

5.4 Conclusions

Online conductivity measurements were utilized in semi-batch emulsion polymerizations, which is the most important latex production process in industry. Seven semi-batch reactions (40 % solids content) were carried out. All reactions had the same seed stage (20 % solids content) and the amount of added SLS amount was varied during the feed stage. The divergence between the two conductivity curves occurred when the amount was of fed SLS not high enough, but the degree of the divergence in these reactions was not as significant as those obtained in the batch emulsion polymerization systems due to the high viscosity of the latexes. For reactions Semi-2.5% and Semi-3.6%, in which the SLS concentration was high compared with the amount of monomer, no obvious difference between the two conductivity curves was found at the end of the reactions. The blender test and turbidity measurements were used to detect the mechanical and electrolyte stability of these latexes. The conductivity ratio (R/T) was used to correlate the conductivity curves to latex stability. A linear relationship was found between them, which is similar to the previous results. This indicates that the online conductivity measurements can be used to predict latex stability in the semi-batch emulsion polymerizations as well as the batch emulsion systems.

5.5 References

[1] P. A. Lovell, in *Emulsion Polymerization and Emulsion Polymers*, P. A. Lovell and M. S. El-Aasser, Eds., John Wiley and Son, Chichester (1997).

[2] C. S. Chern and H. Hsu, *J. Appl. Polym. Sci.*, **55**, 571 (1995).

[3] V. Castelvetro, C. D. Vita, G. Giannini and S. Giaiacopi, *J. Appl. Polym. Sci.*, **102**, 3083 (2006).

[4] S. Sajjadi, *J. Polym. Sci. Part A: Polym. Chem.*, **38**, 3612 (2000).

[5] S. Krishnan, *Ph.D. Dissertation*, Lehigh University (2002).

[6] J. G. Dos Ramos, C. A. Silebi, *Polymer International*, **30**, 445 (1993).

Chapter 6
Online Conductivity Measurements in Batch Emulsion Polymerizations of BMA Using Mixed Surfactants

6.1 Introduction

As introduced in Chapter 1 (1.4), mixed anionic and nonionic surfactants have been widely used in industry to manufacture latex particles. For example, latexes are prepared in the presence of an anionic surfactant and a nonionic surfactant may be added in order to enhance the colloidal stability of the system. The reason for using mixed surfactants is that different types of surfactants can provide different mechanisms to stabilize particles. Anionic surfactants can work on the repulsive forces between two electric double layers surrounding the particles. In contrast, nonionic surfactants can impart two approaching particles with the steric repulsion forces. In addition, nonionic surfactants can improve the chemical and freeze-thaw stability of latexes[1].

Many studies have been carried out previously to investigate the effect of mixed surfactants on the polymerization kinetics[2,3,4] and latex stability. Since this research program only focuses on latex stability, a few papers related to this aspect are

introduced here. Mathai and Ottewill[5,6] reported that when dispersion particles were stabilized by mixtures of ionic and nonionic surfactants, the electrostatic repulsion decreased with increasing steric length of the nonionic surfactants and finally resulted in total domination by the steric stabilization. They claimed that the electrostatic contribution in the potential energy decreased because of shielding. Napper and Netchey[7] reported similar observations. Furthermore, Sung and Piirma[8] used four surfactants with variation in the ethylene oxide (EO group) chain length to investigate the steric chain length effect in the stabilization of model latexes and in the emulsion polymerizations of styrene. A switch in the stabilization mechanism from primarily electrostatic to steric stabilization was observed through coagulation tests.

The competitive adsorption of anionic and nonionic surfactants is another factor, which may affect latex stability when using of the mixed surfactants. Kronberg et al.[9,10] applied a thermodynamic model to calculate the adsorption of the mixed surfactants. Their results showed that when a small amount of Triton X-100 was added to a surface precovered with SLS, the nonionic surfactant adsorbed readily and displaced the anionic surfactant. These results were confirmed by Bolze et al.[11] using small-angle X-ray scattering (SAXS) as a tool to probe the adsorption of the mixed surfactants (SLS/Triton X-405) on the surfaces of polystyrene particles. Colombié et al.[12] studied the competitive adsorption of SLS and Triton X-405 on monodisperse polystyrene particles (92 nm) through serum replacement and ^{1}H NMR spectroscopy. They found that when the mole ratio of SLS to Triton X-405 was 1:1, Triton X-405

adsorbed preferentially if the total surfactant concentration was below 2.5 mM. However, at higher total surfactant concentrations, the particle surfaces became saturated with Triton X-405 and cooperative interactions between the two surfactants took place. An excess amount of the two surfactants was noted on the surfaces, which meant that the surfactants formed a multilayer instead of a monolayer on the surfaces. They also mentioned that the SLS molecules may adsorb in the adsorbed Triton X-405 layer, either by interacting directly with the hydrophobe of the nonionic surfactant or by lateral side chain interactions.

In this chapter, online conductivity measurements were applied in a mixed surfactant system to investigate the relationship between the conductivity curves and latex stability. The contribution of each surfactant to latex stability can also be analyzed. As in the recipes used previously, sodium lauryl sulfate (SLS) was used as the anionic surfactant. Triton X-100 was chosen as the nonionic surfactant, which has a hydrophilic polyethylene oxide group (average number of the EO groups is 9.5) and a hydrophobic group. The structure of Triton X-100 is shown in Figure 6.1. The average molecular weight of Triton X-100 is 625 g/mol. The calculated HLB value is 13.5[13], which means that this surfactant is suitable for oil-in-water emulsions. The CMC of Triton X-100 is from 0.22 to 0.24 mM[13,14]. This range is much lower than the CMC of SLS, which is around 7.8 mM. Triton X-100 is a viscous liquid at room temperature and is easily handled after being gently warmed.

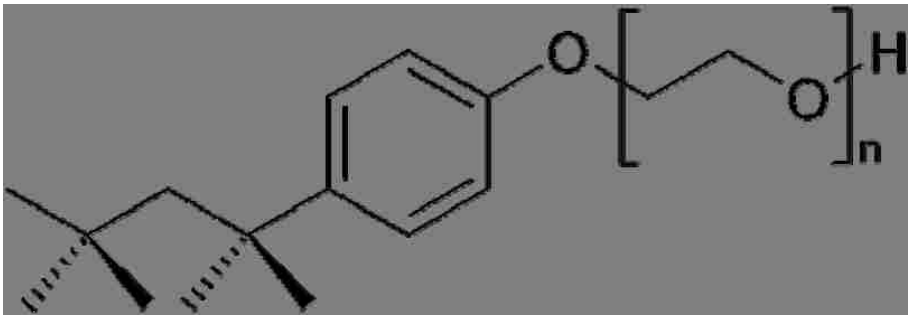

Figure 6.1: *The structure of Triton X-100.*

6.2 Experimental

6.2.1 Materials

10 ppm monomethyl ether of hydroquinone (MEHQ) inhibitor was removed from *n*-butyl methacrylate (BMA, Sigma-Aldrich) by passing the monomer through an inhibitor-removal column (Sigma-Aldrich). Sodium lauryl sulfate (SLS, Fisher Scientific), Triton X-100 (octyl phenol ethoxylate, $C_{14}H_{22}O(C_2H_4O)_n$, n = 9 or 10) (DOW Chemical Company), sodium bicarbonate ($NaHCO_3$, Sigma-Aldrich) and potassium persulfate ($K_2S_2O_8$, Sigma-Aldrich) were used as ionic surfactant, nonionic surfactant, buffer, and initiator, respectively. Citric acid ($C_6H_8O_7$, Sigma-Aldrich), *tri*-sodium citrate ($Na_3C_6H_5O_7$, EM science), diimidium bromide (Sigma-Aldrich), sodium chloride (NaCl, EM science), and chloroform ($CHCl_3$, Sigma-Aldrich) were used for colorimetry tests. All of these chemicals were used as received. Deionized (DI) water was used for all experiments.

6.2.2 Determination of the CMC

The critical micelle concentrations (CMC) of solutions of both Triton X-100 and the SLS/Triton X-100 mixture were determined at room temperature. In the mixed surfactant solutions, the weight ratio of SLS to Triton was varied 3:1, 1:1, and 1:3, respectively. To measure the CMC, the concentrated solution was pumped into 200 g of DI water at a speed of 0.1 mL/min. The changes in the surface tension of the solution were measured by a bubble tensiometer (Sensadyne 6000, ChemDyne Research Corp.) until the surface tension stabilized.

6.2.3 Batch Emulsion Polymerizations of BMA

Batch emulsion polymerizations of BMA were carried out in a 1 L reactor without baffles at 70 °C and stirred at 250 rpm using a 7 cm diameter Rushton impeller with 6 blades. Both the homemade resistance and torroidal probes were used to measure conductivity during the polymerizations. The reactor was blanketed with nitrogen during the polymerizations to prevent O_2 inhibition. $K_2S_2O_8$ initiator was added as an aqueous initiator solution (1.7 mM) to the reactor to start the reaction. During the reactions, the conductivity values obtained from the two probes and the temperature in the reactor obtained from a sensor in the torroidal probe were recorded manually. Samples were taken at periodic intervals to measure the conversion by gravimetry. The particle diameter of the latexes obtained from the reactions was measured by dynamic light scattering (Nicomp 370).

The recipes for the batch emulsion polymerizations of BMA using mixed SLS/Triton X-100 surfactants are shown in Table 6.1. The amount of each component was the same as in the previous recipes shown in Chapter 4 (Table 4.1) except for the surfactant. The mixed surfactants were used in this series of the reactions. To compare these results with those obtained previously, the total surfactant concentrations were chosen as 6, 10, 20, and 30 mM, respectively. Since the weight ratio is widely used in industry instead of the mole ratio, the weight ratio between two surfactants was varied to investigate the effect of each surfactant on latex stability. For each concentration, the weight ratios of SLS to Triton were 3:1, 1:1, and 1:3, respectively (mole ratios

were 6.5:1, 2.2:1, and 1:1.4, respectively). Moreover, the reactions using Triton X-100 as the sole surfactant were also carried out for each concentration.

Table 6.1: Recipes Used for the Batch Emulsion Polymerizations of BMA Using the Triton X-100/SLS Mixture or Triton X-100 alone as surfactant

Reaction	Ingredient (g)					
	H_2O	BMA	$NaHCO_3$	KPS	SLS	Triton X-100
B-6mM-3-1*	600	150	0.280	0.280	0.900	0.300
B-6mM-1-1					0.710	0.710
B-6mM-1-3					0.435	1.306
B-6mM-Triton**					--	2.250
B-10mM-3-1	600	150	0.280	0.280	1.500	0.500
B-10mM-1-1					1.184	1.184
B-10mM-1-3					0.726	2.177
B-10mM-Triton					--	3.750
B-20mM-3-1	600	150	0.280	0.280	3.000	1.000
B-20mM-1-1					2.368	2.368
B-20mM-1-3					1.451	4.353
B-20mM-Triton					--	7.500
B-30mM-3-1	600	150	0.280	0.280	4.500	1.500
B-30mM-1-1					3.552	3.552
B-30mM-1-3					2.178	6.531
B-30mM-Triton					--	11.250

* In the notation “B-6mM-3-1”, B stands for batch emulsion polymerization, 6mM stands for the total concentration of the mixed surfactants based on water phase, and 3-1 stands for the weight ratio of SLS to Triton X-100 (3:1).

** In the notation “B-6mM-Triton”, B stands for batch emulsion polymerization and 6mM-Triton stands for the Triton X-100 concentration (only Triton X-100 and no SLS) based on the water phase.

6.2.4 Partitioning of Triton X-100 in the Aqueous Phase

The partitioning of Triton X-100 in the aqueous phase under the conditions of the batch emulsion polymerizations of BMA was investigated. Five samples were prepared. The components of each sample are based on the reactions using 20 mM total surfactant concentration, and are listed in Table 6.2. Sample 1, which only contained SLS, was used to investigate the partitioning of SLS in the aqueous phase in the presence of BMA. On the other hand, Sample 5, in which only Triton X-100 was added, was used to estimate the partitioning of Triton X-100 in the aqueous phase. The mixed surfactants were used in the other three samples. As shown in the recipes in Table 6.1, the weight ratios of SLS to Triton X-100 were 3:1, 1:1, and 1:3, respectively. All the samples were equilibrated at 70 °C with 250 rpm mixing for 1 h. The aqueous phase of each sample was then obtained using a separatory funnel. After drying in an oven, the partitioning of Triton X-100 in the aqueous phase was calculated based on the mass balance.

Table 6.2: Components of each Sample for Triton X-100 Partitioning Measurements

Component	Sample 1	Sample 2	Sample 3	Sample 4	Sample 5
DI water (g)	100				
BMA (g)	25				
$NaHCO_3$ (g)	0.047				
SLS (g)	0.577 (20 mM)*	0.5 (17.33mM)	0.395 (13.69 mM)	0.242 (8.39 mM)	--
Triton X-100 (g)	--	0.167 (2.67 mM)	0.395 (6.31 mM)	0.726 (11.61 mM)	1.25 (20 mM)

* Concentration based on water phase

6.2.5 Surfactant Concentration Measurements

The concentration of Triton X-100 in the latex serum was measured based on the absorbance of the phenyl ring at 273 nm using UV spectroscopy (Spectronic Genesys 2 UV spectrometer). The concentration of SLS in the aqueous phase was measured using colorimetry. This method was previously used by Urquiola[15] and Colombié[16]. A 200 mL solution of diimidium bromide dye was prepared as follows. 0.1 g of diimidium bromide and 5.0 g of sodium chloride were mixed in 100 mL citrate buffer solution (a mixture of 31.5 mL of 0.1 M citric acid, 18.5 mL of 0.1 M *tri*-sodium citrate and 50 mL DI water, pH = 3.7) and diluted to 200 mL with DI water. 2.0 mL of dye solution was added to 2.0 mL of the diluted SLS solution. The sample was shaken vigorously for 2 minutes to allow the formation of the dye-SLS complex. 4 mL of chloroform was then added. The mixture was shaken for 3 minutes to extract the dye-SLS complex from the aqueous phase to the oil phase. The chloroform phase (bottom layer, purple color) was separated from the aqueous phase. The optical density was measured at 525 nm using a reference of pure chloroform by UV spectroscopy. The calibration curves used to measure the concentrations of Triton X-100 and SLS in the aqueous phase are shown in Figures 6.2 and 6.3. The results show a good linear relationship between optical density and the surfactant concentration. On the other hand, the maximum concentrations, which can be measured based on the calibration curves, are low and less than 1 mM. This means that the samples need to be diluted before the measurements if the surfactant concentrations are high and out of the calibration range.

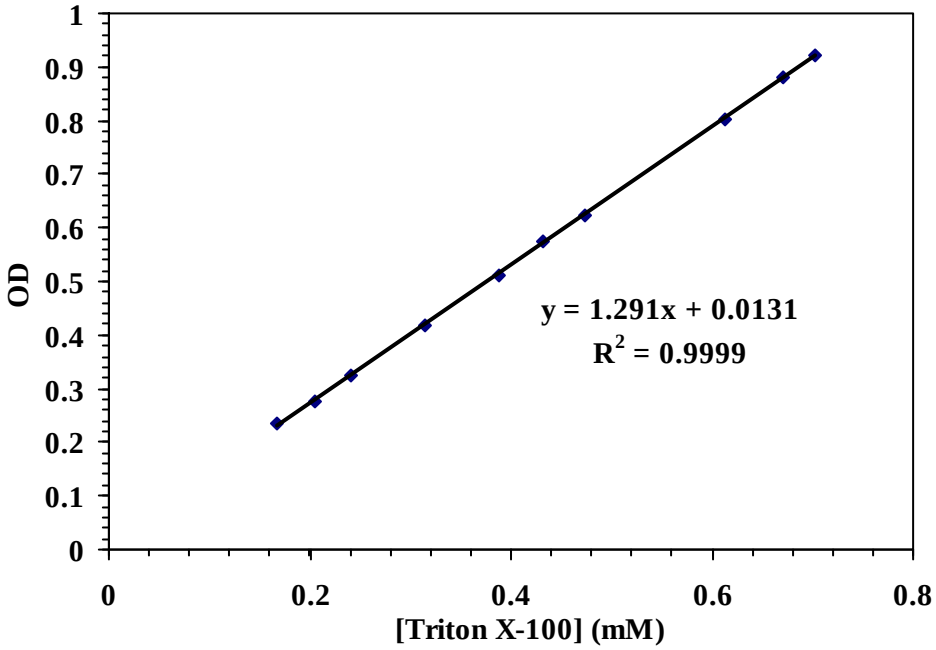

Figure 6.2: *Calibration curve used to determine the concentration of Triton X-100 in the aqueous phase using UV absorption at 273 nm.*

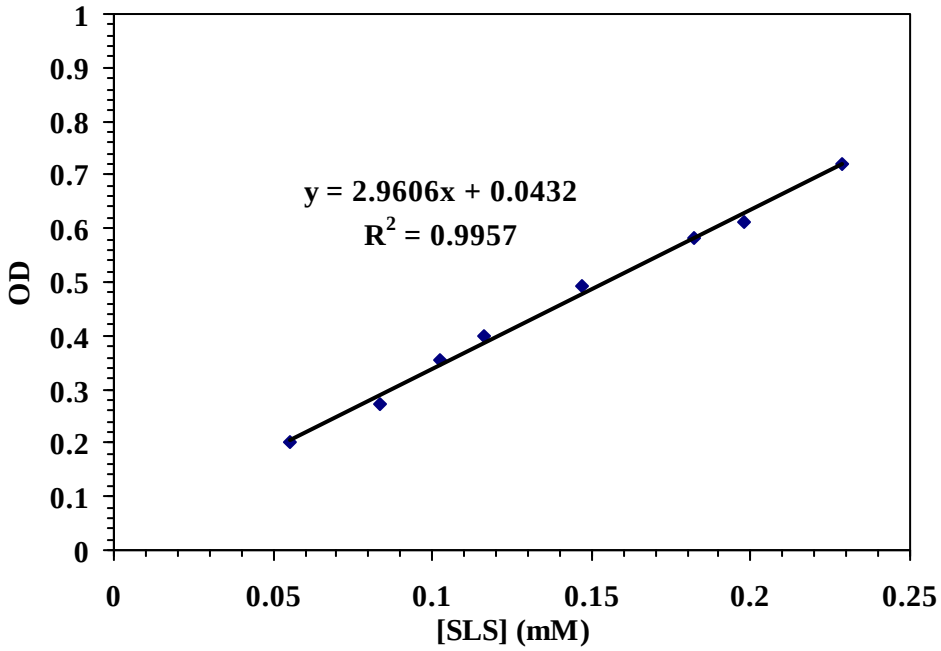

Figure 6.3: *Calibration curve used to determine the concentration of SLS in the aqueous phase using colorimetry at 525 nm (for the absorption of the diimidium bromide dye-SLS complex).*

6.2.6 Packing Area of Triton X-100 and Surface Coverage

To calculate the surface coverage by the mixed surfactants, the packing area of Triton X-100 on the surfaces of PBMA latex particles needed to be measured. A latex was cleaned using a serum replacement cell until the conductivity value of the serum was below 2 μS/cm. The particle size of the cleaned latex was 196 nm and the solids content was 6.6 %. A concentrated Triton X-100 solution (40 mM) was titrated into 150 g of cleaned latex. The dynamic surface tension was measured by a bubble tensiometer. The surface tension decreased as the concentration of Triton X-100 was increased until a plateau was reached, which means that the CMC of Triton X-100 was reached. Because the CMC was measured previously, the packing area of Triton X-100 on the particle surfaces can be estimated based on the surface tension vs. Triton X-100 concentration curve. Based on the calibration curves shown above (Figures 6.2 and 6.3), the concentration of each surfactant in the serum can be measured. The number of each surfactant on each particle then can be calculated using a mass balance. Therefore, the surface coverage of each surfactant can be estimated through the procedure shown in Chapter 3 (3.2.5).

6.2.7 Latex Stability Tests

The blender test and turbidity measurements were carried out to check the mechanical and electrolyte stability of the latexes prepared by the batch emulsion polymerizations with the mixed surfactants (Table 6.1). The procedure for the blender test was the same as used in Chapter 5 (5.2.4) and the details about the turbidity

measurements were presented in Chapter 3 (3.2.4).

6.3 Results and Discussion

6.3.1 Measurements of the CMC

First, the CMC of the Triton X-100 solution was measured using the bubble tensiometer at room temperature. The results are shown in Figure 6.4 (a). The CMC result was not exactly the same as reported in the Sigma data sheet (0.22 to 0.24 mM)[13]. From the figure, it can be seen that the surface tension curve was not a typical curve for a surfactant solution, which normally have a clear plateau after a significant decrease. In this case, the surface tension curve kept decreasing at a very slow rate. Therefore, it was hard to draw the trend lines which would determine the transition point (CMC). This figure shows two ways to draw the trend lines which results in two obviously different CMC values, so the CMC values are reported over a broad range. Because 0.24 mM was a value close to the value shown in the Sigma data sheet, this value was chosen as the CMC of Triton X-100 and used in the following discussion.

The CMC's of the mixed solutions of SLS and Triton X-100 were then measured next. The weight ratios between them were 3:1, 1:1, and 1:3, respectively. The results are shown in Figure 6.4 (b), (c), and (d). The CMCs of these three solutions are 2.0, 1.6, and 0.6 mM, respectively. From these results, it can be seen that the CMC decreased with the increase in the ratio of Triton X-100 to SLS. The CMC decreased from around 7.8 mM, the CMC of the SLS solution at room temperature, to

2.0 mM even though the number of SLS molecules was still dominant in the mixture (the weight ratio is 3:1). To illustrate the interactions between the two kinds of surfactants, the mole ratio between them was calculated and the relationship between the CMC and mole ratio of Triton X-100 in the mixed surfactants is plotted in Figure 6.5. There is a logarithmic relationship between them. This indicates that adding a small amount of Triton X-100 to the SLS solution can significantly change the CMC of the solution. This is caused by the interaction between two different kinds of surfactant molecules (Figure 6.5). Because the Triton X-100 molecule has no charge and is just a long chain, it can enter the space between two SLS molecules and decrease the repulsive forces between them[17]. This results in close packing among the surfactant molecules. So the formation of a micelle needed much fewer molecules compared with the SLS solution, and the CMC decreased significantly. Actually, the curve shown in Figure 6.5 is similar to the results obtained by Kronberg et al.[10]. Based on a thermodynamic model, they theoretically calculated the changes of the CMC values as a function of the mole fraction of NP-EO_{10} (nonylphenol ethoxylates) in the mixture of SLS and NP-EO_{10}.

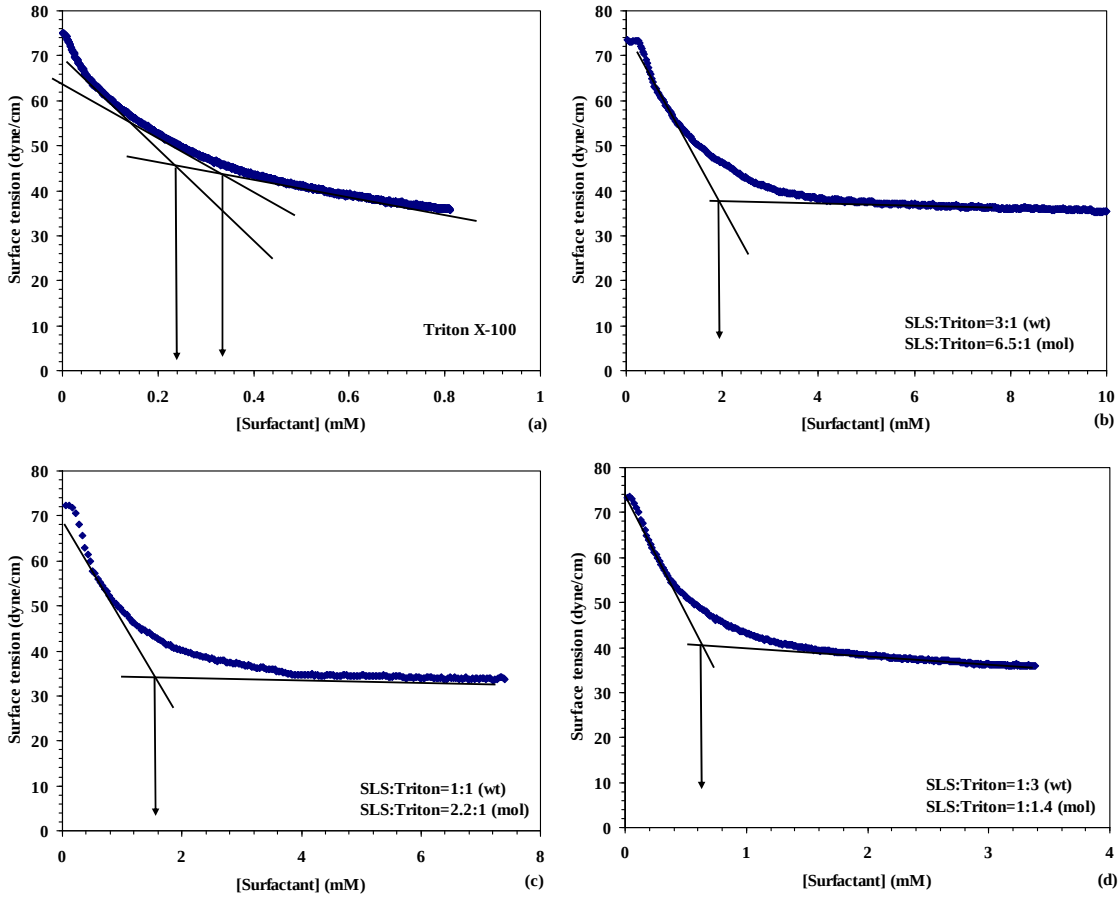

Figure 6.4: *Relationship between surface tension and the surfactant concentration: (a) Triton X-100 solution, (b) SLS/Triton X-100 solution (weight ratio 3:1), (c) SLS/Triton X-100 solution (weight ratio 1:1), and (d) SLS/Triton X-100 solution (weight ratio 1:3).*

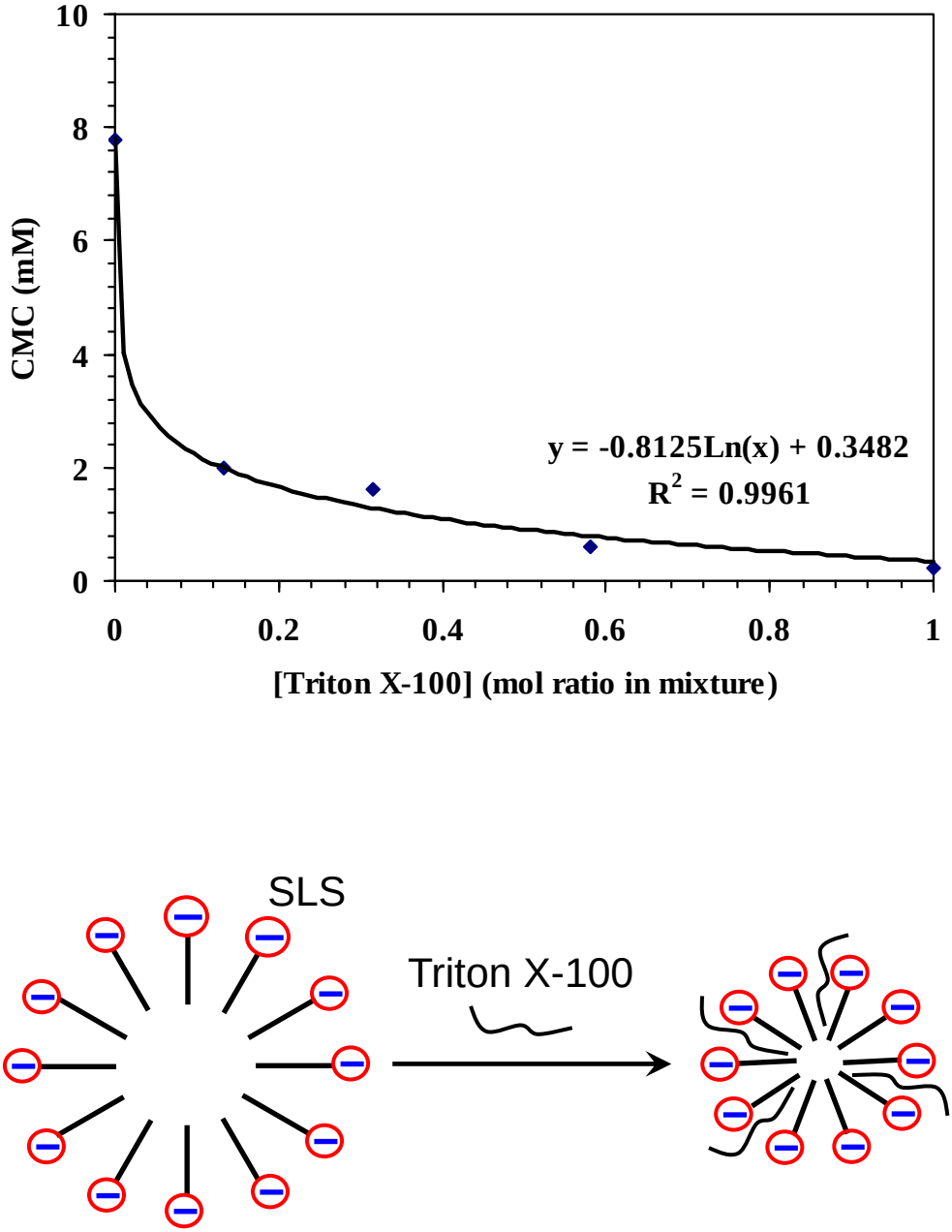

Figure 6.5: *Relationship between the CMC and the mole ratio of Triton X-100 in the mixed surfactant solutions (top) and the effect of Triton X-100 molecules on the formation of micelles in the SLS solution (bottom).*

6.3.2 Batch Emulsion Polymerizations of BMA

The batch emulsion polymerizations of BMA using SLS and Triton X-100 as the mixed surfactants were carried out to investigate the effect of the mixed surfactants on latex stability and the conductivity changes. The recipes used are shown in Table 6.1. The previous results using SLS as the sole surfactant shown in Chapter 4 are also shown in this section for comparison.

The particle sizes of the latexes prepared by the batch emulsion polymerization are shown in Table 6.3. The particle size decreased as expected as the total surfactant concentration increased. Except for the last reaction for each concentration (using Triton X-100 alone), the particle size distributions were fairly narrow and the PDI was small. On the other hand, when using Triton X-100 alone, the particle size distribution was broad. This was caused by coagulum formed during the reactions, which will be discussed below. Some coagulum was still present in the latexes even though the latexes were filtered using a 200 μm metal mesh after the reactions were complete to remove coagulum. For the low concentrations (6 and 10 mM) of the mixed surfactants, the particle size increased with an increase in the ratio of Triton X-100. For high concentrations of the mixed surfactant (20 and 30 mM), there were no major changes in the particle size as the ratio of Triton X-100 to SLS was varied.

The kinetic curves of all of the reactions are shown in Figure 6.6. For each

concentration, the reaction rate decreased as the ratio of Triton X-100 to SLS was increased. Especially, using only Triton X-100, the reaction rate was much slower than in the other cases. For the high concentrations (20 and 30 mM), using SLS or the mixed surfactants, the reactions were completed in 30 minutes. On the other hand, the reactions carried out using Triton X-100 alone needed more than 3 hours for completion. From these curves, it can be seen that the nucleation process took a long period of time, which may also cause the broad particle size distributions. Moreover, coagulum was formed during the reactions carried out when using Triton X-100 alone. Figure 6.7 shows photographs of the coagulum taken right after reaction B-6mM-Triton was completed and after air drying. A great deal of coagulum was adsorbed on the surfaces of the impeller and probes, which caused the low solids content of the latex at the end of the reaction. The coagulum percentage decreased (24.2, 10.6, 7.4, and 1.2 %, respectively), with the increase in the concentration of Triton X-100. On the other hand, using SLS or the mixed surfactants, there was no coagulum present in the latexes and the coagulum adsorbed on the surfaces of the reactor was negligible. These results clearly showed that even though the surfactant concentration is much higher than the CMC, Triton X-100 was not a good surfactant to stabilize particles during the batch emulsion polymerizations compared with SLS. This is caused by the partitioning of Triton X-100 in the aqueous phase under the reaction conditions, which will be discussed later (6.3.4).

Table 6.3: Particle Size of the Latexes Obtained from the Batch Emulsion Polymerizations Shown in Table 6.1

Latexes	D_n (nm)	D_V (nm)	PDI
B-20%-6mM	162	169	1.07
B-6mM-3-1	153	153	1.00
B-6mM-1-1	166	170	1.04
B-6mM-1-3	198	209	1.08
B-6mM-Triton	92	1493	8.08
B-20%-10mM	120	122	1.03
B-10mM-3-1	117	117	1.00
B-10mM-1-1	111	117	1.09
B-10mM-1-3	137	139	1.03
B-10mM-Triton	129	1021	5.28
B-20%-20mM	92	98	1.12
B-20mM-3-1	79	89	1.25
B-20mM-1-1	88	94	1.14
B-20mM-1-3	89	99	1.22
B-20mM-Triton	48	299	8.04
B-20%-30mM	85	89	1.09
B-30mM-3-1	79	86	1.16
B-30mM-1-1	68	80	1.37
B-30mM-1-3	85	93	1.18
B-30mM-Triton	42	158	5.98

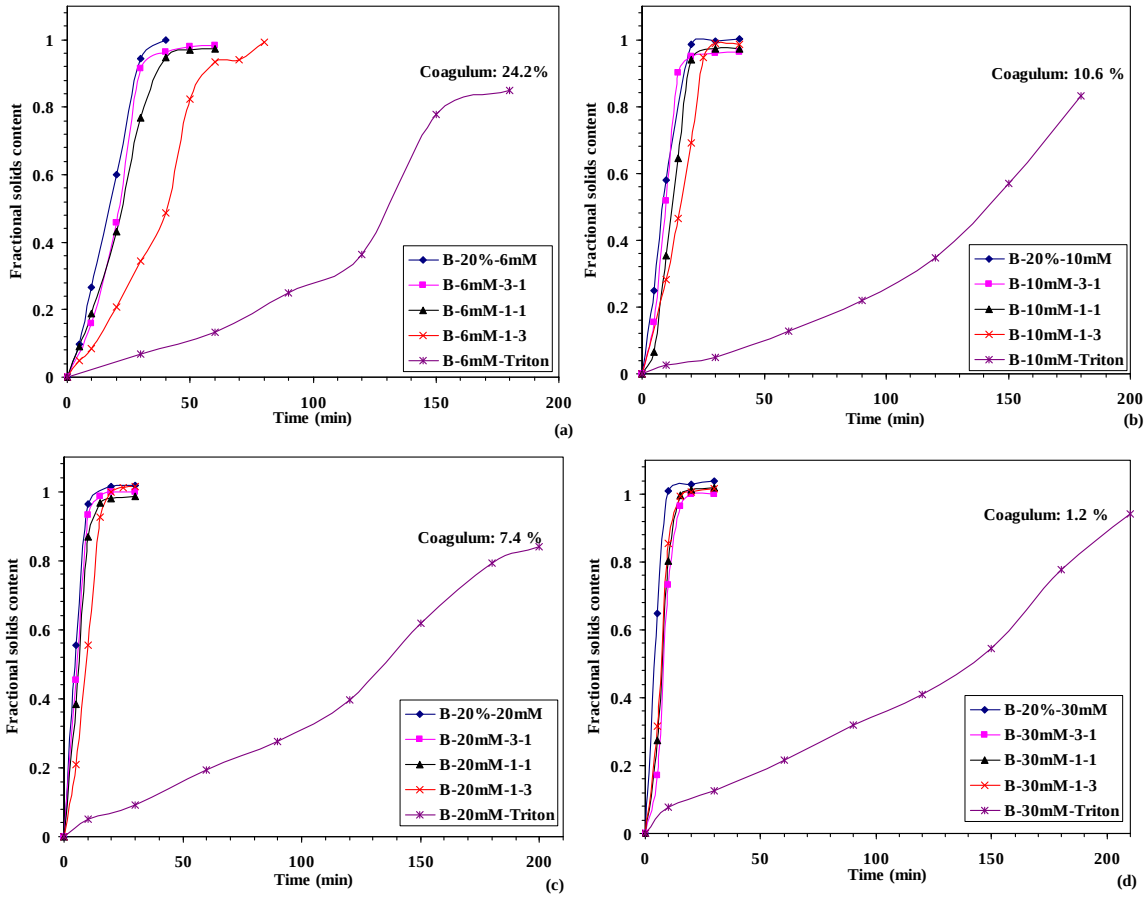

Figure 6.6: *Fractional solids content vs. time curves for the batch emulsion polymerizations using the different total surfactant concentrations: (a) 6 mM, (b) 10 mM, (c) 20 mM, and (d) 30 mM.*

Figure 6.7: *Picture of the coagulum formed during reaction B-6mM-Triton taken after the reaction (top) and after air drying (bottom).*

6.3.3 Online Conductivity Measurements

The conductivity profiles obtained during the reactions using the mixed surfactants and Triton X-100 as the sole surfactant are shown in Figures 6.8 to 6.11. At the beginning of each reaction, the conductivity value obtained from the homemade resistance probe was smaller than the value obtained from the torroidal probe, which is supposed to represent the true conductivity value. This difference is caused by the structure of the homemade probe and dispersed insulator materials in the continuous aqueous phase, such as monomer droplets and nonionic surfactant molecules. The details and evidence concerning this phenomenon were discussed previously (Chapter 4). For each concentration, as the ratio of Triton X-100 to SLS increased, the conductivity curve obtained from the torroidal probe decreased. The reason for this is that the nonionic surfactant had no charge and did not contribute to conductivity. Therefore, the conductivity of the whole system decreased.

Except for Figure 6.11 (a) and (b), there was an obvious gap between the two conductivity curves obtained from the two probes at the end of each reaction. This indicated that some polymer particles plated onto the surfaces of the electrodes of the homemade resistance probe during the reactions. The final conductivity ratio (R/T) between the two curves was calculated as described previously. The results are listed in Table 6.5. From these results, it can be seen that for each concentration, the R/T value was largest in the reactions using only SLS and were smallest in the reactions using Triton X-100 alone. For 6 mM total surfactant concentration, three reactions

using the mixed surfactants had similar R/T values, which were around 0.1. Actually, this value is very small and indicates that the surfaces of the electrodes are almost fully covered by deposited coagulum. In this case, the resistance probe loses sensitivity and cannot be used to predict latex stability. For the other three concentrations, the R/T values decreased with an increase in the ratio of Triton X-100 to SLS, which predicts that Triton X-100 only slightly contributes to latex stability compared with SLS. This means that for the same total surfactant concentration, the more Triton X-100 used, the less stable is the latex. Moreover, because the R/T values in the reactions using only SLS are larger than the ones in the mixed surfactants, it predicted that using only SLS is a better choice to stabilize the latex compared with using the mixed surfactants of SLS and Triton X-100. This result was unexpected, because mixtures of ionic and nonionic surfactants are often used to improve latex stability. However, the conductivity curves predict a contradictory result for this system. Whether this prediction is true needs to be proven by the results from the blender tests and turbidity measurements and will be discussed later.

During most of these reactions, a second increase in conductivity curves obtained from the resistance probe occurred. As discussed previously (Chapter 4), the second increase may be related to the disappearance of monomer droplets, which is considered as the end of the second interval of emulsion polymerization. The results of this series of reactions also show some clues to support the previous analysis. In Figure 6.9 (d), Figure 6.10 (d), and Figure 6.11 (d), the second increase in

conductivity curves can be seen clearly. Due to the relatively slow reaction rate during these reactions, the conversion when this increase occurred could be obtained from the kinetic curve within a small error. The results of these three reactions showed that the second increase occurred at a conversion between 40 and 50 %, which is in the range of the end of the second interval. For 6 mM total surfactant concentration (Figure 6.8), the second increase was not significant compared with the other three concentrations. This is caused by the high surface coverage of the electrodes by plating. From the figures, it can be seen that the conductivity curves obtained from the homemade resistance probe decreased to low values at early times in each reaction, which indicated that the degree of plating reached a high level. At this point, the homemade resistance probe lost sensitivity.

Table 6.4: Summary of the Results of the Final Conductivity Ratio

Reaction	R/T
B-20%-6mM	0.491
B-6mM-3-1	0.103
B-6mM-1-1	0.110
B-6mM-1-3	0.114
B-6mM-Triton	0.032
B-20%-10mM	0.628
B-10mM-3-1	0.314
B-10mM-1-1	0.176
B-10mM-1-3	0.143
B-10mM-Triton	0.091
B-20%-20mM	1.020
B-20mM-3-1	0.680
B-20mM-1-1	0.603
B-20mM-1-3	0.349
B-20mM-Triton	0.269
B-20%-30mM	1.080
B-30mM-3-1	0.972
B-30mM-1-1	0.948
B-30mM-1-3	0.895
B-30mM-Triton	0.296

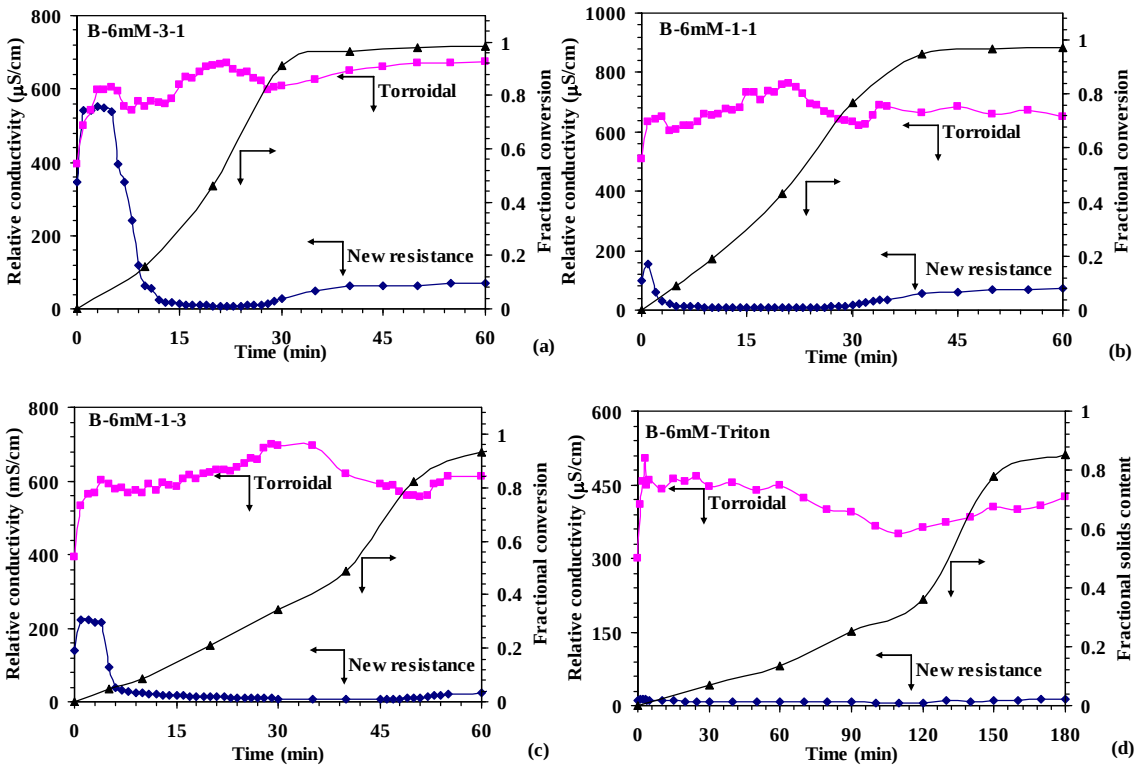

Figure 6.8: *Relative conductivity and fractional conversion vs. time curves for the batch emulsion polymerizations using 6 mM total surfactant concentration with different weight ratios of SLS to Triton X-100: (a) 3:1, (b) 1:1, (c) 1:3, and (d) only Triton X-100.*

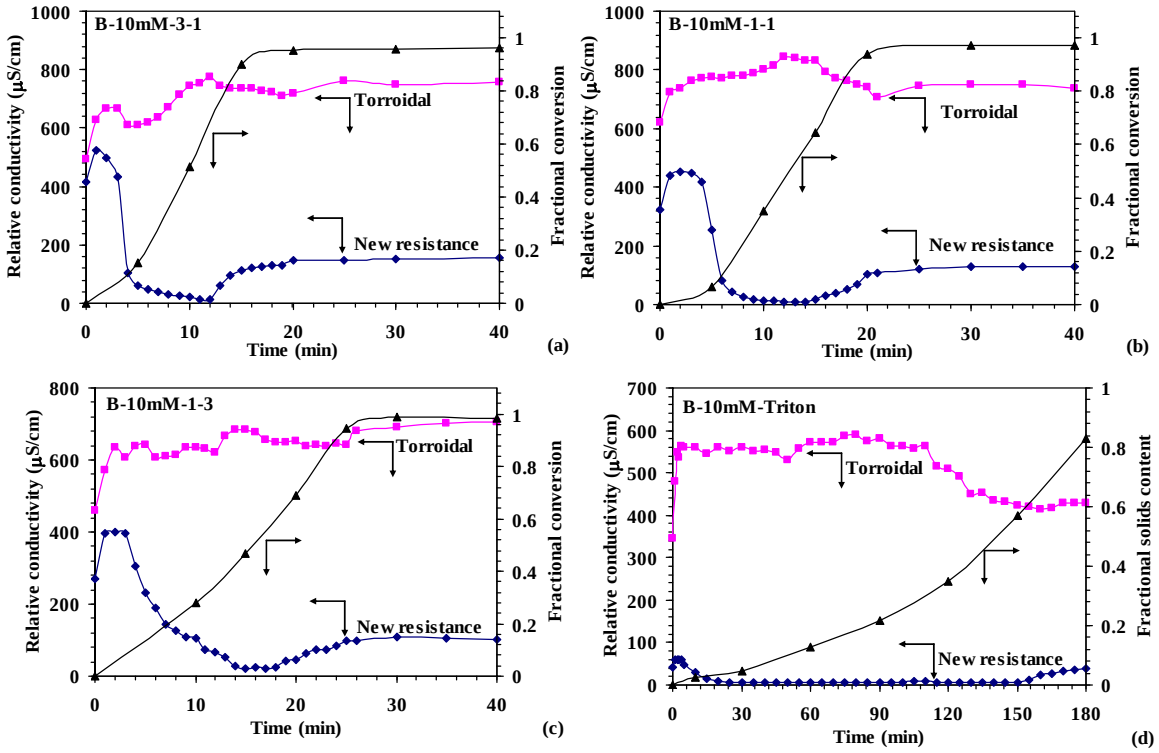

Figure 6.9: *Relative conductivity and fractional conversion vs. time curves for the batch emulsion polymerizations using 10 mM total surfactant concentration with different weight ratios of SLS to Triton X-100: (a) 3:1, (b) 1:1, (c) 1:3, and (d) only Triton X-100.*

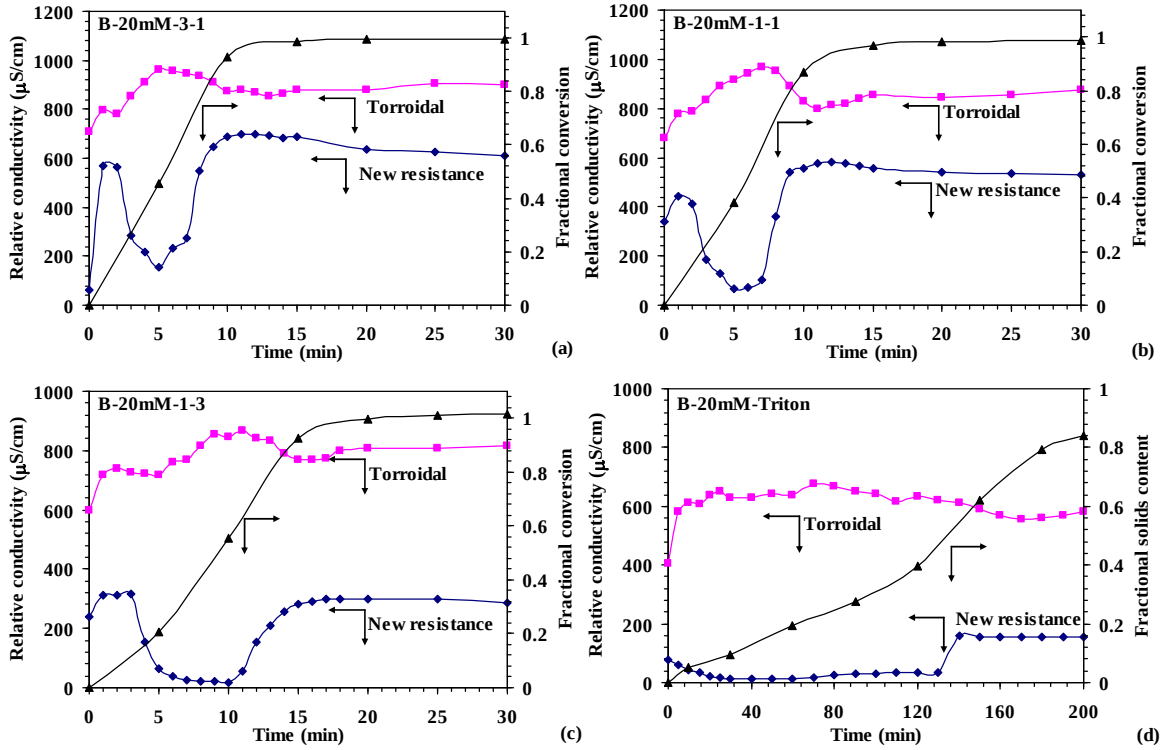

Figure 6.10: *Relative conductivity and fractional conversion vs. time curves for the batch emulsion polymerizations using 20 mM total surfactant concentration with different weight ratios of SLS to Triton X-100: (a) 3:1, (b) 1:1, (c) 1:3, and (d) only Triton X-100.*

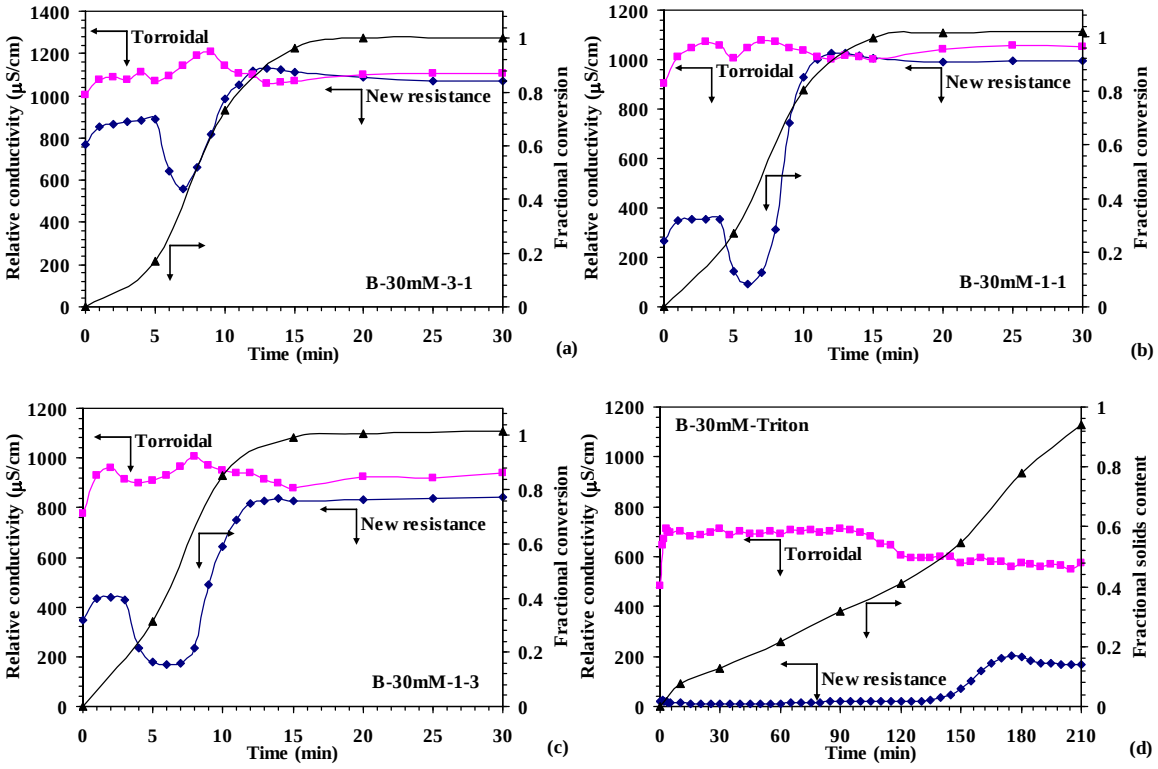

Figure 6.11: *Relative conductivity and fractional conversion vs. time curves for the batch emulsion polymerizations using 30 mM total surfactant concentration with different weight ratios of SLS to Triton X-100: (a) 3:1, (b) 1:1, (c) 1:3, and (d) only Triton X-100.*

6.3.4 Partitioning of Triton X-100 in the Aqueous Phase

As shown in Table 6.2, there was only SLS and no Triton X-100 present in the first sample. The results showed that 86.2 % of SLS was distributed in the aqueous phase, which meant that the remaining surfactant was associated (adsorbed or dissolved) with the oil phase. This value is slightly lower than the result (91 %) shown in Colombie's paper[18] for a polystyrene system. If assuming the percentage of SLS associating with the oil phase is constant and is not affected by the presence of Triton X-100, the partitioning of Triton X-100 (Table 6.2, samples 2 to 4) between the two phases can then be calculated based on the mass balance. These results are shown in Figure 6.12. From these results, it can be seen that the partitioning of Triton X-100 in the aqueous phase is low (less than 5 %) if only Triton X-100 is used as the surfactant in the recipe. Almost all of Triton X-100 is dissolved in the monomer phase and cannot play a role in nucleating particles before the monomer droplets disappear during the emulsion polymerizations. Therefore, the real concentration of Triton X-100 in the aqueous may be very low even though the concentration is high in the recipes. This is the reason why the reaction rate was slow and coagulum was formed in the reactions if only Triton X-100 was used. These results are consistent with the results obtained by Özdeğer[19] in a styrene and Triton X-405 system. The partitioning of Triton X-100 increased with an increase in the SLS concentration. This may be caused by the formation of micelles. Some of the Triton X-100 molecules may be trapped among the SLS molecules to form mixed micelles, which would influence the partitioning of Triton X-100 between the aqueous phase and monomer phase.

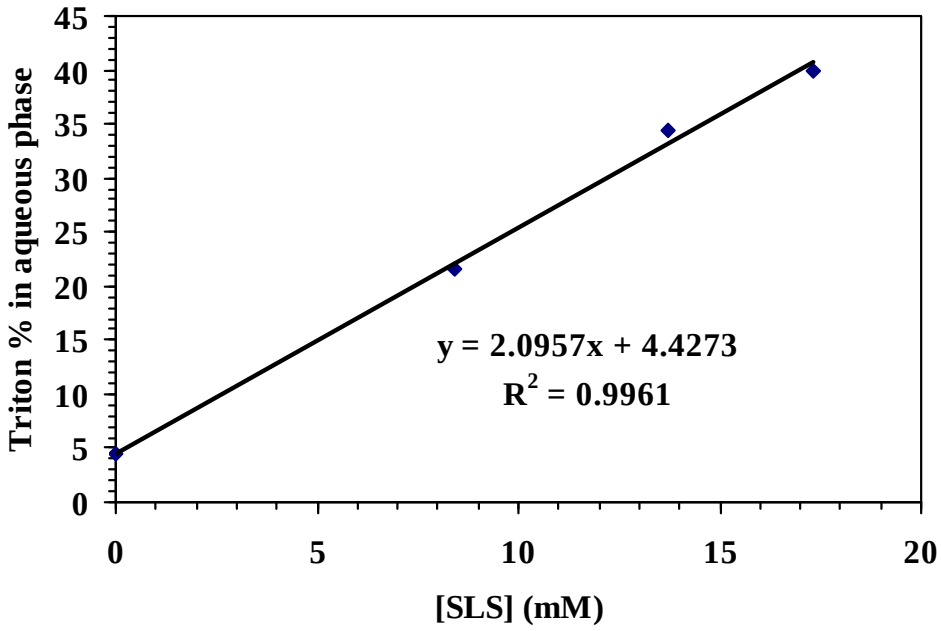

Figure 6.12: *Relationship between the partitioning of Triton X-100 and the concentration of SLS in the aqueous phase (Table 6.2).*

6.3.5 Latex Stability Tests and Correlation

Blender test and turbidity measurements were carried out to investigate the mechanical and electrolyte stability of the final latexes prepared by the reactions described previously (Table 6.1). The results are summarized in Table 6.5. Because the reactions using only Triton X-100 formed a great deal of coagulum and were considered as unsuccessful reactions, the latexes prepared in these reactions were not used to test stability. The percent coagulum obtained from the blender test increased and the ccc obtained from the turbidity measurements decreased with an increase in the ratio of Triton X-100 to SLS. Both of these results indicate that latex stability decreased as the amount of Triton X-100 was increased for a fixed total surfactant concentration. The results also show that Triton X-100 has a much smaller contribution to latex stability compared with SLS and it is not a good nonionic surfactant for BMA. This may be caused by the short hydrophilic chain (the average number of the EO groups is 9.5) in a Triton X-100 molecule. The results from both the blender tests and turbidity measurements are consistent with the prediction obtained from the conductivity curves and proved that the prediction of the conductivity measurements is correct.

Because the homemade resistance probe lost sensitivity due to the high degree of plating when the total surfactant concentration was 6 mM, the correlation between the conductivity curves and latex stability was based on the results of the other three surfactant concentrations shown in Tables 6.4 and 6.5. Figure 6.13 shows

the percent coagulum vs. R/T curves. From Figure 6.13 (top), it can be seen that there was a linear relationship between them for each concentration. The slopes of these curves obtained with 10 and 20 mM total surfactant were similar. However, the slope of the 30 mM curve was much larger than the other two. This may be caused by the overly high concentration of the surfactants based on the blender test results. From the results obtained from latex B-20%-20mM, it can be seen that the percent coagulum obtained during the blender test was 1.3 %, which means that the latex can be stabilized by this amount of SLS. When the surfactant concentration increased to a higher level, such as 30 mM, there was no major change in the results found from the blender test. However, the use of the higher surfactant concentrations may have caused the relatively higher R/T values. Therefore, the 30 mM line exhibits a steeper slope. Moreover, in Figure 6.13 (top), two groups of data points were used to analyze the contribution of SLS and Triton X-100 to mechanical stability. First, the concentrations of SLS and Triton X-100 were 8.67 and 1.33 mM for point (a), and they were 8.39 and 11.61 mM for point (b). Obviously, both points had a similar SLS concentration but much different Triton X-100 concentration. However, the percent coagulum for points (a) and (b) was similar. This illustrates that the effect of Triton X-100 on the mechanical stability was small. Second, the SLS concentrations at points (c), (d), and (e) were 13.69, 10.00, and 12.58 mM, respectively. The corresponding concentrations of Triton X-100 were 6.31, 0, and 17.42 mM, respectively. These three points exhibited similar results for the percent coagulum. The results also show that the efficiency of Triton X-100 in stabilizing the latexes

during the blender test was low. However, one thing needs to be pointed out here. The listed surfactant concentrations are based on the recipes. They are not the concentrations on the latex particle surfaces. To investigate the contribution of each surfactant to latex stability accurately, the surface coverage of each surfactant on the particles needs to be measured. This will be presented in the following section.

All of the results obtained previously (Chapters 4, 5, and 6) using the homemade resistance probe are shown in Figure 6.13 (bottom) except for the results for the 30 mM concentration. In both the batch and semi-batch emulsion polymerization systems, there was a linear relationship between the percent coagulum and R/T. The slope of the semi-batch curve was larger than the one for the batch process. However, the data points obtained from the semi-batch process were around the line of the batch system. Therefore, all points can be roughly considered to fall on one line. Through this line, the mechanical stability of the final latexes can be predicted by the online conductivity measurements.

Figure 6.14 (top) shows the correlation between the ccc obtained from the turbidity measurements and R/T for this series of the reactions. The slopes of the three lines were similar. The final correlation using all of the previous results (Chapters 4, 5, and 6) is shown in Figure 6.14 (bottom). The slope of the semi-batch curve was much greater than that of the batch curve and thus all the data were not be fitted by one line. This may be caused by the need for dilution before the turbidity measurements was

carried out. Because the solids content of the batch system (20 %) and the semi-batch system (40 %) were not the same, they needed to be diluted with different amounts of DI water. The relationship between the ccc and R/T demonstrates that the online conductivity measurements can be used to predict the electrolyte stability of the final latexes.

Table 6.5: Summary of the Results of the Blender Tests and Turbidity Measurements

Samples	Percent coagulum	ccc (M)
B-20%-6mM	41.1	0.522
B-6mM-3-1	69.7	0.440
B-6mM-1-1	75.9	0.368
B-6mM-1-3	76.3	0.312
B-20%-10mM	35.4	0.560
B-10mM-3-1	47.5	0.446
B-10mM-1-1	55.5	0.370
B-10mM-1-3	65.0	0.287
B-20%-20mM	1.3	0.616
B-20mM-3-1	23.5	0.577
B-20mM-1-1	35.5	0.483
B-20mM-1-3	43.6	0.403
B-20%-30mM	0.5	0.699
B-30mM-3-1	6.9	0.683
B-30mM-1-1	24.2	0.669
B-30mM-1-3	35.7	0.642

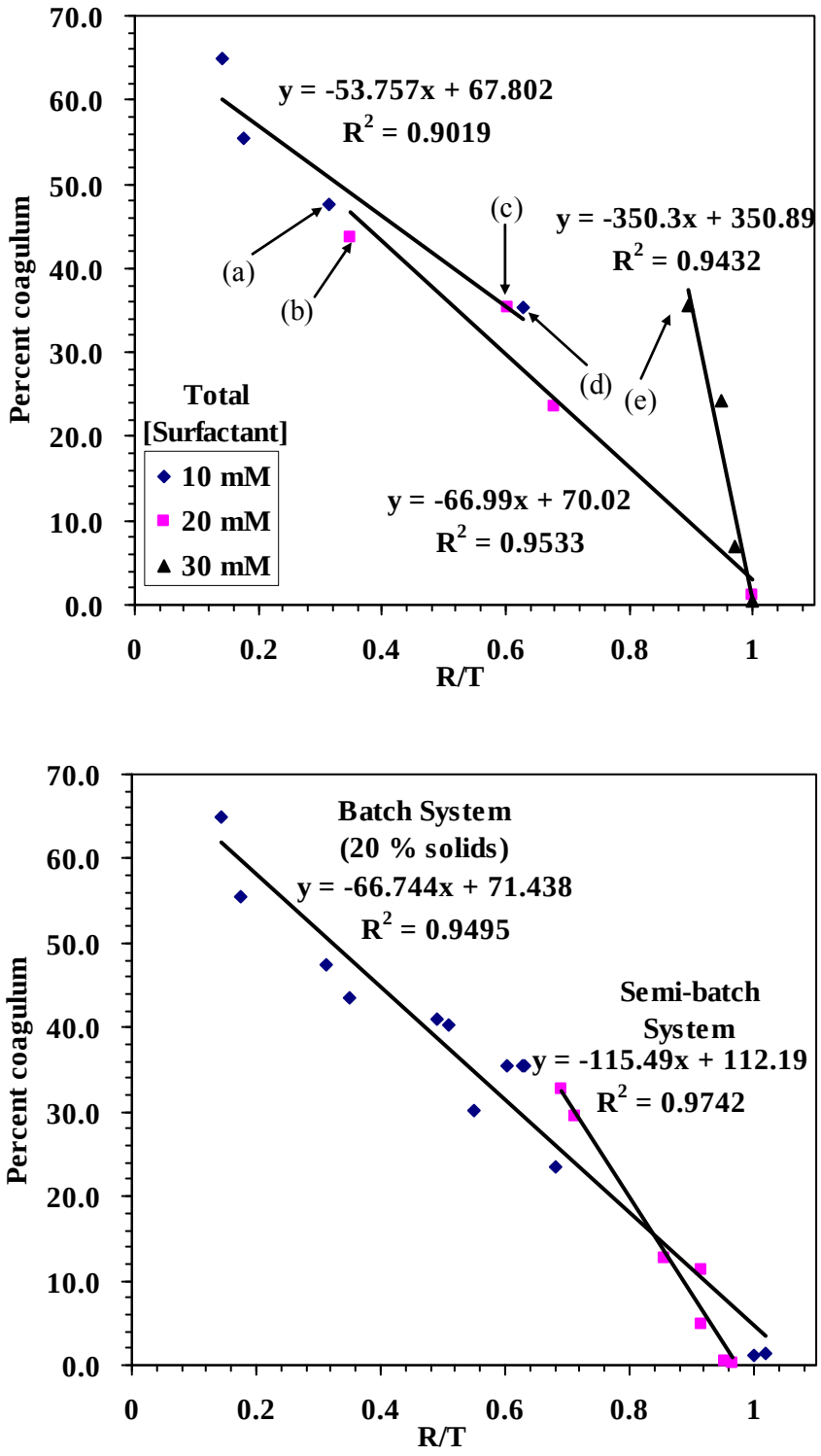

Figure 6.13: *Relationship between the percent coagulum and R/T obtained from this series of the reactions using the mixed surfactants (top) and obtained from all of the results using the homemade resistance probe (bottom).*

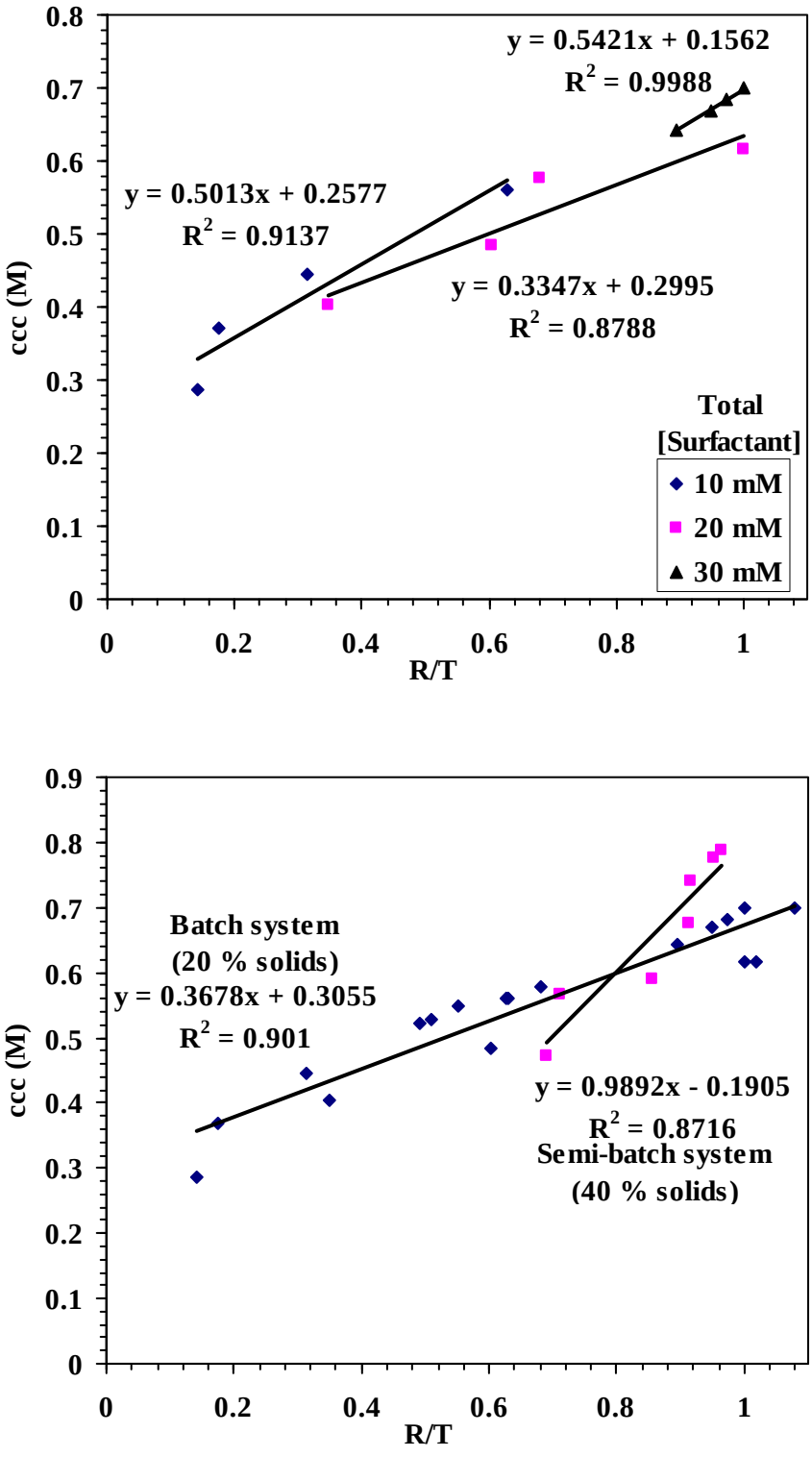

Figure 6.14: *Relationship between the ccc and R/T obtained from this series of the reactions using the mixed surfactants (top) and obtained from all of the results using the homemade resistance probe (bottom).*

6.3.6 Packing Area of Triton X-100 and Surface Coverage

As discussed in the last section, the surface coverage needs to be known to analyze the contribution of each surfactant to latex stability. To calculate the surface coverage, the packing area of Triton X-100 was measured using surface tension measurements. The shape of the curve is similar to the one used for the measurements of the CMC (Figure 6.4 (a)) and the results show that the concentration of Triton X-100 was 1.9 mM when the micelles were formed in the aqueous phase. From the Sigma data sheet, the CMC of Triton X-100 lies in a range between 0.22 and 0.24 mM. Choosing 0.24 mM as the CMC, the concentration of Triton X-100 on the particle surfaces can be obtained based on a mass balance. The packing area of Triton X-100 can then be calculated and the result is 84 $Å^2$. This value is larger than the one reported by Porcel[20] (50 $Å^2$) and Kronberg[21] (60 $Å^2$).

The serum of each latex was obtained by filtration in the serum replacement cell and the concentrations of each surfactant in the serum were measured using the method described previously (6.2.5). The results are summarized in Table 6.6. As expected, for each fixed total surfactant concentration, the surface coverage of Triton X-100 increases as the weight ratio of Triton X-100 increases in the recipes. At the same time, the surface coverage of SLS decreases with the increase in the weight ratio of Triton X-100 due to the reduction in the amount of SLS in the recipes. The contribution of each surfactant to latex stability can easily be analyzed through some comparisons. For example, for latexes B-20%-10mM and B-10mM-1-3, the former

was covered by SLS (26.2 %) and the latter is covered by Triton X-100 (28.0 %) and SLS (13.1 %). For the latter, the total coverage is more than the former and the coverage of SLS is half of the former, but the former shows obviously better stability than the latter as shown in Table 6.5. Similar results can also be found from comparisons of the other samples. The results clearly show that the contribution of SLS to latex stability is much larger than the one of Triton X-100. What is the reason for this? Why do the mixed surfactants not improve latex stability compared with the SLS as the sole surfactant? These questions will be answered in the next chapter.

Table 6.6: Summary of the Results Related to the Surface Coverage of Triton X-100 and SLS

	D_V (nm)	Adsorption ($\times 10^{22}$ g/nm^2)		Coverage	
		Triton	SLS	Triton (%)	SLS (%)
B-20%-6mM	169	--	1.69	--	19.1
B-6mM-3-1	153	0.43	1.58	3.4	17.9
B-6mM-1-1	170	1.33	1.39	10.8	15.7
B-6mM-1-3	209	3.09	1.04	25.0	11.7
B-20%-10mM	122	--	2.32	--	26.2
B-10mM-3-1	117	0.59	2.00	4.8	22.6
B-10mM-1-1	117	1.55	1.59	12.6	18.0
B-10mM-1-3	139	3.46	1.16	28.0	13.1
B-20%-20mM	98	--	3.52	--	39.8
B-20mM-3-1	89	1.00	3.02	8.1	34.1
B-20mM-1-1	94	2.55	2.52	20.6	28.4
B-20mM-1-3	99	4.97	1.63	40.3	18.5
B-20%-30mM	89	--	4.91	--	55.5
B-30mM-3-1	86	1.45	4.35	11.7	49.1
B-30mM-1-1	80	3.27	3.21	26.5	36.2
B-30mM-1-3	93	7.02	2.29	56.8	25.8

6.4 Conclusions

The homemade resistance probe and torroidal probes were used to monitor conductivity changes during the batch emulsion polymerizations of BMA using mixture of SLS and Triton X-100 as surfactants. The conductivity results predicted that latex stability should decrease with an increase in the ratio of Triton X-100 to SLS for a fixed total surfactant concentration, which was the opposite of what was expected. Blender tests and turbidity measurements were used to investigate the

mechanical and electrolyte stability of the final latexes. The results proved that the prediction of the conductivity results was correct. All results obtained using the homemade probe were plotted together in one figure. The linear relationships between R/T and the percent coagulum obtained from the blender test, and between R/T and the ccc obtained from the turbidity measurements were established. These results illustrate that the conductivity probes can be used as online sensors to monitor latex stability during the course of the emulsion polymerizations of BMA. Moreover, the surface coverage of each surfactant on the particle surfaces was calculated. The results proved that the contribution of Triton X-100 to latex stability was much smaller compared to SLS. This is the reason why latex stability decreased as the weight ratio of Triton X-100 to SLS increased in the recipes when the total surfactant concentration was fixed.

6.5 References

[1] C. S. Chern, *Prog. Polym. Sci.*, **31**, 443 (2006).

[2] K. Ouzineb, M. F. Heredia, C. Graillat, T. F. McKenna, , *J. Polym. Sci. A: Polym. Chem.*, **39**, 2832 (2001).

[3] L. J. Chen, S. Y. Lin, C. S. Chern and S. C. Wu, *Colloid Surfaces A*, **122**, 161 (1997).

[4] R. G. Gilbert, in *Emulsion Polymerization, A Mechanistic Approach*, Academic Press, London (1995).

[5] R. H. Ottewill, in *Nonionic Surfactants*, M. J. Schick Ed., Surfactant Series, Marcel Dekker, New York, Vol. 1 (1966).

[6] K. G. Mathai and R. H. Ottewill, *Trans. Faraday Soc.*, **62**, 759 (1966).

[7] D. H. Napper and A. J. Netschey, *J. Colloid Interface Sci.*, **237**, 528 (1971).

[8] A. Sung and I. Piirma, *Langmuir*, **10**, 1393 (1994).

[9] M. Hulden and B. Kronberg, *J. Coat. Technol.*, **66**, 67 (1994).

[10] B. Kronberg, M. Linstrom and P. Stenius, in Phenomena in *Mixed Surfactant Systems*, J. H. Scamehorn, Ed., ACS Symposium Series 311, American Chemical Society, Washington. DC (1986).

[11] J. Bolze, K. D. Horner and M. Ballauf, *Colloid Polym. Sci.*, **274**, 1099 (1996).

[12] D. Colombié, K. Landfester, E. D. Sudol and M. S. El-Aasser, *Langmuir*, **16**, 7905 (2000).

[13] Sigma data sheet.

[14] G. E. Tiller, *Anal. Biochem.*, **141**, 262 (1984).

[15] B. Urquiola, *Ph.D. Dissertation*, Lehigh University (1997).

[16] D. Colombié, *Ph.D. Dissertation*, Lehigh University (1999).

[17] M. J. Schick and D. J. Manning, *J. Am. Chem. Soc.*, **43**, 133 (1966).

[18] D. Colombié, E. D. Sudol, and M. S. El-Aasser, *Macromolecules*, **33**, 7283 (2000).

[19] E. Özdeğer, E. D. Sudol, M. S. El-Aasser and A. Klein, *J. Polym. Sci.: Part A*, **35**, 3819 (1997).

[20] R. Porcel, A. B. Jodar, M. A. Cabrerizo, R. Hidalgo-Alvarez and A. Martin-Rodriguez, *J. Colloid Interface Sci.*, **239**, 568 (2001).

[21] B. Kronberg, P. Stenius and G. Igeborn, *J. Colloid Interface Sci.*, **102**, 418 (1984).

Chapter 7
Theoretical Calculations of Latex Stability Based on the DLVO and Extended DLVO Theories

7.1 DLVO Theory

7.1.1 Introduction

The stability of surface charged particles in a dispersion system depends on the electrostatic interactions, which arise from the electrical double layer surrounding the particles. The electrostatic stability can be calculated from the DLVO theory. This theory was developed independently in the 1940s by Derjaguin and Landau[1] and Verwey and Overbeek[2]. It is a classical theory to describe the interactions between two charged particles in terms of the potential energies when they approach each other. The total energy (V_T) is the addition of the energy resulting from van der Waals attractive forces (V_A), the energy resulting from the electrostatic repulsive forces (V_R), and the Born repulsion (V_B) as shown in eqn (7.1). The Born repulsion is a strong short-range repulsion when the distance between two particles is on the order of atomic dimensions and the orbitals of atoms overlap. It is usually represented as a cut-off potential at a distance of about one atomic diameter[3]. For long-range calculations, V_B does not need to be considered.

$$V_T = V_A + V_R + V_B \tag{7.1}$$

As shown in Figure 7.1[4], a deep minimum in the total potential energy curve, termed the primary minimum, occurs at a very short distance (h) between particle surfaces. It determines the closest distance between two particles. The depth is related to twice the dispersive contribution to the surface energy[5]. In the primary minimum, coagulation of particles occurs and this process is irreversible. At an intermediate distance, the electrostatic repulsion is larger than the attractive contribution and hence there is a maximum (V_m) in the curve, which is referred to as the primary maximum. V_m serves as the energy barrier in a dispersion system. If the collision energy is larger than V_m, particles will coagulate together and the system will be unstable. As the distance between two particle surfaces increases, the repulsive forces show an exponential decay and the attractive forces dominate the total potential energy again. Therefore, the curve shows a minimum known as the secondary minimum. In this case, a liquid film is retained between two particles and flocculation occurs[6]. It is possible to redisperse the flocculated particles by removing electrolyte from the system or applying small amounts of mechanical energy. The depth of the secondary minimum can affect the rate of flocculation[7,8].

The DLVO theory is used to study latex stability and related parameters in many publications. Rubio-Hernández[9] investigated a relationship between the electrophoretic mobility and the stability factor of cationic polystyrene latex particles in alcohol-water mixtures. Moreover, the possible hydrophobic effects were quantitatively evaluated for the interaction between positively charged polystyrene

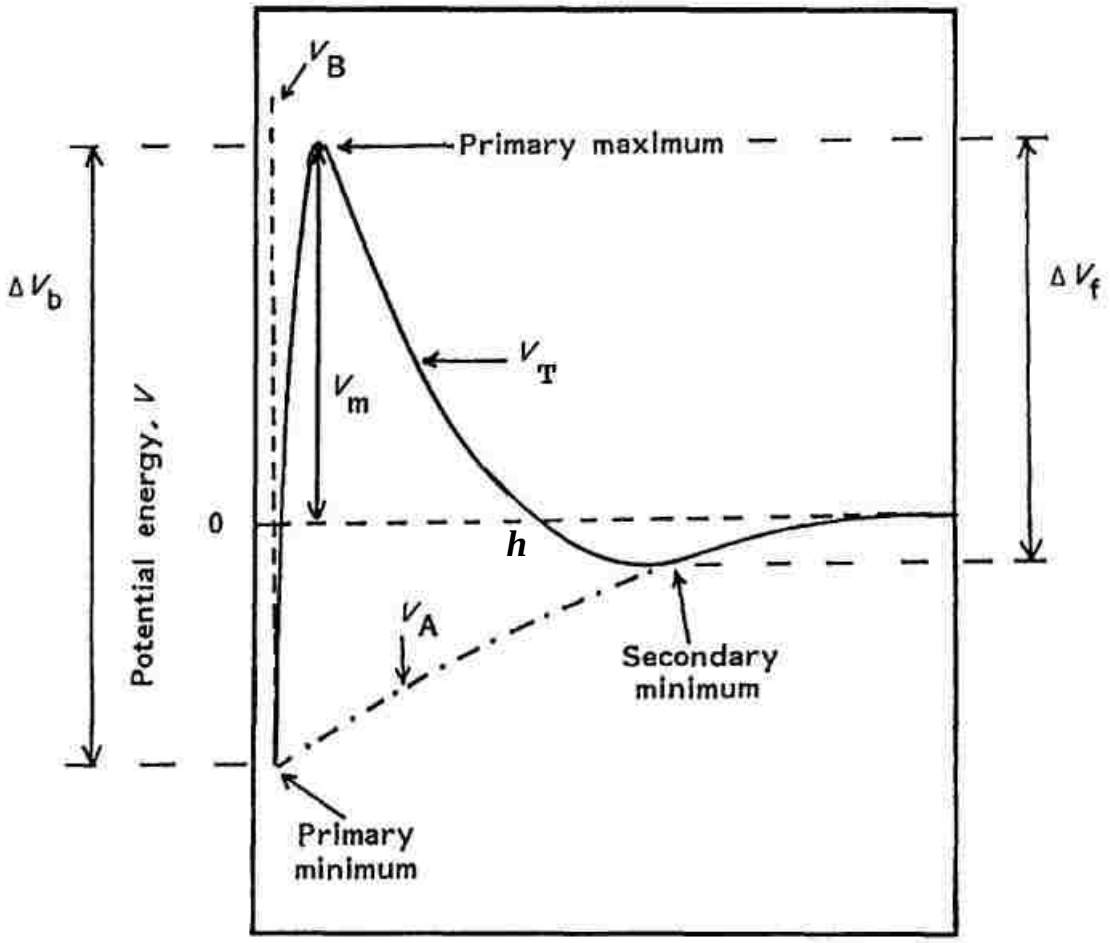

Figure 7.1: *Schematic representation of a total potential energy (V_T) profile as a function of interparticle distance (h). V_A is the energy resulting from the van der Waals attractive forces; V_R is the energy resulting from the electrostatic repulsive forces; and V_T is the total energy of interaction*[4].

particles in order to understand the zeta-potential at the critical coagulation concentration (ccc). Ishikawa *et al.*[10] used the DLVO theory to study the effects of pH and electrolyte on the stability of three poly(methacrylate)-based latexes. They calculated the Hamaker constant (A) of these latexes and the total potential energies based on their results. Tsaur and Fitch[11] investigated the effects of the surface charge density on the stability of monodisperse polystyrene latexes through coagulation kinetics. They theoretically calculated A and the Stern potential (ψ_δ) using their experimental data. Fortuny *et al.* [12] studied the stability of poly(butyl acrylate-*co*-methyl methacrylate) latexes stabilized by an anionic surfactant sodium dodecyl sulfate (SDS), an electrosteric surfactant with a short ethylene oxide chain, or simply with sulfate end groups through turbidity measurements. Urbina-Villalba *et al.*[13] used emulsion stability simulations to evaluate the stability ratio (W) of a polystyrene suspension. They established a relationship between W obtained through turbidity measurements and V_m calculated using the DLVO theory.

In the previous chapters, the stability of the latexes prepared by the batch and semi-batch BMA emulsion polymerizations were compared using the blender test and turbidity measurements. Theoretical calculations will be carried out in this chapter to explain latex stability from the view of the DLVO and extended DLVO theories. Especially, in Chapter 6, the results showed that the mixed surfactants decreased latex stability compared with using SLS as the sole surfactant at a fixed total surfactant concentration, which was the opposite of what was expected. The questions raised by

these results will be answered through calculations based on the extended DLVO theory. Moreover, the key factors that can decide the effect of nonionic surfactants on latex stability, will also be analyzed.

7.1.2 Model

As shown in eqn (7.1), the van der Waals attractive forces (V_A) and electrostatic repulsive forces (V_R) need to be calculated in order to plot the curve of the total potential energy. In this section, the model used to calculate both forces will be discussed.

First, the attractive energy (V_A) between two particles is calculated based on the theory proposed by Hamaker[14] and can be expressed as eqn (7.2).

$$V_A = -\frac{A}{12}\left[\frac{1}{x^2+2x} + \frac{1}{x^2+2x+1} + 2\ln\left(\frac{x^2+2x}{x^2+2x+1}\right)\right] \tag{7.2}$$

where $x = h/(2a)$, h is the distance between the surfaces of two particles, a is the radius of the particles, and A is the Hamaker constant. When $a>>h$, V_A can be calculated using eqn (7.3).

$$V_A = -\frac{Aa}{12h} \tag{7.3}$$

To calculate the Hamaker constant of PBMA, a simple group contribution method[15] is applied. This method attributes the surface free energy of a macromolecule, which is related to the Hamaker constant, to the contribution of each chemical group. The values calculated using this method show great agreement with the experimental data

presented in some publications. For example, the calculated Hamaker constant of poly(methyl methacrylate) is 7.7×10^{-20} J and the experimental result is 6.3×10^{-20} J[16]. Based on this method, the Hamaker constant of PBMA (A_{11}) is 7.2×10^{-20} J. Since the presence of the medium also affects the value of the Hamaker constant, the Hamaker constant of PBMA dispersed in an aqueous phase can be expressed as eqn (7.4).

$$A = (\sqrt{A_{11}} - \sqrt{A_{22}})^2 \tag{7.4}$$

where A_{22} is the Hamaker constant of water, which is reported as 3.70×10^{-20} J [17]. Therefore, the Hamaker constant of PBMA dispersed in the aqueous phase is 5.7×10^{-21} J.

Second, the repulsive potential (V_R) between two charged particles was calculated. Based on Overbeek's calculation[18],

if $\kappa a >> 1$,

$$V_R = 2\pi\varepsilon_r\varepsilon_0(4kT/e)^2 a\gamma^2 \exp(-\kappa h)/v^2 \tag{7.5}$$

$$\gamma = [\exp(ve\psi_\delta/2kT) - 1]/[\exp(ve\psi_\delta/2kT) + 1] \tag{7.6}$$

where ε_r (78.5) is the dielectric constant of water at 25 ºC; ε_0 (8.85×10^{-12} C^2/Nm^2) is the vacuum permittivity; k (1.381×10^{-23} J/K) is the Boltzmann constant; T (298.15 K) is the absolute temperature; e (1.6×10^{-19} C) is the fundamental unit of electricity; ψ_δ is the Stern potential; κ is the Debye parameter; and v is the magnitude of the charge. κ can be calculated using eqn (7.7).

$$\frac{1}{\kappa} = \sqrt{\frac{\varepsilon_r \varepsilon_0 kT}{2v^2 e^2 n_\infty}} \tag{7.7}$$

where n_∞ is the bulk ionic number concentration and is expressed in terms of the molarity M (mole/liter) by eqn (7.8).

$$n_\infty = 1000 N_A M \tag{7.8}$$

where $N_A = 6.022 \times 10^{23}$ is Avogadro's number. When $v = 1$, for a symmetrical electrolyte,

$$\frac{1}{\kappa} = \frac{3.04}{\sqrt{M}} \times 10^{-10} \tag{7.9}$$

Normally, the zeta potential is used to replace the Stern potential (ψ_δ) because the zeta potential is easy to measure. However, this value is measured in a dilute system, which is not accurate for a latex having a typical solids content, such as 20 % or 40 %. Moreover, the zeta potential measured by electrophoresis is inexact, because the zeta potential is the potential at the shear plane of a particle and the location of this plane relative to the Stern layer is unknown. In this section, ψ_δ is calculated based on the surface potential (ψ_0), which is directly related to surface charge density (σ). Therefore, the electrostatic surface potential ψ_0 needs to be calculated first through eqn (7.10)[19].

$$\psi_0 = \frac{2RT}{F} \sinh^{-1}\left(\frac{2\pi F\sigma}{4\pi\varepsilon_0\varepsilon_r RT\kappa}\right) \tag{7.10}$$

where F (96485 C/mol) is the Faraday constant; R (8.314 J/(mol K)) is the ideal gas constant; and σ is the surface charge density which can be obtained using eqn (7.11)

$$\sigma = veN_S \tag{7.11}$$

where N_S is the number of charged sites per unit area which can be calculated based on the results of the surface coverage of each latex. When v=1, ψ_δ has the relationship to ψ_0 as follows[20].

$$\psi_\delta = \frac{2RT}{F}\ln(\frac{\exp B + 1}{\exp B - 1}) \tag{7.12}$$

where

$$B = (\frac{8\pi F^2 n_\infty}{\varepsilon_0 \varepsilon_r N_A RT})^{\frac{1}{2}}\delta + \ln(\frac{\exp(F\psi_0 / 2RT) + 1}{\exp(F\psi_0 / 2RT) - 1}) \tag{7.13}$$

where δ is the thickness of the Stern layer, which is assumed to be 0.141 nm[21].

Through the discussion above, all of the parameters used in the equations of the DLVO theory are clearly shown. The Hamaker constant (A) is theoretically calculated. The electrolyte concentration consists of three parts: the buffer ($NaHCO_3$), the free SLS present in the aqueous phase, and the ions formed by the dissolution and decomposition of KPS. The last one can be negligible due to the small amount compared with the other two. The concentration of $NaHCO_3$ is used as the amount in the recipes and the concentration of the free SLS was measured previously. To simplify the mathematical calculations, $NaHCO_3$ and SLS are considered as symmetric salts with the valence of 1. The contributions to the surface charge density (σ) are from two parts: the adsorbed SLS molecules and the sulfate group present from the decomposition of KPS. The former term can be calculated based on the results of the surface coverage. The contribution of the latter to the surface charge density is much smaller compared with the adsorbed SLS if the SLS concentration is

high in the recipes, but it is not be negligible in the case where low SLS concentrations were used, such as for latexes B-5%-0.6mM and B-5%-1.2mM. Therefore, the amount of the sulphate group exposed on the particle surfaces needs to be estimated. According to the research of Santos *et al.*[22], the half-life ($t_{1/2}$) of KPS varies under the different conditions. In the presence of SLS and fixed pH (pH = 7), $t_{1/2}$ is 277 min. This value is used in the calculations due to the similar situations. Using eqn (7.14), the decomposition rate constant (k_d) can be calculated. The KPS concentration (I) at a given time (t) is then calculated through eqn (7.15).

$$t_{1/2} = \frac{0.693}{k_d} \tag{7.14}$$

$$I = I_0 e^{-k_d t} \tag{7.15}$$

where I_0 is the initial concentration of KPS. The reaction times for the batch and semi-batch emulsion polymerizations are assumed as 30 min and 180 min. If supposing that all of the sulfates groups formed from the decomposition of KPS are located on the surfaces, the surface charge density contributed from KPS can be estimated. For example, it is 1.8 μC/cm^2 for latex B-5%-0.6mM. This value is smaller than the result 3.8 μC/cm^2 shown in Egen's research, who worked on the surfactant-free emulsion polymerization of various methacrylates[23].

When V_m equals zero, attractive interactions dominate and the dispersion system becomes unstable. Any collision between two particles will result in coagulation. Under this condition, the critical coagulation concentration (ccc) can be

estimated through the DLVO theory. Two equations below need to be satisfied to achieve this condition.

$$V_R = -V_A \tag{7.16}$$

$$\frac{dV_R}{dh} = -\frac{dV_A}{dh} \tag{7.17}$$

Through the mathematical analysis, it is found that when $h = 1/\kappa$, these two equations can be satisfied. The ccc then can be obtained using eqn (7.18), because γ is a function of ψ_δ, which is related to the electrolyte concentration. Moreover, in eqn (7.18), the particle size (a) can be cancelled, which means that the ccc is not related to the particle size based on the DLVO theory.

$$-\frac{Aa}{12h} + 2\pi\varepsilon_r\varepsilon_0(4kT/e)^2 a\gamma^2 \exp(-1) = 0 \tag{7.18}$$

7.1.3 Results and Discussion

Based on the results shown in previous chapters, theoretical calculations were carried out. All of the parameters related to the calculations are summarized in Table 7.1. V_A and V_R were calculated independently, and V_T was then obtained using eqn (7.1). Taking latex B-5%-0.6mM as an example, the results are shown in Figure 7.2. Because V_R is much bigger than V_A, V_R dominates the curve of V_T and V_m is more than 300 kT. Moreover, the secondary minimum does not occur in the curve of V_T.

The V_T curves for the 5 %, 20 % and 40 % solids content latexes are summarized in Figures 7.3, 7.4, and 7.5, respectively. V_m in the V_T curve, which represents the energy barrier between two particles, can be used to demonstration the

level of latex stability. However, the results are obviously unreasonable. For example, in the 5 % solids content system (Figure 7.3), latex B-5%-0.6mM has the largest V_m value, which indicates that this latex has the highest stability, even more than latex B-5%-7.8mM. Similar results are obtained in Figure 7.4, which shows that latex B-20%-5mM has better stability compared to latexes B-20%-20mM and B-20%-30mM. Obviously, these results are wrong and contradict the results of the blender and turbidity tests. This is caused by some assumption in the DLVO theory, which is not suitable under the experimental conditions. The limitations of this theory and a correction will be discussed next.

Table 7.1: Summary of the Major Parameters of PBMA Latexes Prepared Previously

Samples	D_v (nm)	σ (μC/cm^2)	ψ_0 (mV)	Electrolyte Concentration (mM)
B-5%-0.6mM	214	2.07	78	6.7
B-5%-1.2mM	186	1.91	72	7.2
B-5%-2.4mM	160	3.35	96	8.1
B-5%-7.8mM	75	13.04	163	8.8
B-20%-5mM	208	6.66	164	2.2
B-20%-6mM	169	5.95	152	2.8
B-20%-8mM	147	7.31	164	2.6
B-20%-10mM	122	7.34	168	2.3
B-20%-20mM	98	10.98	175	3.9
B-20%-30mM	89	14.55	186	4.4
Semi-0.7%	107	4.48	117	6.3
Semi-1.0%	117	6.45	131	7.3
Semi-1.4%	107	8.44	146	7.1
Semi-1.7%	118	11.23	158	7.8
Semi-2.0%	111	12.47	163	8.0
Semi-2.5%	109	15.45	172	8.6
Semi-3.6%	108	22.07	183	11.2

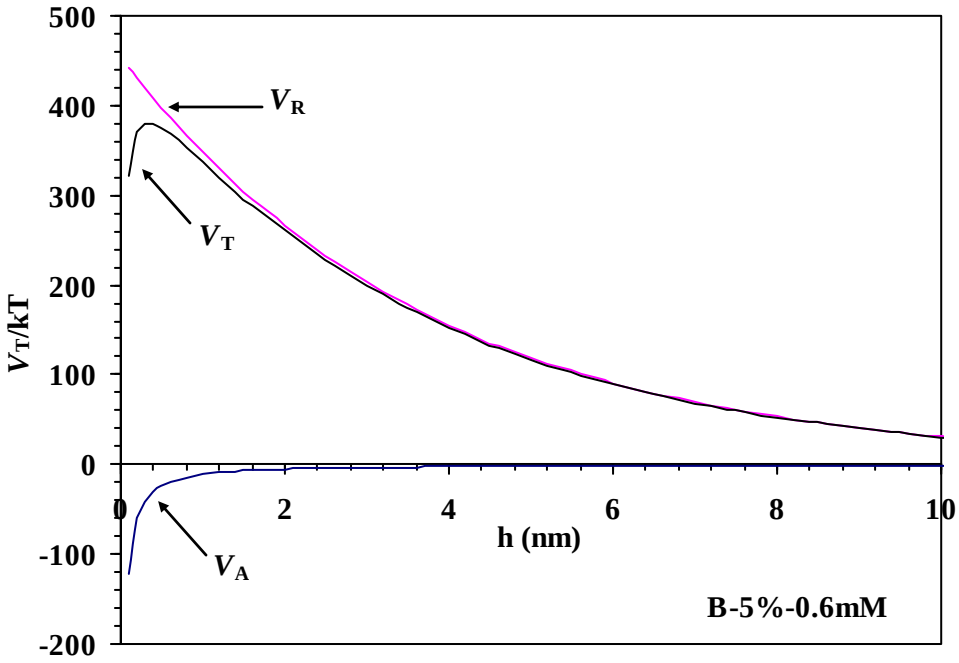

Figure 7.2: *The total potential energy (V_T), the attractive potential energy (V_A), and the repulsive potential energy (V_R) curves as a function of particle surface distance (h) for latex B-5%-0.6mM.*

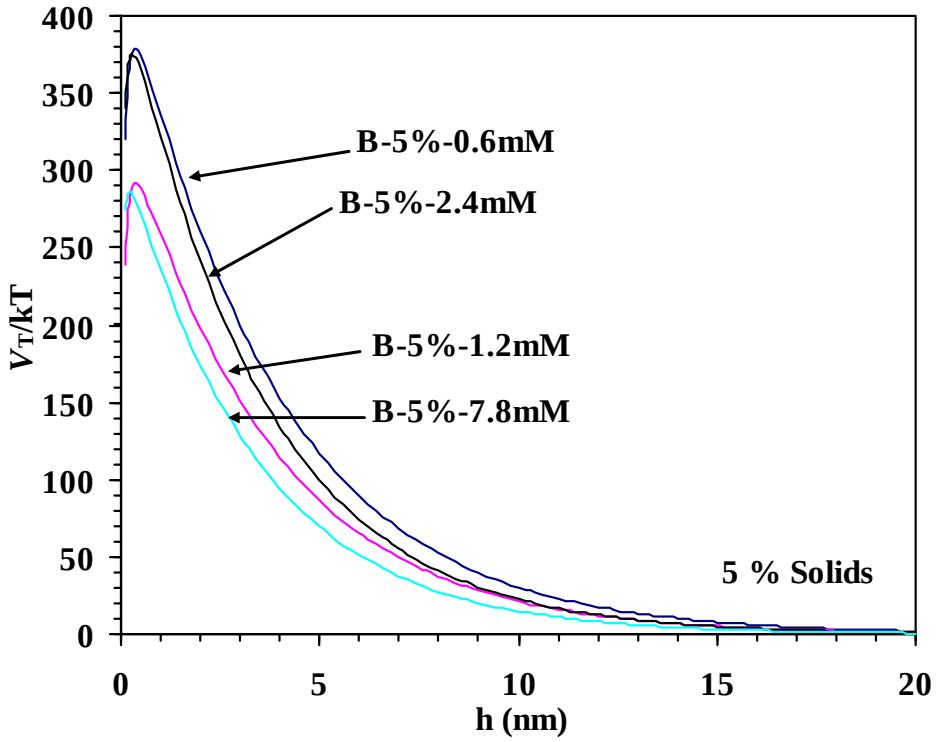

Figure 7.3: *The total potential energy (V_T) curves as a function of particle surface distance (h) for the 5 % solids content latexes in the original electrolyte concentration.*

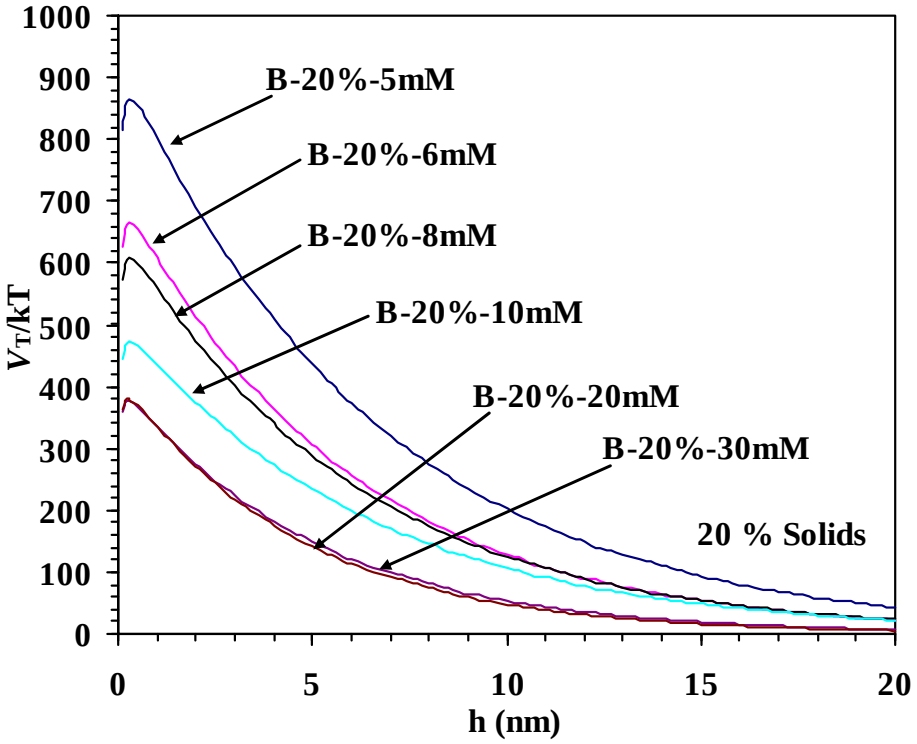

Figure 7.4: *The total potential energy (V_T) curves as a function of particle surface distance (h) for the 20 % solids content latexes in the original electrolyte concentration.*

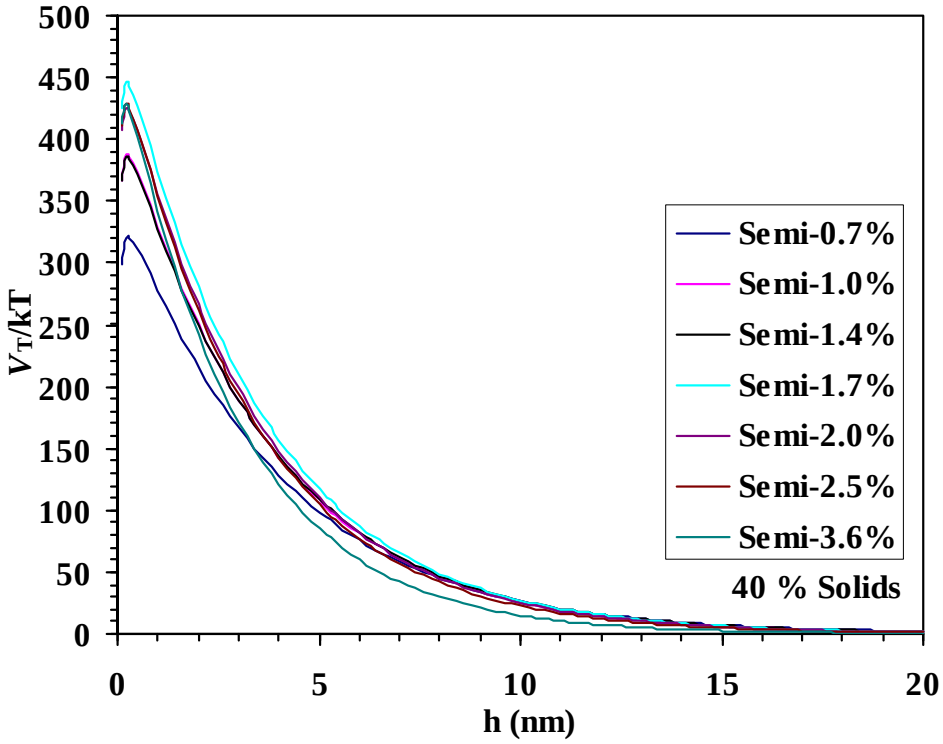

Figure 7.5: *The total potential energy (V_T) curves as a function of particle surface distance (h) for the 40 % solids content latexes in the original electrolyte concentration.*

To prevent some mathematical problems during the development of the DLVO theory, a simple assumption was made at the very beginning of this theory[2], which was that the surface potential should be very low (less than 25 mV). In this case, there is a linear relation between the surface potential and surface charge density. If the value of $e\psi_0$/kT is on the order of between 5 and 10, this assumption is a very poor approximation. Unfortunately, almost all of the $e\psi_0$/kT values for the latexes prepared in this research are in this range. The real relationsjip (no approximation) between the surface charge density and surface potential based on eqn (7.10) is shown in Figure 7.6. From this figure, it can be seen that 25 mV is a very low value and the surface charge density should be less than 2 $\mu C/cm^2$ to satisfy this assumption when the electrolyte concentration is 0.1 M. Moreover, the required surface charge density should even be much smaller if the electrolyte concentration is on the order of 10^{-3} M. The electrolyte concentrations of the prepared latexes were between 2 and 10 mM and the surface charge density varied from 2.0 to 14.4 $\mu C/cm^2$. From Figure 7.6, it can be seen that the relationship between the surface charge density and surface potential is far from linear and almost reaches a plateau. This is the reason why the theoretical calculation gives unreasonable results. Moreover, the contribution of the particle size to V_R is too large in eqn (7.5). This can be demonstrated through a comparison between the variables of latexes B-20%-5mM and B-20%-20mM shown in Table 7.1. The surface charge density of latex B-20%-20mM is almost 2 times that of latex B-20%-5mM. However, the surface potential only increases less than 10 % because the ψ_0 *vs.* σ curve is in the plateau range. On the other hand, the particle size of latex

B-20%-5mM is 2 times larger than the latex B-20%-20mM. The V_R is primarily influenced by the particle size in this case. Therefore, using these results in the calculations will result in the phenomenon whereby latex B-20%-5mM to have a larger V_m value than latex B-20%-20mM. The domination of the particle size in eqn (7.5) can also be illustrated using the results of the 40 % solids content latexes (Figure 7.5). These latexes were synthesized using the same recipe in the seed stage and they have similar particle size. The V_T curves of these latexes are close and there is no obvious contradiction in the V_m values with the trend in latex stability.

As shown in Figure 7.6, the initial slope of the 10^{-3} M curve is large. When the curve reaches a plateau, the errors between the values calculated based on the linear and the true values are large. The errors significantly decrease as the electrolyte concentration increases. Especially, if the electrolyte concentration increases to the order of 10^{-1} M, the errors become much smaller and are good enough to make theoretical calculations. For example, if the electrolyte concentration is 0.1 M, the error in the linearity approximation is less than 10 % when the surface charge density is 3.3 $\mu C/cm^2$; if the electrolyte concentration is 0.3 M, the error is about 20 % when the surface charge density is 10.0 $\mu C/cm^2$. Therefore, the V_T curves were calculated again using a high electrolyte concentration value instead of the original electrolyte concentration shown in Table 7.1. The electrolyte concentrations used for the 5 %, 20 % and 40 % solids content latexes are 0.1, 0.3 and 0.3 M, respectively. Table 7.2 shows the comparison of the changes in the surface and Stern potentials of these

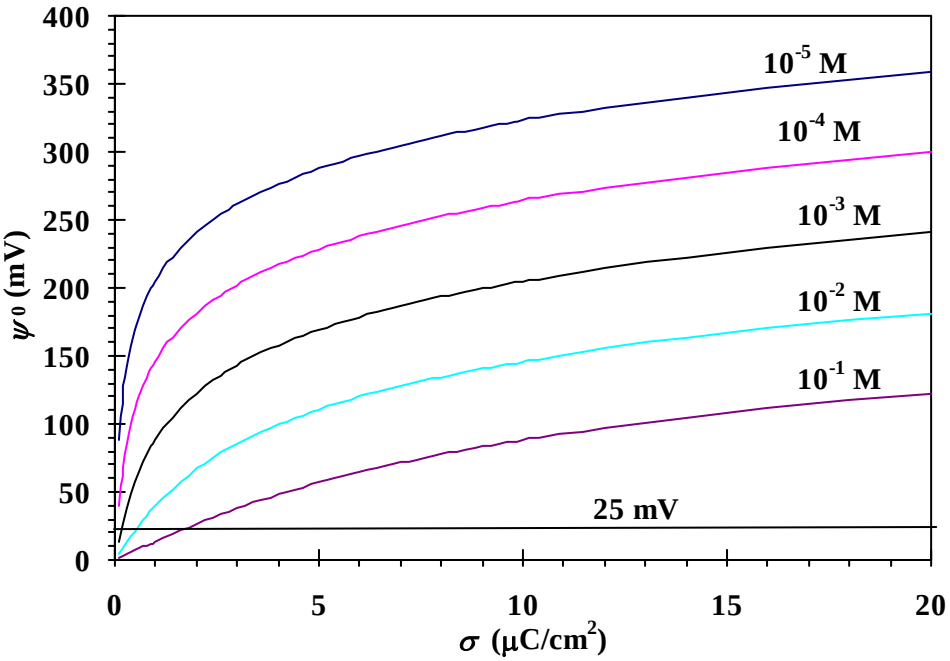

Figure 7.6: *Surface potential (ψ_0) as a function of the surface charge density (σ) at different electrolyte concentrations.*

latexes for the different electrolyte concentrations. The potentials significantly decrease as the electrolyte concentration increases.

Table 7.2: Comparison of the Surface and Stern Potentials for the Different Electrolyte Concentrations

Samples	σ ($\mu C/cm^2$)	Low salt concentration*		High salt concentration**	
		ψ_0 (mV)	ψ_δ (mV)	ψ_0 (mV)	ψ_δ (mV)
B-5%-0.6mM	2.07	78	74	27	23
B-5%-1.2mM	1.91	72	69	25	22
B-5%-2.4mM	3.35	96	90	42	35
B-5%-7.8mM	13.04	163	141	101	80
B-20%-5mM	6.66	164	152	47	35
B-20%-6mM	5.95	152	141	43	32
B-20%-8mM	7.31	164	151	50	38
B-20%-10mM	7.34	168	155	50	38
B-20%-20mM	10.98	175	156	67	49
B-20%-30mM	14.55	186	163	80	57
Semi-0.7%	4.48	117	108	33	26
Semi-1.0%	6.45	131	120	45	34
Semi-1.4%	8.44	146	131	56	42
Semi-1.7%	11.23	158	139	68	50
Semi-2.0%	12.47	163	142	73	53
Semi-2.5%	15.45	172	147	83	59
Semi-3.6%	22.07	183	151	100	68

***** The original electrolyte concentration

****** The electrolyte concentration used in the calculations (0.1 M for the 5 % solids content latexes; 0.3 M for the 20 % and 40 % solids content latexes)

The new results are shown in Figures 7.7, 7.8, and 7.9. The results look reasonable and show the correct trend in latex stability, even though V_R is underestimated for the high surface charge conditions. All of the new results are consistent with the results obtained previously by the blender and turbidity tests except for latex B-20%-5mM. These results show that the DLVO theory can only work at the high electrolyte concentrations if the surface charge density is high.

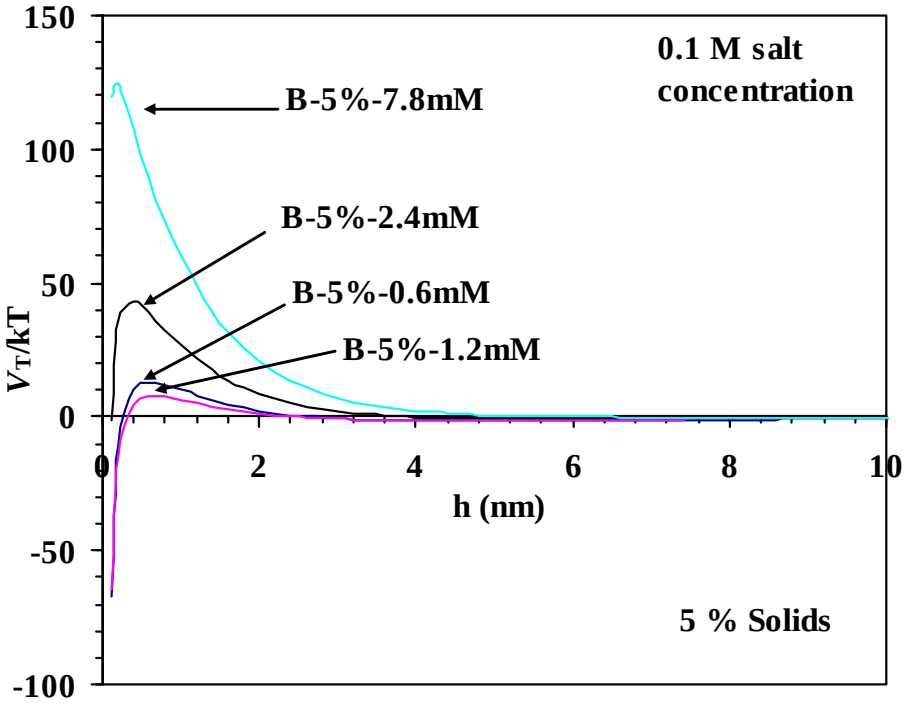

Figure 7.7: *The total potential energy (V_T) curves as a function of particle surface distance (h) for the 5 % solids content latexes and 0.1 M (1:1) electrolyte concentration.*

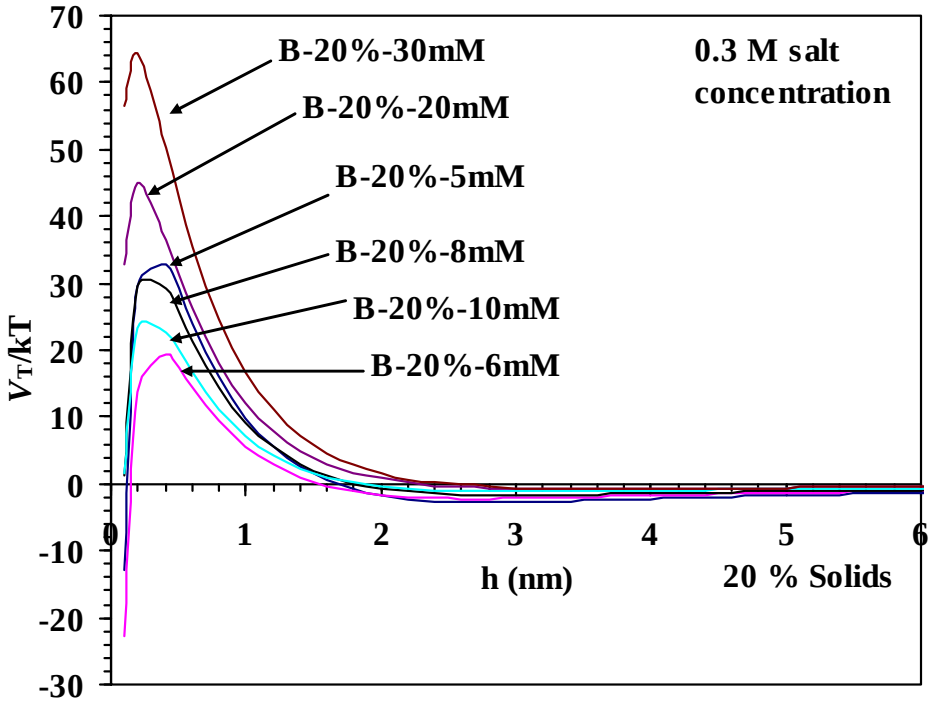

Figure 7.8: *The total potential energy (V_T) curves as a function of particle surface distance (h) for the 20 % solids content latexes and 0.3 M (1:1) electrolyte concentration.*

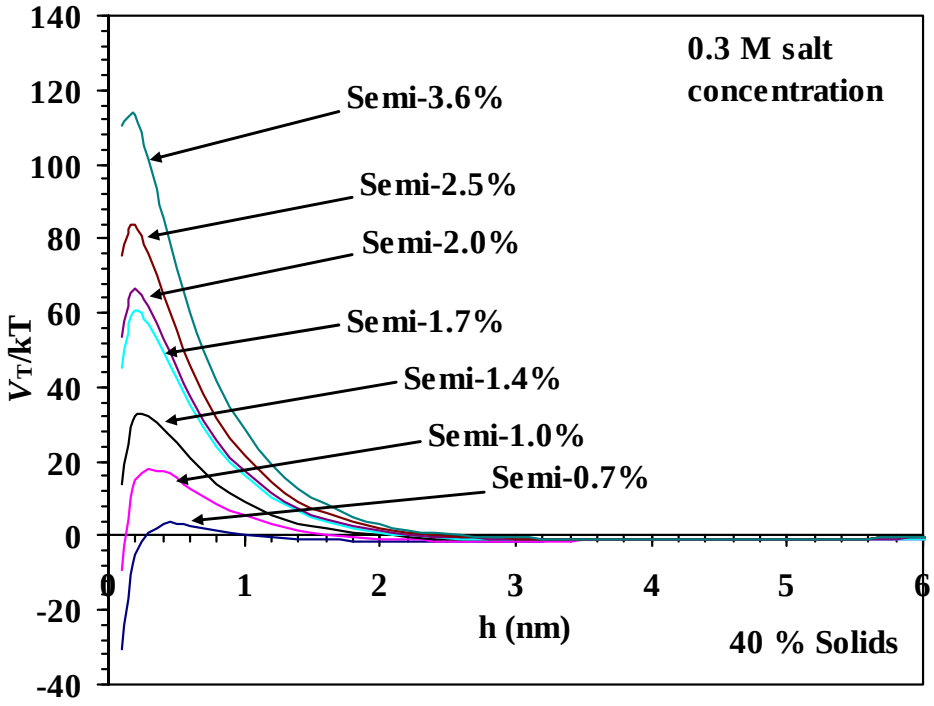

Figure 7.9: *The total potential energy (V_T) curves as a function of particle surface distance (h) for the 5 % solids content latexes and 0.3 M (1:1) electrolyte concentration.*

The ccc is theoretically calculated using eqn (7.18) and the results obtained from the calculations and the turbidity measurements are shown in Table 7.3. From this table, it can be seen that the error is small if σ is in the intermediate level; on the other hand, the error is large if σ is too low or too high, which are caused by different reasons. First, in the case of the low surface charge density values, such as latexes B-5%-0.6mM and B-5%-1.2mM, it is caused by the estimation of the KPS decomposition rate. Due to the low SLS concentration on the particle surfaces, the contribution of the decomposed KPS to σ is large, but this part is roughly estimated using the same decomposition rate constant and the same reaction time for the different recipes. This causes the large error between the experimental data and the theoretical values. Second, in the case of the very high surface charge density values, such as latexes B-5%-7.8mM and B-20%-30mM, the large error is caused by the poor approximation of the DLVO theory. From Figure 7.6, it can be seen that the error between the linear approximation and true curve is still large in the high surface charge density range (more than 10 $\mu C/cm^2$), even though the electrolyte concentration is on the order of 0.1 M.

Table 7.3: Comparison of the ccc's Obtained from the Calculations and the Turbidity Measurements for the Latexes Prepared Using SLS as the Sole Surfactant

	σ (μC/cm^2)	ccc (M)	
		Experimental	**Theoretical**
B-5%-0.6mM	2.07	0.445	0.150
B-5%-1.2mM	1.91	0.531	0.137
B-5%-2.4mM	3.35	0.581	0.255
B-5%-7.8mM	13.04	0.682	0.942
B-20%-5mM	6.66	0.527	0.509
B-20%-6mM	5.95	0.522	0.460
B-20%-8mM	7.31	0.550	0.561
B-20%-10mM	7.34	0.560	0.612
B-20%-20mM	10.98	0.616	0.879
B-20%-30mM	14.55	0.699	1.140
Semi-0.7%	4.48	0.471	0.351
Semi-1.0%	6.45	0.566	0.500
Semi-1.4%	8.44	0.590	0.648
Semi-1.7%	11.23	0.675	0.825
Semi-2.0%	12.47	0.741	0.897
Semi-2.5%	15.45	0.777	1.051
Semi-3.6%	22.07	0.787	1.348

Some efforts were made to overcome the limitations in the DLVO theory, but it was found that the corrections would not give more practical meanings after the calculations of the stability ratio (W). W can be calculated using the following equation[24].

$$W = 2a\int_0^\infty \frac{\exp(V_T/kT)}{(h+2a)^2}dh \tag{7.19}$$

Overbeek[25] estimated the value of W through eqn (7.20) if there is a sharp peak in the curve calculated based on the DLVO theory.

$$W = \frac{1}{2\kappa a}\exp\frac{V_m}{kT} \tag{7.20}$$

So W can be estimated using the maximum value (V_m) in the curve. At a low electrolyte concentration, W is huge based on eqn (7.20). For example, for latex B-5%-1.2mM, having the lowest surface charge (1.91 μC/cm^2) and a V_m/kT value of 292 at the original electrolyte concentration, W is 7.9×10^{124}. This value is reasonable even though it is huge because this latex is stable and can be stored for many years if no additional salt is added to the sample. W can also be estimated using the results of the blender test through eqn (7.21) based on von Smoluchowski's theory[26].

$$-\ln(1-c)=\frac{4\phi St}{\pi W} \tag{7.21}$$

where ϕ is the volume fraction of particles, S is the shear rate, c is the fraction of particles coagulated at t time. Taking samples B-20%-5mM and B-20%-30mM as examples, using the results of the blender test, the ratio of W between them can be obtained.

$$\frac{W_{30}}{W_5}=\frac{\ln(1-0.4)}{\ln(1-0.005)}=102$$

where W_{30} and W_5 are the stability ratios of samples B-20%-30mM and B-20%-5mM. This result shows that W of sample B-20%-30mM is 102 times larger than that of sample B-20%-5mM, which is a significant difference. However, if V_m/kT is calculated using eqn (7.20),

$$(\frac{V_m}{kT})_{30}-(\frac{V_m}{kT})_5=\ln(2\kappa_{30}a_{30}W_{30})-\ln(2\kappa_5 a_5 W_5)=\ln(\frac{\kappa_{30}a_{30}W_{30}}{\kappa_5 a_5 W_5})=3.98$$

this result indicates that the difference in V_m/kT between the two samples is less than 4. Even though the calculation of V_m/kT is not accurate at the original electrolyte concentration using the DLVO theory, it is more than 800 for sample B-20%-5mM.

Therefore, the difference in V_m/kT between the two samples is too small (4 *vs.* 800) and the two curves will be very close even though the equations used for the DLVO theory are corrected. This is caused by the exponential relation between V_m/kT and W, which means that a small change in V_m will cause a significant change in W. As a result, the corrections for the DLVO curves at a low electrolyte concentration will not give more practical significance and the efforts to achieve this were abandoned.

7.2 Extended DLVO Theory

7.2.1 Introduction

Even though the DLVO theory successfully explains the long-range interactions observed in many systems, it fails to predict the stability in many well-known cases, such as the unexpected stability of latexes at high salt concentrations[27] and the stability of soap films[28]. This is caused by the existence of other interaction forces between two particles besides van der Waals attractive forces (V_A) and the electrostatic repulsive forces (V_R). These forces mainly include solvation or hydration forces[29,30], hydrophobic forces[31,32] and steric forces. Liang *et al.* wrote a good review describing these other forces[33]. The theories about these forces are referred to as the extended DLVO or non-DLVO theory. In this section, only steric forces are discussed due to the content of this research.

Steric stabilization was first used as a term by Heller and Pugh[34], which may be differentiated from protective action by the absence of any electrostatic component.

The prediction of the steric interactions between two spheres covered by grafted polymers has been studied since then[35,36]. Vincent *et al.*[37,38] established a quantitative model to study steric stabilization based on the ideas of Smitham *et al.*[39] and Meier[40], in which the steric interaction is visualized as the consequence of two stabilizing contributions. As shown in Figure 7.10[41], the two contributions are osmotic and elastic. First, when $\delta < h < 2\delta$ (δ is the thickness of the adsorbed layer), the adsorbed polymer chains form an overlapped range and generate a higher density of polymer. This causes a difference in the osmotic pressure of the solvent in this region. Second, when $h < \delta$, the elastic compression of the adsorbed chains occurs. This limitation of the available volume leads to a loss in the configuration entropy of the chains.

The model of Vincent *et al.* is widely used to calculate the effect of steric forces on latex stability. Ortege-Vinuesa *et al.*[42] investigated the effects of interfacial properties on the colloidal stability of monodisperse polymer colloids using sulfonate polystyrene (PS) and styrene-hydroxyethyl methacrylate copolymer (PSHEMA) latexes prepared by surfactant-free emulsion polymerizations. They theoretically calculated *A* and *W* for both of the latexes and compared the theoretical values and experimental results. Peula *et al.*[43] studied the colloidal stability mechanisms of polystyrene latexes with acetal functionality (core-shell structures). After calculating *A* and the diffuse potential based on the calculation of *W*, they predicted the ccc for the different latexes at different pH values. Lozsán *et al.*[44] studied the effect of steric interactions on the stability of oil-in-water emulsions by the means of emulsion

stability simulations. In their research, hexadecane in water emulsions was stabilized with nonylphenol ethoxylated surfactants with different chain lengths and W was calculated using the half life time of the number of drops per unit volume. An empirical relationship between W and V_m was found.

7.2.2 Model

In the extended DLVO theory, V_T is the summation of V_A, V_R and the potential energy generated by other forces. In this research, the steric forces are considered (V_S) and V_T can be expressed in eqn (7.22).

$$V_T = V_A + V_R + V_S \tag{7.22}$$

As discussed before, V_S consists of two parts: osmotic (V_{osm}) and elastic (V_{elas}).

$$V_S = V_{osm} + V_{elas} \tag{7.23}$$

When $\delta < h < 2\delta$, only V_{osm} needs to be taken into account.

$$V_{osm} = \frac{4\pi akT}{v_1}\varphi^2(\frac{1}{2} - \chi)(\delta - \frac{h}{2})^2 \tag{7.24}$$

where δ is the thickness of the adsorbed layer, v_1 is the volume of a single molecule of the solvent, φ is the effective volume fraction of the nonionic surfactant in the adsorbed layer, and χ is the Flory–Huggins solvency parameter for the polymer. When $h < \delta$, V_{osm} needs to be calculated using another equation and V_{elas} needs to be taken into account.

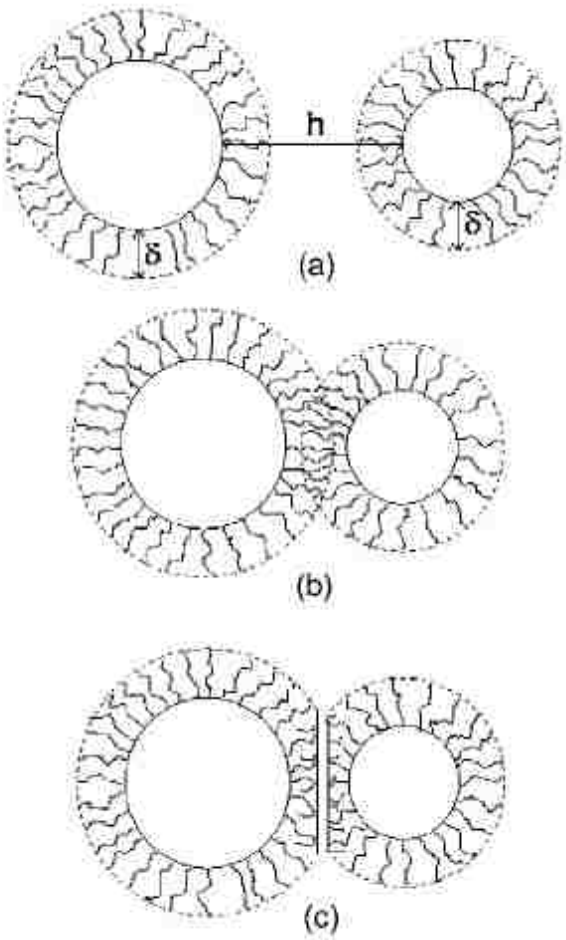

Figure 7.10: *Schematic representation of steric interaction between two particles covered by polymer layers: (a) $h > \delta$, (b) $\delta < h < 2\delta$, and (c) $0 < h < \delta$* [41].

$$V_{osm} = \frac{4\pi akT}{v_1}\varphi^2(\frac{1}{2}-\chi)\delta^2(\frac{h}{2\delta}-\frac{1}{4}-\ln\frac{h}{\delta}) \quad (7.25)$$

$$V_{elas} = \frac{2\pi akT}{M_W}\varphi\delta^2\rho\{\frac{h}{\delta}\ln[\frac{h}{\delta}(\frac{3-h/\delta}{2})^2]-6\ln\frac{3-h/\delta}{2}+3(1-\frac{h}{\delta})\} \quad (7.26)$$

where M_W is the molecular weight of a single nonionic surfactant molecule, and ρ is the density of the nonionic surfactant.

For Triton X-100, $v_1 = 3.01\times10^{-29}$ m^3/molecule, $M_w = 1.04\times10^{-24}$ kg/molecule, $\rho = 982$ kg/m^3, $\chi = 0.45$. The unknown parameters are δ and φ. Different papers have used different numbers to fit their experimental data. The effective volume fraction (φ) of Triton X-100 is reported to be as 0.0125 in several papers[44,45], so this value was chosen to use in the following calculations. The thickness (δ) of a saturated monolayer of Triton X-100 is reported to be as 2.0 nm[46,47]. The relationship between the thickness (δ) and the amount of the adsorbed Triton X-100 (Γ) can be calculated based on the mass balance through the following equations:

$$\frac{4}{3}\pi\rho[(a+\delta)^3-a^3]\varphi = 4\pi a^2\Gamma \quad (7.27)$$

where ρ is the density of Triton X-100.

$$\frac{\Gamma}{\Gamma_s} = \frac{(a+\delta)^3-a^3}{(a+\delta_s)^3-a^3} \quad (7.28)$$

where Γ_s is the amount of Triton X-100 forming a saturated monolayer and δ_s is the thickness of the monolayer (2.0 nm). The packing area of Triton X-100 (84 Å^2) was reported in Chapter 6 (6.3.6), so Γ_s can be calculated and the thickness for different coverages can also be calculated.

7.2.3 Results and Discussion

To estimate V_S resulting from the adsorbed Triton X-100, the thickness of the adsorbed layer needs to be calculated. The surface coverage of Triton X-100 was estimated in the previous chapter and the results were shown in Table 6.6. Using eqn (7.28), the thickness on each latex was calculated and the results are shown in Table 7.4. From the results, it can be seen that the adsorbed Triton X-100 layer is relatively thin. Even for latex B-30mM-1-3, which used the highest amount of Triton X-100 in this series of reactions, the adsorbed Triton X-100 is about half the amount needed to form a saturated monolayer and the thickness is only 1.2 nm. This is one of the reasons for the small contribution of Triton X-100 to latex stability, which will be discussed next.

Using the thicknesses reported in Table 7.4 and the fixed φ (0.0125), the V_S curves for samples B-6mM-3-1, B-6mM-1-1 and B-6mM-1-3 were calculated as shown in Figure 7.11. From the scale of the V_S/kT values, it is clearly seen that V_S is much smaller compared with V_R generated by the electrostatic forces shown in Figure 7.8. The V_T curves for the reactions with the fixed total surfactant concentration of 6 mM are shown in Figure 7.12. The V_T curve for latex B-20%-6mM (only SLS, no Triton X-100) is added in this figure for comparison. V_m decreases as the ratio of Triton X-100 to SLS increases. These results represent the same trend as the results obtained from the blender and turbidity tests and prove that the prediction obtained from the conductivity ratio measured during the polymerizations is correct. The

reason for this can be analyzed through the changes in V_R and V_S. When the total surfactant concentration is fixed, the amount of SLS in the recipes decreases with an increase in the weight ratio of Triton X-100 to SLS, which also decreases the amount of adsorbed SLS on the particle surfaces, resulting in the decrease in σ. Taking 6 mM as an example, σ for latexes B-20%-6mM, B-6mM-3-1, B-6mM-1-1 and B-6mM-1-3 are 0.0595, 0.0556, 0.0494 and 0.0385, respectively. The maximum values of V_R decreases from 73.1 to 59.8, 55.3, and 45.0 kT, respectively. On the other hand, the maximum values of V_S only increase from 0 to 0.00011, 0.025, and 0.542 kT, respectively. The increase in the potential energy resulting from the steric forces is too small compared with the decreases in the electrostatic forces. This is the reason why the increase in the amount of Triton X-100 results in a decrease in latex stability for the fixed total surfactant concentration. Moreover, one thing that needs to be pointed out here is that the electrolyte concentration used in the calculations is 0.3 M instead of the original concentrations used in the latexes. Since the original concentrations are less than 0.01 M, V_m for the original concentrations should be much larger than V_m shown in Figure 7.12 due to the effect of the electrolyte concentration on ψ_0, which means that the effect of the decrease in σ on V_R is much larger than the one for the 0.3 M concentration.

Table 7.4: Amount of Triton X-100 Absorbed and Thickness on the Particle Surfaces

Latex	Amount of adsorbed Triton X-100 (μmol/m^2)	Thickness (nm)
B-6mM-3-1	0.069	0.1
B-6mM-1-1	0.213	0.2
B-6mM-1-3	0.495	0.5
B-10mM-3-1	0.094	0.1
B-10mM-1-1	0.260	0.3
B-10mM-1-3	0.562	0.6
B-20mM-3-1	0.160	0.2
B-20mM-1-1	0.408	0.4
B-20mM-1-3	0.796	0.8
B-30mM-3-1	0.232	0.2
B-30mM-1-1	0.523	0.5
B-30mM-1-3	1.123	1.2

The V_T calculated curves for the latexes prepared using the fixed total surfactant concentrations of 10, 20, and 30 mM are shown in Figures 7.13, 7.14, and 7.15, respectively. Similar conclusions can be obtained from these figures, which also demonstrate that the prediction from the conductivity ratio is correct.

Comparisons of the measured and theoretically calculated ccc's are shown in Table 7.5. Because the potential energy generated by the steric forces is negligibly small, the potential energy generated by the electrostatic forces dominates latex stability. Therefore, as discussed previously, the error is less than 10 % if σ is not too high (less than 0.08 μC/cm^2). On the other hand, if σ is more than 0.1 μC/cm^2, the error is over 40 %.

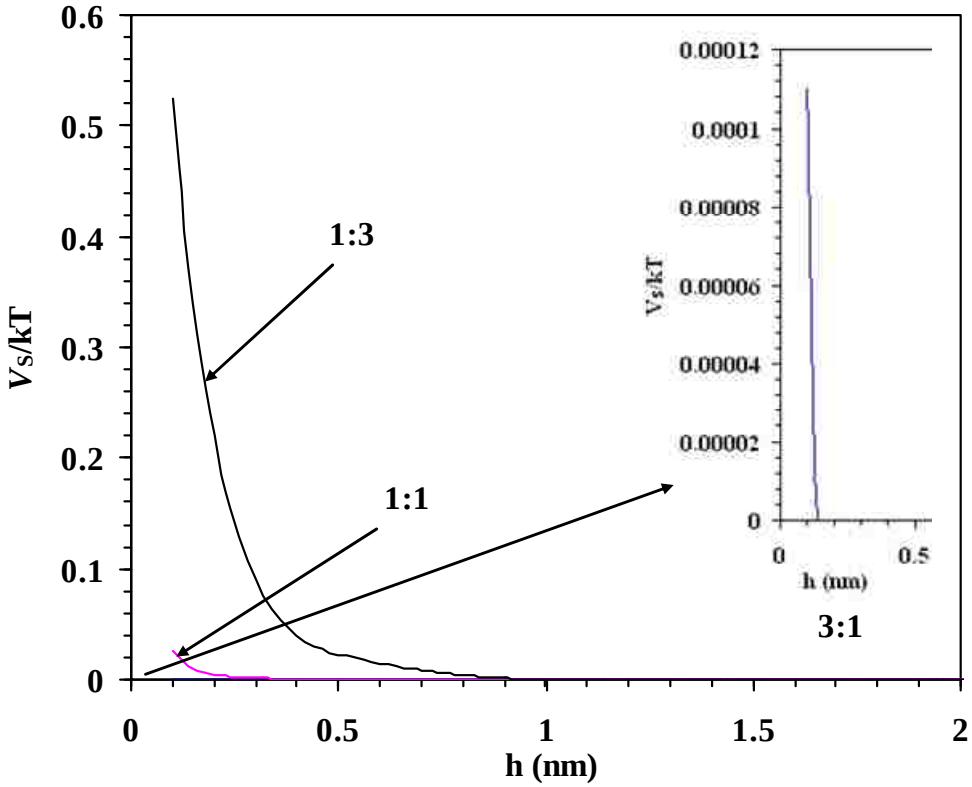

Figure 7.11: *Potential energy curves resulting for the steric forces (V_S) as a function of interparticle distance (h) for samples B-6mM-3-1, B-6mM-1-1 and B-6mM-1-3. The ratios in the figure are the weight ratios of SLS to Triton X-100 for a fixed total surfactant concentration (6 mM).*

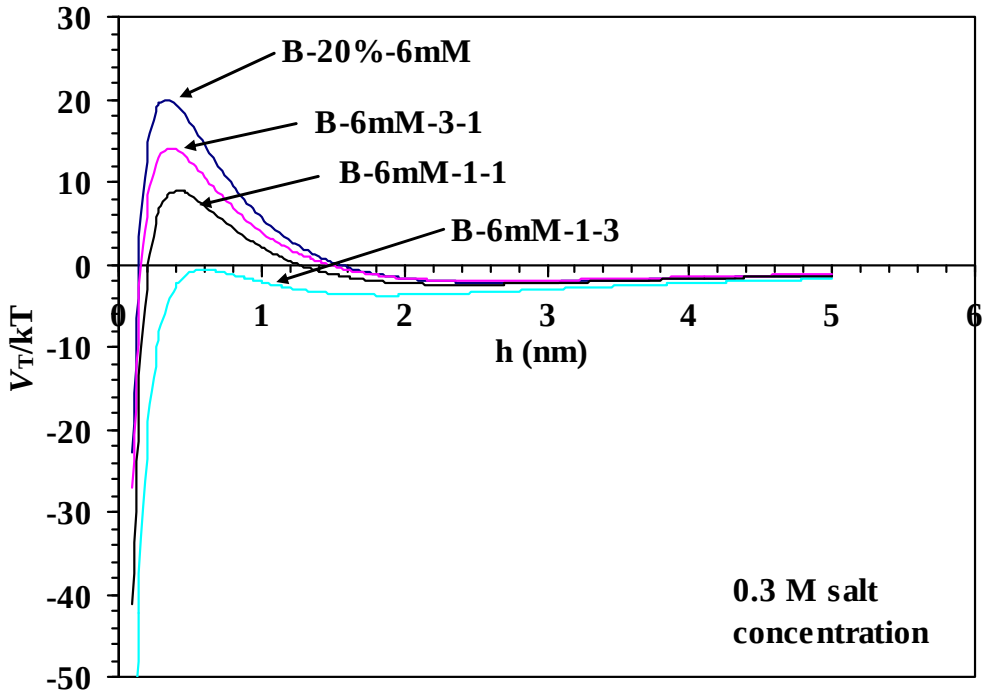

Figure 7.12: *V_T as a function of interparticle distance (h) for the latexes prepared with a fixed total surfactant concentration of 6 mM and different weight ratios between SLS and Triton X-100.*

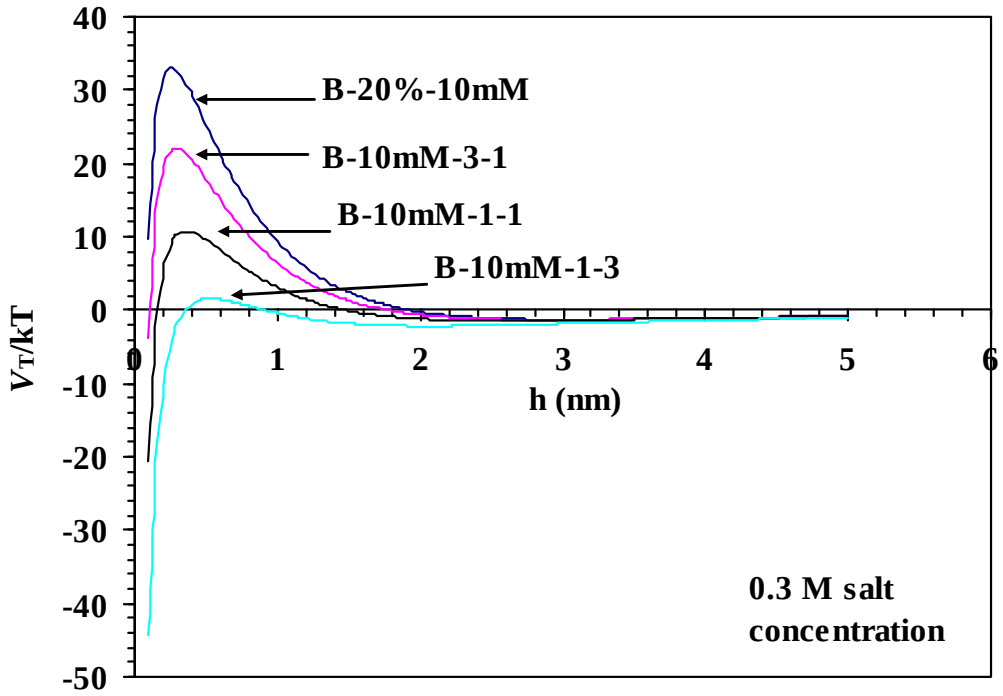

Figure 7.13: *V_T as a function of interparticle distance (h) for the latexes prepared with a fixed total surfactant concentration of 10 mM and different weight ratios between SLS and Triton X-100.*

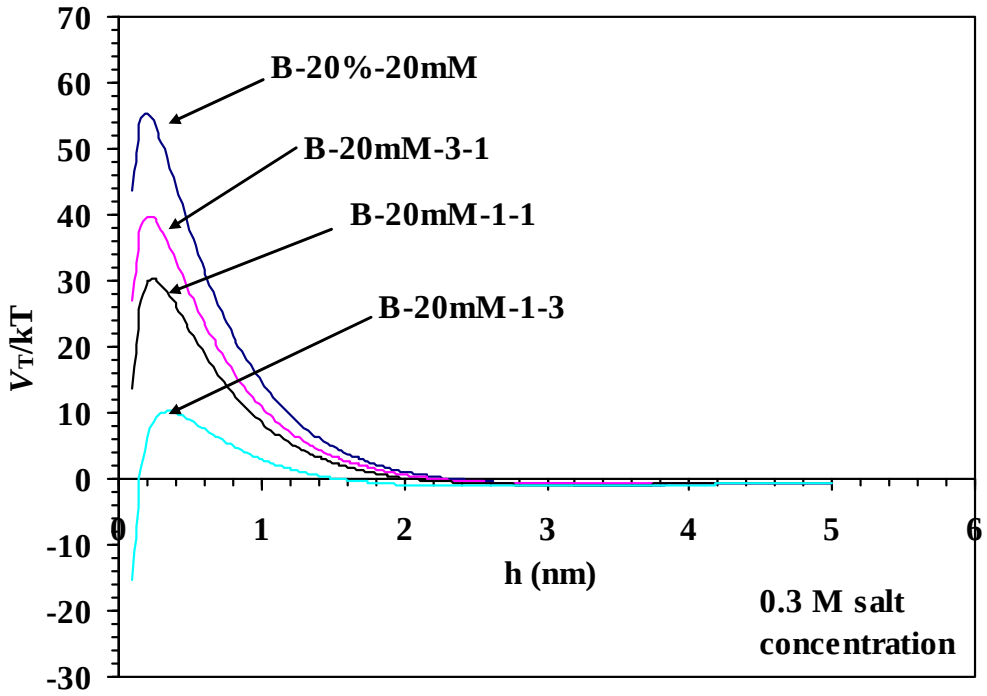

Figure 7.14: *V_T as a function of interparticle distance (h) for the latexes prepared with a fixed total surfactant concentration of 20 mM and different weight ratios between SLS and Triton X-100.*

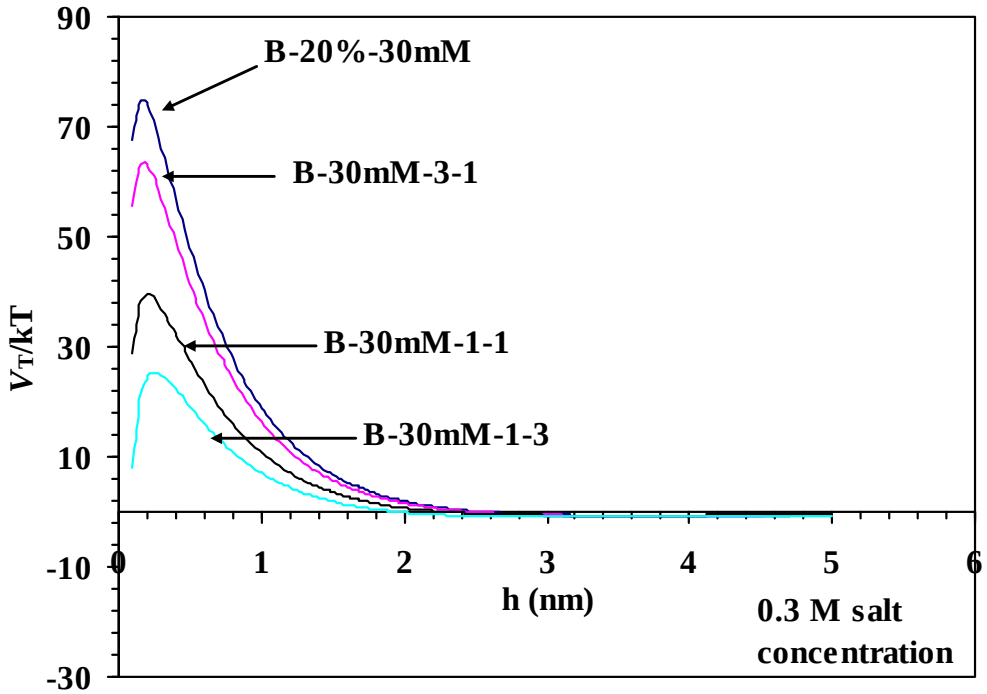

Figure 7.15: *V_T as a function of interparticle distance (h) for the latexes prepared with a fixed total surfactant concentration of 30 mM and different weight ratios between SLS and Triton X-100.*

Table 7.5: Comparison of the ccc's Obtained from the Calculations and the Turbidity Measurements for the Latexes Prepared Using the Mixed Surfactants

Latex	σ (μC/cm^2)	ccc (M)	
		Experimental	Theoretical
B-20%-6mM	0.0595	0.522	0.460
B-6mM-3-1	0.0556	0.440	0.431
B-6mM-1-1	0.0494	0.368	0.382
B-6mM-1-3	0.0385	0.312	0.296
B-20%-10mM	0.0799	0.560	0.612
B-10mM-3-1	0.0689	0.446	0.535
B-10mM-1-1	0.0553	0.370	0.433
B-10mM-1-3	0.0413	0.287	0.325
B-20%-20mM	0.1196	0.616	0.879
B-20mM-3-1	0.1027	0.577	0.776
B-20mM-1-1	0.0859	0.483	0.665
B-20mM-1-3	0.0564	0.403	0.474
B-20%-30mM	0.1660	0.699	1.140
B-30mM-3-1	0.1470	0.683	1.042
B-30mM-1-1	0.1088	0.669	0.832
B-30mM-1-3	0.0781	0.642	0.741

From eqns (7.24), (7.25), and (7.26), it can be seen that the thickness of the adsorbed layer (δ) and the effective volume fraction of the nonionic surfactant in the adsorbed layer (φ) are the important parameters determining the degree of steric stability. The nonionic surfactant used in this research failed to provide better latex stability. The major reason is that both δ and φ are small at the same time. This shows the principle behind the usage of nonionic surfactants for latex stability. Further calculations were carried out to analyze the role of these two parameters in latex stability. The results are shown in Figures 7.16 and 7.17. For these calculations, the particle diameter was assumed to be 117 nm.

In Figure 7.16, δ is fixed at 2.0 nm. It can be seen that the maximum value of V_S increases as φ increases. Compared with Figure 7.12, if φ equals 0.0375, the maximum value of V_S will have a similar magnitude as V_R, which means that the steric forces have a similar contribution to latex stability as the electrostatic forces. Because φ is mainly influenced by the length of the EO groups in the structure of the nonionic surfactant, this demonstrates that a longer EO group can provide better stability. The average length of the EO groups in Triton X-100 is 9.5 and φ is 0.0125. As a comparison, the average length of the EO groups in Triton X-405 is 40 and φ should be much larger than 0.0125. Obviously, Triton X-405 can provide better stability than Triton X-100 if the other parameters are the same.

Figure 7.17 shows the effect of δ on the potential energy generated by the steric forces. δ depends on the number of the EO groups and the amount adsorbed (surface coverage by the nonionic surfactant). As discussed above, the nonionic surfactant with more the EO groups has a larger δ value for the same coverage. Moreover, for the same nonionic surfactant, increasing the amount adsorbed can also improve latex stability. For example, δ is 2.0 nm for a saturated monolayer of Triton X-100, which causes a low maximum value of V_S in the curve. If the amount of the adsorbed Triton X-100 is increased to form multiple layers, δ may be doubled. This will generate a much larger potential energy. From the analysis above, it can be concluded that the length of the EO repeat unit in the nonionic surfactant and the amount adsorbed are the critical parameters to decide latex stability.

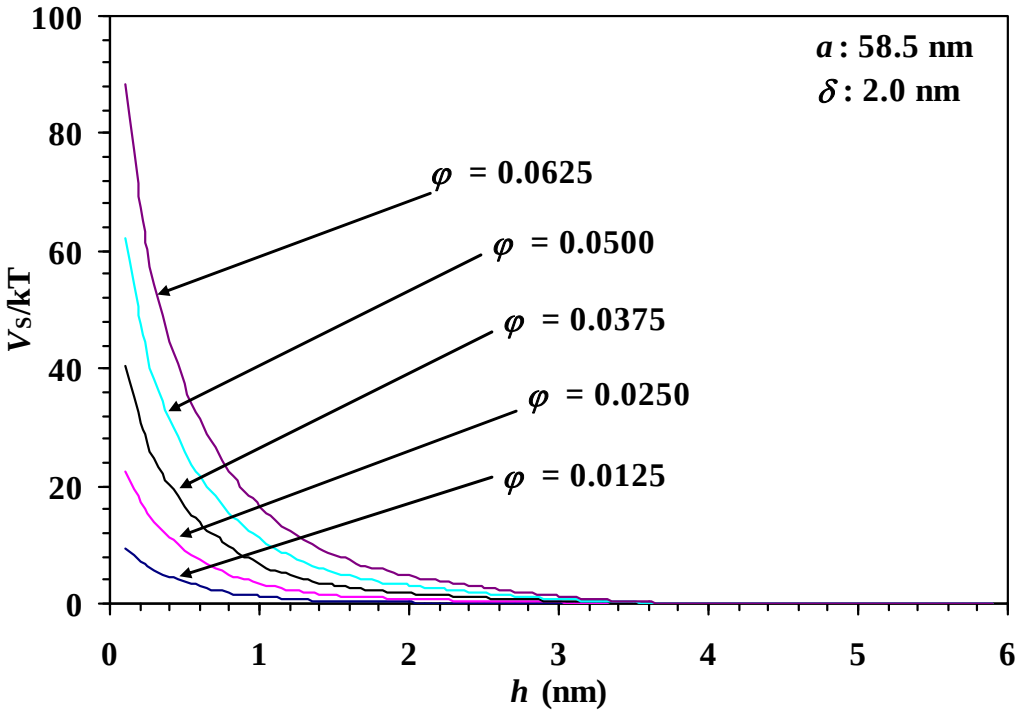

Figure 7.16: *Effect of the effective volume fraction (φ) on the potential energy (V_S) generated by the steric forces.*

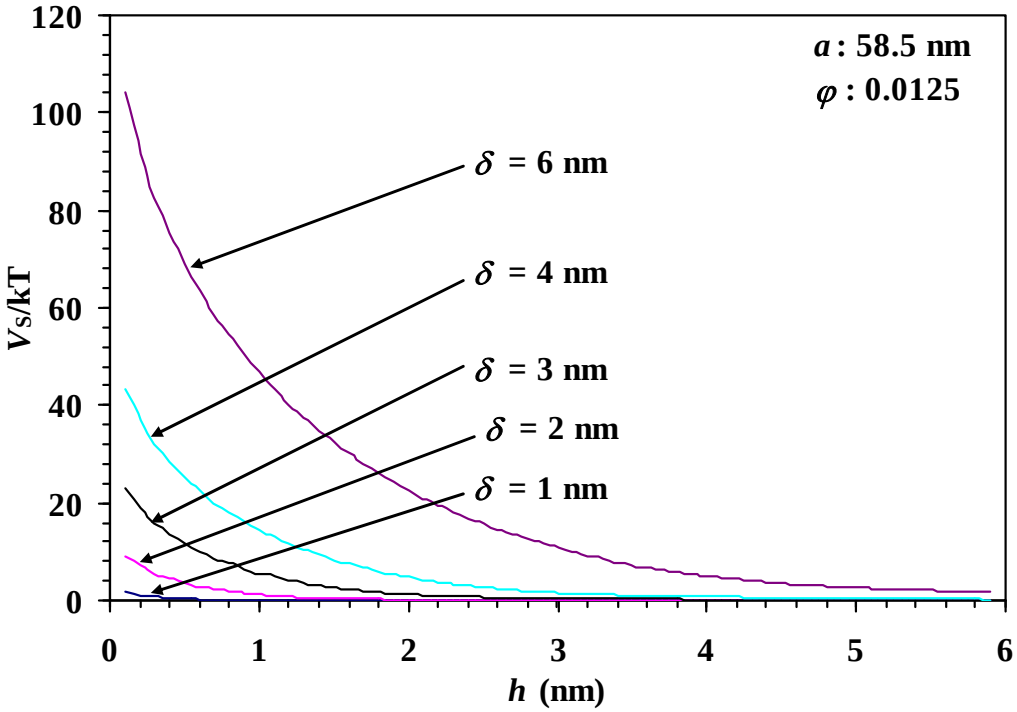

Figure 7.17: *Effect of the thickness of the adsorbed layer (δ) on the potential energy (V_S) generated by the steric forces.*

7.3 Conclusions

Theoretical calculations were carried out to estimate latex stability based on the data obtained previously using the DLVO and extended DLVO theories. The potential energy generated by the electrostatic forces was calculated based on the DLVO theory. The results showed that significant errors and a wrong trend were obtained if the equations were employed for the low electrolyte concentrations. This is caused by the basic assumptions of the DLVO theory. After adjusting the electrolyte concentrations to a high level instead of the original concentrations in the latexes, the calculated results became reasonable and exhibited the same trends as the experimental results. The potential energy generated by the steric forces, which is introduced by the nonionic surfactant, was estimated using the extended DLVO theory. The results explained the major reason why latex stability decreased as the weight ratio of Triton X-100 to SLS was increased. When the total mixed surfactant concentration was fixed, the increase in the weight ratio of Triton X-100 to SLS reflected a decrease in the amount of SLS, which caused the amount of adsorbed SLS on the particle surfaces to decrease. However, the calculated results showed that the contribution of Triton X-100 to latex stability was negligibly small compared with SLS, so the increased potential energy generated by Triton X-100 cannot make up for the decreased potential energy due to the decrease in SLS. This phenomenon is explained by two reasons. One is that the EO group in Triton X-100 is too short; the other is that the amount adsorbed is too low due to the low concentration of Triton X-100 used in the recipes. Furthermore, the changes in the potential energy generated

by the steric forces were analyzed through variations of the thickness of the adsorbed layer (δ) and the effective volume fraction of the nonionic surfactant (φ). The results showed that these two parameters significantly affected the degree of latex stability. Based on these results, a conclusion regarding the usage of the nonionic surfactants can be summarized: a nonionic surfactant with a long repeat unit and high surface coverage of the polymer particles needs to be applied to improve latex stability. Finally, these theoretical calculations also proved that the predictions of latex stability from the conductivity ratio were correct.

7.4 References

[1] B. V. Derjaguin and L. Landau, *Acta Physicochim,* USSR, **14**, 633 (1941).

[2] E. J. W. Verwey and J. Th. G. Overbeek, *Theory of Stability of Lyophobic Colloids,* Elsevier, Amsterdam (1948).

[3] J. N. Israelachvili, in *Intermolecular and Surface Forces*, Academic Press, London (1985).

[4] R. H. Ottewill, in *Emulsion Polymerization and Emulsion Polymers*, P. A. Lovell and M. S. El-Aasser Eds., John Wiley and Son, Chichester (1997).

[5] F. M. Fowkes, *Ind. Eng. Chem.*, **56**, 40 (1964).

[6] G. C. Jeffrey and R. H. Ottewill, *Colloid Polym. Sci.*, **266,** 173 (1988).

[7] D. C. Prieve, *J. Colloid Interface Sci.*, **73**, 539 (1980).

[8] G. Urbina-Villalba, *Langmuir*, **21**, 6675 (2005).

[9] F. J. Rubio-Hernández, *J. Non-Equilib. Thermdyn.*, **21**, 153 (1996).

[10] Y. Ishikawa, Y. Katoh and H. Ohshima, *Colloids Surf. B*, **42**, 53 (2005).

[11] S. Tsaur and R. M. Fitch, *J. Colloid Interface Sci.*, **115**, 463 (1986).

[12] M. Fortuny, C. Graillat and T. F. McKenna, *Ind. Eng. Chem. Res.*, **43**, 7210 (2004).

[13] G. Urbina-Villalba, A. Lozsan, K. Rahn and M. S. Romero-Cano, *Comput. Phys. Commun.*, **180**, 2129 (2009).

[14] H. C. Hamaker, *Physica*, **4**, 1058 (1937).

[15] J. Vial and A. Carre, *Int. J. Adhesion and Adhesive*, **11**, 140 (1991).

[16] J. P. Friends, and R. J. Hunter, *J. Colloid Interface Sci.* **44**, 456 (1971).

[17] J. A. Kitchener and J. H. Schenkel, *Trans. Faraday Soc.*, **56**, 161 (1960).

[18] J. Th. G. Overbeek, *Pure Appl. Chem.*, 52, 1151 (1980).

[19] P. J. Feeney, D. H. Napper and R. G. Gilbert, *Macromolecules,* **20**, 2922 (1987).

[20] A. S. Dunn and L. C. Chong, *Br. Polymer J.* **2**, 49 (1970).

[21] H. Schlüter, *Colloid Polym. Sci.,* **271**, 246 (1993).

[22] A. M. Santos, Ph. Vindevoghel, C. Graillat, A. Guyot and J. Guillot, *J. Polym. Sci. A*, **34**, 1271 (1996).

[23] M. Egen and R. Zentel, *Macromol. Chem. Phys.*, **205**, 1479 (2004).

[24] N. Fuchs, *Z. Phys.*, **89**, 129 (1917).

[25] J. Th. G. Overbeek, in *Colloid Science*, H. R. Kruyt eds. (1960).

[26] M. von Smoluchowski, *Z. Physik. Chem.*, **92**, 155 (1917).

[27] B. V. Derjaguin, T. N. Voropaye, B. N. Kabanov and A. S. Titiyevs, *J. Colloid Sci.*, **19**, 113 (1964).

[28] J. S. Clunie and J. F. Goodman, *Nature*, **216**, 1203 (1967).

[29] N. V. Churaev and B. V. Derjaguin, *J. Colloid Interface Sci.*, **103**, 542 (1985).

[30] S. Leikin, V. A. Parsegian, D. C. Rau and R. P. Rand, *Annu. Rev. Phys. Chem.*, **44** 369 (1993).

[31] J. N. Israelachvili and R. M. Pashley, *J. Colloid Interface Sci.*, **98**, 500 (1984).

[32] Y. I. Rabinovich and B. V. Derjaguin, *Colloids Surf.*, **30**, 243 (1988).

[33] Y. Liang, N. Hilal, P. Langston and V. Starov, *Adv. Colloid Interface Sci.*, **134-135**, 151 (2007).

[34] W. Heller and T. L. Pugh, *J. Chem. Phys.*, **22**, 1778 (1954).

[35] F. T. Hesselink, *J. Phys. Chem.*, **75**, 2094 (1971).

[36] R. H. Otewill, *J. Colloid Interface Sci.*, **58**, 357 (1977).

[37] B. Vincent, P. F. Luckham and F. A. Waite, *J. Colloid Interface Sci.*, **73**, 508 (1980).

[38] B. Vincent, J. Edwards, S. Emmett and A. Jones, *Colloid Surf.*, **18**, 261 (1986).

[39] J. B. Smitham, R. Evans and D. H. Napper, *J. Chem. Soc., Faraday Trans. 1*, **71**, 285 (1975).

[40] D. J. Meier, *J. Phys. Chem.*,**75**, 2094 (1971).

[41] A. Lozsan, M. Garcia-Sucre and G. Urbina-Villalba, *Phys. Review E*, **72**, 061405 (2005).

[42] J. L. Ortega-Vinuesa, A. Martin-Rodriguez and R. Hidalgo-Alvarez, *J. Colloid Interface Sci.*, **184**, 259 (1996).

[43] J. M. Peula, R. Santos, J. Forcada, R. Hidalgo-Alvarez and F. J. de las Nieves, *Langmuir*, **14**, 6377 (1998).

[44] A. Lozsán, M. Garcia-Sucre, G. Urbina-Villalba, *J.Colloid Interface Sci.*, **299**, 366 (2006).

[45] M. S. Romero-Cano, A. M. Puertas and F. J. de las Nieves, *J. Chem. Phys.*, **112**, 8654 (2000).

[46] P. Johnson, *Langmuir*, **9**, 2318 (1993).

[47] M. S. Romero-Cano, A. Martin-Rodriguez and F. J. de las Nieves, *Langmuir*, **17**, 3505 (2001).

Chapter 8
Conclusions and Recommendations

8.1 Conclusions

Online conductivity measurements as a method was developed to predict the stability of a latex, in which two different types of conductivity probes (resistance and torroidal) were used to measure conductivity changes at the same time. This method was applied in non-reactive and reactive systems. In the reactive system, both batch and semi-batch emulsion polymerizations of BMA were carried out. SLS and a mixture of SLS and Triton X-100 were chosen as the surfactants in the recipes. Blender tests and turbidity measurements were used as tools to estimate the mechanical and electrolyte stability of the final latexes. Theoretical calculations were also carried out to analyze latex stability based on the DLVO and extended DLVO theories. The conclusions of this study are summarized as follows:

In the non-reactive system, latexes with high, intermediate, and low conversions were used to determine latex stability and conductivity. The results indicated that there was no obvious relationship between the conductivity curves and latex stability. Therefore, online conductivity measurements could not be used as a tool to predict latex stability if no polymerization reaction was carried out.

The online conductivity measurements were used in batch (5 and 20 % solids content) and semi-batch emulsion polymerization (40 % solids content) systems. The relative conductivity curves obtained from the torroidal probe showed similar shapes. On the other hand, the profiles of the conductivity curves obtained from the resistance probe changed with variations in the SLS concentration. There was an obvious divergence between the two conductivity curves if the SLS concentration was not high enough (less than 2.4 mM for 5 % solids content and 10 mM for 20 % solids content). This was caused by polymer plating on the surfaces of the electrodes of the resistance probe. The final conductivity ratio (R/T) between the two conductivity curves could be used to represent the degree of plating on the surfaces of the electrodes. The blender test and turbidity measurements were performed to check the mechanical stability and the electrolyte stability of the final latexes, respectively. The percent coagulum obtained after the blender test was used to represent the mechanical stability and the critical coagulation concentration (ccc) estimated through the turbidity measurements was used to indicate electrolyte stability. R/T was correlated to the percent coagulum and ccc, respectively. There was a linear relationship between them, which indicated that the online conductivity measurements could be used to predict latex stability in the batch and semi-batch emulsion polymerization systems.

The commercial resistance probe showed poor repeatability and limited sensitivity due to the structure and surface properties of this type of probe. Therefore, a homemade resistance probe was built and used to measure conductivity during the

course of the emulsion polymerizations. Because the homemade probe had larger surface area and the electrodes were totally exposed to the reaction mixture, this probe provided better sensitivity compared to the commercial resistance probe and the new results were much more reliable than the old results. However, this probe had a disadvantage, which was that the measurements obtained from this probe were easily affected by the presence of insulated materials, such as monomer droplets.

The reason for the second increase in the conductivity curves obtained using the resistance probe in the middle of the emulsion polymerizations was investigated. Some indirect evidence was obtained through the analysis of the kinetic curves and a batch emulsion polymerization using AIBN as initiator. The results showed that this increase was related to the disappearance of the monomer droplets.

SEM and AFM were used to investigate the morphology of coagulum formed in the early stages of an emulsion polymerization reaction. The results showed that coagulum might be formed at very low conversions on gold film surfaces. This provided a direct and strong evidence to prove that the divergence between the two conductivity curves was caused by the deposited coagulum.

A mixture of SLS and Triton X-100 was used as surfactants in batch emulsion polymerizations of BMA. The conductivity results predicted that latex stability should decrease with an increase in the ratio of Triton X-100 to SLS for a

fixed total surfactant concentration, which was the opposite of what was the expected. The blender test and turbidity measurements were used to investigate the mechanical and electrolyte stability of the final latexes. The results proved that the prediction of the conductivity results was correct. Linear relationships between R/T and the percent coagulum obtained from the blender test, and between R/T and the ccc obtained from the turbidity measurements were established. These results illustrated that the two conductivity probes could be used as online sensors to monitor latex stability during the course of the emulsion polymerizations of BMA. Moreover, the surface coverage of each surfactant on the particle surfaces was calculated. The results proved that the contribution of Triton X-100 to latex stability was much smaller compared to SLS.

The DLVO and extended DLVO theories were applied to theoretically calculate the energy barrier between two polymer particles. The DLVO theory was used to calculate the energy potential caused by the electrostatic forces between the particles. Some unreasonable results were obtained, caused by an assumption of the DLVO theory, which was not suitable for the experimental results. After changing the electrolyte concentration to the order of 0.1 M, the equations based on the DLVO theory showed much smaller errors and the new results were more reasonable. The extended DLVO theory was used to calculate the energy potential for the latexes prepared using a mixture of SLS and Triton X-100 as the surfactants. Both the electrostatic and steric forces were considered in the calculations. The theoretically calculated results were consistent with the ones obtained from the conductivity curves

and latex stability tests. Moreover, the results also gave an explanation for the unexpected results, which was that the mixed surfactants did not improve latex stability. This was caused by the low potential energy generated by Triton X-100 due to its structure and the low surface coverage. Therefore, the contribution of Triton X-100 to latex stability was much smaller compared to SLS.

8.2 Recommendations

Studies of online conductivity measurements and latex stability are very limited. So far, only a few papers have been published regarding this aspect. This research presented a view of the relationship between the conductivity curves and latex stability. Further work needs to be carried out in the future to provide more experimental results and fundamental theories concerning this relationship. As the final part of this research, several recommendations are listed below:

First, the homemade resistance probe used in this research provides better sensitivity and repeatability compared with the commercial one, but the back-to-back configuration of the electrodes has a disadvantage, which causes the measured conductivity values to be smaller than the true values in the presence of the insulated materials, such as monomer droplets. In this case, it is hard to detect accurately when the divergence between the two conductivity curves occurs during the course of emulsion polymerizations. This means that online conductivity measurements cannot be precisely judged when the deposited polymer occurs. Therefore, a better

homemade probe needs to be machined to overcome this disadvantage.

Second, the recipes used in this research are very simple compared with the recipes used in industry. Therefore, if online conductivity measurements can be applied to a complicated recipe, especially an industrial recipe, the feasibility of this method to real industrial applications can be determined.

Third, Triton X-100 was used as a nonionic surfactant in this research. The results showed that this surfactant was not a good stabilizer of the polymer particles due to its short EO group. A nonionic surfactant, which contains a longer EO group (such as Triton X-405), can be used in the further studies. The results obtained from the latex stability tests can be compared with the calculated results based on the DLVO and extended DLVO theories. In the meantime, the online conductivity measurements can be used to predict latex stability in such a system. If the prediction from the conductivity curves is correct, it will provide more evidences to prove the relationship between the online conductivity measurements and latex stability. Moreover, other types of surfactants can also be evaluated in emulsion polymerization systems. These results can expand the applicability of online conductivity measurements.

Lastly, a model for the deposition processes occurring during the course of the emulsion polymerizations of BMA can be established in a fundamental study. In

this model, a lot of the parameters need to be considered, such as the agitation rate, the flow direction, the surface properties of the electrodes and the interactions between the surfaces of the electrodes and polymer particles. This model will be used to analyze the reasons why the deposited coagulum can be formed early in the reaction at low conversions during the course of emulsion polymerizations.

VITA

Funian Zhao was born on October 25th, 1979, in Langfang, Hebei Province, China. He is the elder son of Baozhong Zhao and Binmei Sun. He entered Tianjin University in Tianjin, China in 1998. He chose Biochemical Engineering as his major due to the curiosity of biology and chemistry. As a senior student, he handled the research about the fermentation of recombinant E.coli.

In 2002, he stayed in Tianjin University and became a graduate student. His advisor was Professor Yiru Gan. His research was about the separation and quantitative analysis of tetracyclines by HPLC with a coulometric electrode array system. He published a paper to introduce the method he established.

After receiving his Master degree, he entered Lehigh University and joined the Emulsion Polymers Institute to pursue a Ph.D. degree in 2005. This was a huge decision for him because he changed his focus from biochemical engineering to emulsion polymers, which was a totally new area for him. Through hard working, self-learning and the help from his advisor, Professor Andrew Klein, he accomplished this change within several months. His research was about the online conductivity measurements and latex stability. He successfully completed this project. He presented some of his results at an ACS conference in Anaheim, CA (2011). He is planning to publish four papers based on his research.